

**The roles of glycerol in *Candida albicans* biofilm formation and invasion.**

A Dissertation

Submitted to the

Carnegie Mellon University

In partial fulfillment of the requirements for

the degree of Doctor of Philosophy

By

Jigar V. Desai

July, 2014

Copyright by

Jigar V. Desai

2014

## ABSTRACT

The fungal pathogen *Candida albicans* is a leading cause of device-associated and other nosocomial infections. The traits of biofilm formation and invasion into an underlying surface are important for *Candida* to cause disease. In this dissertation, I describe my work, which reveals a novel role for glycerol in *C. albicans* biofilm formation and hyphal invasion. Through genome-wide expression profiling it was observed that glycerol biosynthetic genes were highly up-regulated in biofilms relative to the planktonic (suspension) cultures. Consistent with this observation, cells in a biofilm also accumulated higher amounts of glycerol than non-biofilm cells. In order to study the impact of glycerol on biofilm formation I made a deletion mutant, *rhr2Δ/Δ*, in the gene encoding glycerol-3-phosphatase. Under in vitro conditions, the *rhr2Δ/Δ* mutant has reduced biofilm biomass and reduced adherence to silicone. The mutant is also severely defective in biofilm formation in the rat venous catheter model of biofilm infection. Surprisingly, genome-wide expression profiling showed that the *rhr2Δ/Δ* mutant has reduced expression of the cell-surface adhesin genes: *ALS1*, *ALS3*, and *HWP1*, as well as many other genes that are up regulated in biofilms. The role of Rhr2 in adherence and biofilm formation depends on adhesin gene expression as overexpression of any of the adhesin genes restores biofilm formation by *rhr2Δ/Δ* in vitro and in vivo. Thus, our findings indicate that glycerol plays a regulatory role in biofilm gene expression and that the adhesin genes are among the functional Rhr2-regulated genes.

I observed that the functional significance of biofilm glycerol accumulation lies in its ability to generate turgor to drive hyphal invasion. I showed that using an assay for invasive growth into elastic polyacrylamide. Using mathematical and biophysical approaches, I show that *C. albicans* can generate turgor equivalent to 20 atm in order to invade. Additionally, I show that several mutants with deletions in biofilm and hyphal regulator genes are defective in invasion, thus

implying a critical role for biofilm formation and hyphal morphogenesis in invasion. The glycerol-deficient hyphae, however, cannot invade even when they are hyperadherent and enmeshed in a confluent biofilm. Thus, my observations suggest that *Candida* hyphae can generate high turgor while in a biofilm which is required for invasion into elastic substrata. I predict that turgor is required for hyphal invasion of mucosal surfaces as well, and that is significant for the pathogenicity of this fungus.

Among the other biofilm up-regulated genes, I focused my attention on *SHB17* that encodes the enzyme sedoheptulose biphosphatase, involved in nonoxidative arm of ribose biosynthesis. I made deletion mutant strains and analyzed the mutants for their abilities to form biofilm. I observed the mutant to have a moderate loss of biofilm biomass. The mutant biofilm, however, contained hyphae that were more slender in appearance than either the wild type or the complemented strain. I additionally observed that the mutant phenotype is biofilm specific and ribose-dependent, as the mutant biofilms grown in ribose-containing growth medium do not display the slender hyphal phenotype. Thus, these observations suggest that biofilm growth drives higher flux through the nonoxidative arm of ribose synthesis. Any alterations to this flux can affect the cell morphology.

In the course of Rhr2 studies, I developed an improved method for biofilm imaging. I applied this approach to analyze the roles of the adhesin Als1 and biofilm regulators Bcr1 and Brg1 in biofilm formation. These studies helped to establish that Als1 stimulates Brg1 activity in Bcr1-dependent manner.

**To my family.**

## **ACKNOWLEDGEMENT**

I thank the past and present members of the Mitchell lab: Saranna Fanning and Carol Woolford, for their guidance with my experiments, their resourcefulness and lively chats about the things beyond lab; Tatyana Aleynikova, who always kept everything ready for my experiments and has enlightened me with her worldly wisdom about handling almost any crisis; and Wenjie Xu, for his excellent intellectual feedbacks on my work and thesis. I also thank the two exceptional undergraduates: Tammy Ying and Dagny Cooke for their contributions to my work.

I thank our collaborators: Dr. Scott G. Filler and Dr. Norma Solis, for their support with the mouse model of oropharyngeal candidiasis; Dr. David R. Andes and Kaitlin F. Mitchell, for analyzing our strains in the rat venous catheter model of biofilm infection; Dr. Vincent M. Bruno, for his help with RNAseq; and Dr. Cornelius J. Clancy, Dr. Minh-Hong Nguyen and Dr. Shaoji Cheng for their help in analyzing our strains in the intraabdominal candidiasis model.

I thank the members of my committee: Dr. John L. Woolford, Jr. and Dr. Cornelius J. Clancy for their valuable guidance over the years. I also thank Dr. Dannie Durand and Dr. Luisa Hiller for their help.

I am grateful to my advisors, Dr. Aaron P. Mitchell and Dr. Frederick Lanni for giving me this privilege to work under their tutelage. Their patience, enthusiasm and unwavering support have helped me to remain focused even during the most testing times. I especially appreciate that, despite their busy schedules, they always had time for discussions, troubleshooting and answering any question that occurred to me at any time.

I thank my friends: Sahil, Madhu, Sneha, John, Ram, Phu, Shantanu, Dharik and Lina for giving me the most memorable four years of my life.

Most of all I am thankful to my family: my parents, Mr. Vinod B. Desai and Mrs. Dipika V. Desai, for believing in me and giving me what I needed to advance; my sister, Parita, for teaching me

how to live carefree; and finally my fiancée, Darshini, for her unconditional love, support, and for always being there for me.

# Contents

ABSTRACT .....	3
ACKNOWLEDGEMENT .....	6
LIST OF TABLES .....	11
LIST OF FIGURES .....	12
Introduction .....	13
Biofilm structure and development .....	13
Cell morphology and biofilm formation .....	16
Biofilm-associated gene expression .....	19
The cell surface and adherence .....	21
Extracellular matrix material .....	27
Biofilm metabolism.....	30
Biofilm drug resistance .....	32
Regulatory role of glycerol in <i>Candida albicans</i> biofilm formation .....	33
Work disclaimer .....	33
Introduction.....	33
Results.....	36
Biofilm-responsive gene expression and function .....	36
Rhr2 function in adherence and biofilm formation.....	39
Rhr2 impact on biofilm gene expression .....	44
Functional basis of the <i>rhr2</i> $\Delta/\Delta$ mutant biofilm defect.....	47
Glycerol and biofilm gene-regulation.....	50
Discussion .....	54
Methods.....	58
Media and Strain Construction .....	58
RNA sample preparation for RNAseq analysis .....	59
Yeast-cell reporter expression assay in mixed biofilms.....	60

Fluconazole sensitivity assay .....	61
RNA sequencing and differential expression analysis .....	61
NanoString data collection and analysis .....	62
Quantitative RT PCR .....	62
Adherence analysis .....	63
Confocal imaging of biofilms .....	63
Virulence assay .....	64
In vivo biofilm assay .....	64
Biofilm biomass estimation .....	65
Glycerol assay .....	65
Caspofungin sensitivity assay .....	66
Active penetration by <i>Candida albicans</i> hyphae .....	67
Introduction .....	67
Results .....	69
Theoretical modeling for hyphal invasion in an infinite elastic solid .....	69
Genetic control of invasive growth .....	76
Biofilm formation and filamentation are necessary, but are not sufficient for invasion .....	80
Discussion .....	83
Methods .....	85
Media and Strain Construction .....	85
RNA sample preparation .....	85
Quantitative RT PCR .....	85
Polyacrylamide gel preparation .....	86
Elastic modulus measurement .....	86
Confocal imaging of invasion .....	87
Glycerol assay .....	88
Adhesin-dependent regulation of biofilm maturation .....	90
Introduction .....	90

Results .....	92
Role of Als1 in biofilm maturation .....	92
Involvement of Brg1 in adhesin-dependent gene expression response .....	95
Functional relationship between Bcr1, Als1 and Brg1 .....	97
Discussion .....	99
Methods .....	101
Biofilm embedding for microscopy .....	101
Functional role of a ribose biosynthetic gene <i>SHB17</i> in biofilm development .....	102
Introduction .....	102
Results .....	104
Function of <i>SHB17</i> in biofilm development .....	104
<i>SHB17</i> functions to maintain a normal hyphal morphology in biofilms .....	106
<i>SHB17</i> 's function in hyphal morphology depends on its role in ribose biosynthesis .....	108
Discussion .....	110
Methods .....	112
Appendix .....	113
Table of the strains .....	113
Plugins for biofilm image processing .....	117
A mathematical model for cell fate decision in <i>Candida albicans</i> .....	123
Phenotypic screen to uncover genes with potential roles in biofilm development .....	132

## LIST OF TABLES

Table 1: Transcription factors encoding genes that have a role in hyphal invasion.....	78
Table 2: Transporter encoding genes, up-regulated in a <i>C. albicans</i> biofilm. ....	111
Table 3: Strains used in this disserataion. ....	113
Table 4: Estimated values of the parameters regulating the white-opaque cell switching. ....	128
Table 5: Phenotypic profile for biofilm up-regulated gene mutants. ....	132

## LIST OF FIGURES

Figure 1: Biofilm gene expression and phenotypic screen for insertion mutants in biofilm up-regulated genes.....	38
Figure 2: <i>RHR2</i> is required for biofilm formation in vitro through its role in glycerol biosynthesis.	41
Figure 3: Glycerol is required for biofilm gene expression response. ....	45
Figure 4: The function of <i>RHR2</i> in adhesin gene expression is required for silicone adherence and biofilm formation in vitro. ....	48
<b>Figure 5: The function of <i>RHR2</i> in adhesin gene expression is required for biofilm formation in vivo.</b> .....	<b>49</b>
Figure 6: A hunt for the possible regulator(s) that mediate the biofilm gene expression response of glycerol. ....	52
Figure 7: <i>Candida albicans</i> hyphae employ turgor to invade an elastic substratum.....	74
Figure 8: <i>SFL2</i> functions in invasive hyphal orientation.....	79
Figure 9: Biofilm hyphae defective in glycerol accumulation cannot invade. ....	81
Figure 10: <i>ALS1</i> is required for a mature biofilm formation in YPD medium. ....	94
Figure 11: Functional connections between <i>ALS1</i> and <i>BRG1</i> .....	96
Figure 12: Functional relationship between <i>BCR1</i> , <i>ALS1</i> and <i>BRG1</i> . ....	98
Figure 13: Function of <i>SHB17</i> in <i>C. albicans</i> in biofilm development. ....	105
Figure 14: <i>SHB17</i> functions to maintain a normal biofilm hyphal morphology.....	107
Figure 15: <i>SHB17</i> 's function to maintain normal biofilm-hyphal-morphology depends on its metabolic role in ribose biosynthesis.....	109
Figure 16: Imaging and quantification of <i>YWP1</i> reporter expression in a biofilm. ....	119
Figure 17: An image of a ramp, constructed to correct intensity attenuation arising while biofilm serial-image-stack acquisition. ....	121
Figure 18: A wiring diagram of the transcriptional circuit regulating the white-opaque cell switch in <i>C. albicans</i> .....	123
Figure 19: Time-course of the cell-switch model output in terms of normalized protein concentrations of the four transcription factors. ....	127
Figure 20: Relative sensitivity coefficients for the RNA and protein species' concentrations w.r.t the 21 parameters. ....	129
Figure 21: Overall sensitivity for the cell-switch model w.r.t the 21 parameters. ....	130

# Introduction

The human commensal *Candida albicans* is the leading fungal colonizer of implanted medical devices and a frequent cause of nosocomial infections (Finkel and Mitchell, 2011; Kojic and Darouiche, 2004). Several *Candida* species, including *C. albicans*, are part of the mucosal flora of most healthy individuals, and reside in the gastrointestinal and genitourinary tracts. These organisms are thus poised to cause infection when a suitable niche becomes available. The use of broad-spectrum antibiotics is an additional risk factor for *Candida* infections, probably because bacterial competitors that are eliminated would otherwise keep fungal populations in check. The extreme resistance of biofilm cells to antifungal therapy is a further complication, and often the infected device has to be removed and replaced to prevent recurrent infection (Finkel and Mitchell, 2011). Here, we focus mainly on biofilm formation by *C. albicans*, the most intensively studied of the *Candida* species.

## **Biofilm structure and development**

The first published image of a *Candida* biofilm on an implanted catheter came from the pioneering study of Marrie and Costerton (Marrie and Costerton, 1984). This and many subsequent reports of *Candida* biofilms on devices prompted Hawser and Douglas to develop an in vitro system to study *Candida* biofilm development on catheter material discs (Hawser and Douglas, 1994). Their scanning electron micrographs provided the first glimpse of *C. albicans* biofilm architecture, which has since been studied by confocal imaging as well. *C. albicans* can grow either as individual oval cells (called yeast cells or blastospores) or as long cylindrical, filamentous cells attached end-to-end (called pseudohyphae or hyphae, distinguished by specifics of cell structure (Berman and Sudbery, 2002)). Biofilms grown in vitro under a variety of conditions have a basal substrate-bound layer of yeast cells that ranges from 20 to 100 microns in depth under many conditions. Filamentous cells project from the basal layer, and can extend for several hundred microns. Yeast cells are often found to bud from the filamentous cells, especially in the apical regions of the biofilm. Amorphous extracellular matrix material is found throughout the biofilm,

which can appear aggregated (shown here) or dispersed (Daniels et al., 2013), depending on staining and fixation. A three-dimensional reconstruction reveals a very dense basal region beneath loosely packed filamentous cells. The loose packing of the upper region may facilitate solvent access to the basal region.

Fungi are non-motile, and biofilm structure thus reflects the sequence of cell division events that occurs during biofilm development. Chandra et al. analyzed time-courses of *C. albicans* biofilm development on two different substrates, and proposed that biofilm development occurs in stages (Chandra et al., 2001). They used a yeast cell inoculum because yeast cells are more likely than long filamentous cells to be able to disseminate to new sites. In the early stage, individual yeast cells adhered to the substrate. They then proliferated as yeast to produce microcolonies, and coalescence of microcolonies yielded the basal layer of the biofilm. Biofilm development then entered an intermediate stage of high metabolic activity along with the emergence of hyphae and production of extracellular matrix material. In the final maturation stage, there was extensive accumulation of extracellular matrix material. The images did not show the presence of apical yeast cells, and they may have been obscured by intensely stained matrix. The authors also found that greatly reduced susceptibility to fluconazole, amphotericin B, nystatin, and chlorhexidine was acquired at the time of transition to the intermediate stage, concomitant with the increase in metabolic activity and accumulation of matrix material. This finding is in keeping with more recent studies that reveal that drug binding by extracellular matrix is a major source of biofilm drug resistance (see below).

The final step in biofilm formation can be considered to be the release of cells, permitting colonization of new sites and, unfortunately, disseminated infection (Blankenship and Mitchell, 2006). Uppuluri et al. (Uppuluri et al., 2010) found that cell dispersal occurs throughout biofilm development and does not represent a temporally distinct stage. Cells released from biofilms were mainly yeast cells, not filaments. Remarkably, the released cells were phenotypically distinct from cells grown planktonically for the same amount of time in the same medium. The released cells displayed higher levels of adhesion to plastic or endothelial cells, probably due to

their increased propensity to produce hyphae. In addition, the released cells were more virulent than planktonic cells in a disseminated infection model. Thus biofilm dispersion yields a unique class of yeast cells with increased ability to create new biofilms and cause infection.

Do biofilms follow the same developmental steps described above during a true catheter infection? One cannot reason from first principles to reach a conclusion about how representative an in vitro model may be. We believe that the simplest approach to validate in vitro observations is to use an animal model of biofilm-based infection. There are animal models (Tournu and Van Dijck, 2012) for venous catheter infection (Andes et al., 2004; Chandra et al., 2011), urinary catheter infection (Wang and Fries, 2011), and denture stomatitis infection (Nett et al., 2010b). There is also a subcutaneous catheter model that cultures biofilm cells in a host environment, though it may not resemble in detail a device currently in use (Tournu and Van Dijck, 2012). Finally, there are animal models for both oral and vaginal mucosal infections, which are in essence biofilms that form on mucosal tissue (reviewed in (Ganguly and Mitchell, 2011)). Mucosal biofilms are, however, more complex than in vitro biofilms as they consist of multiple microbial species and host cells (Ganguly and Mitchell, 2011; Morales and Hogan, 2010; Peleg et al., 2010). Several commonly observed cohabitating bacterial species have been studied for their impacts on *C. albicans* biofilm formation (Morales and Hogan, 2010; Peleg et al., 2010). These studies have identified several direct and indirect bacterial-*Candida* interactions that affect biofilm structure, primarily via an impact on cell morphology (Morales and Hogan, 2010; Peleg et al., 2010). The different cell morphologies, as discussed below, play important roles in biofilm developmental cycle and invasive life-style of *C. albicans*.

## Cell morphology and biofilm formation

Under most conditions, both yeast and filamentous cells are required for *C. albicans* biofilm formation. Initial support for this conclusion came from mutants that were locked in either yeast or filamentous growth states (Baillie and Douglas, 1999), though the genetic basis for the mutant phenotypes was uncertain. Each mutant produced an altered biofilm with reduced biomass or cell density. A random insertion mutant screen further substantiated a role of hyphal morphogenesis in biofilm development (Richard et al., 2005). Mutants with insertions in the genes *NUP85*, *MDS3*, *SUV3* and *KEM1* were identified as biofilm-defective, and there was no known molecular or functional connection among them. However, they were all defective in hypha formation in several media. In addition, in mixed biofilms formed with wild-type cells, each mutant produced only yeast cells. Therefore, the mutations caused defects in filamentation in the context of a biofilm, arguably the most relevant situation to assay. Ramage et al. found that two well established hyphal-defective mutant strains, *efg1Δ/Δ* and *efg1Δ/Δ cph1Δ/Δ*, were defective in forming biofilms (Ramage et al., 2002c). These mutants yielded only sparse substrate-attached cells, not a true basal layer. Remarkably, though, the substrate-attached mutants displayed no susceptibility to fluconazole and only moderate susceptibility to amphotericin B. These findings indicated that surface-bound growth is sufficient to induce the antifungal resistance of biofilm cells, and were consistent with the finding from Chandra et al. (Chandra et al., 2001) that resistance increases substantially before a biofilm fully matures.

Why are filamentous growth forms so important for biofilm formation? Insight into the answer came from the transcription factor Bcr1 (Nobile and Mitchell, 2005), identified in the first systematic screen of *C. albicans* transcription factor mutants. The *bcr1Δ/Δ* mutant was defective in biofilm formation, and also failed to form hyphae under some conditions. Importantly, though, in mixed biofilms formed with wild-type cells, mutant cells yielded abundant hyphae. Also, the non-adherent cells produced by the mutant under biofilm-inducing conditions included hyphae. These results suggested that the mutant produces hyphae that are defective in a function required for biofilm formation. Transcript profiling and functional analysis pointed to the same conclusion: Bcr1 is required for expression of genes for cell surface adherence proteins (called

adhesins), such as *ALS1*, *ALS3*, and *HWP1*. Many of these genes, including *ALS3* and *HWP1*, are induced strongly during hyphal growth. Importantly, overexpression of adhesin genes *ALS1*, *ALS3*, or *HWP1* in a *bcr1ΔΔ* mutant background restored biofilm formation ability, both in vitro and in a catheter infection model (Nobile et al., 2006a). This study was the first to provide evidence that hyphae are required for biofilm formation because of their cell surface adhesins.

For invasion as well, hyphae play a prominent role. Microscopic analyses of infected tissues and device-surfaces showed a predominant presence of invading hyphae (Brand, 2012). The hyphae invade via an active or a passive mechanism (Zhu and Filler, 2010). In the well-characterized passive mechanism, *Candida* hyphae induce their endocytosis by the epithelial cells. The surface proteins, Als3 and Ssa1, act as invasins to induce endocytosis (Phan et al., 2007; Sun et al., 2010). This mechanism is passive because the epithelial cells can endocytose the dead hyphae and the invasin-coated beads (Phan et al., 2007). The invasins induce endocytosis via interacting with E-cadherin or EGFR/HER2 or both, that activates the clathrin-dependent endocytic pathway (Phan et al., 2007; Zhu et al., 2012). At an early stage after the initial fungal attachment, this mechanism is true for several cell types, as demonstrated using a panel of cell lines (Zhu and Filler, 2010). Gastrointestinal epithelial cells, on the other hand, do not support endocytosis (Dalle et al., 2010; Wachtler et al., 2012). The hyphae invade via an active mechanism in this case. Two different mechanisms have been suggested for active invasion: the first involves protease-mediated invasion, while the second involves a turgor-mediated, forceful penetration by *Candida* hyphae. For the protease-mediated invasion, genes from the **S**ecreted **A**spartyl **P**roteinase (SAP) family have been analyzed for their roles in epithelial invasion and damage. Dalle et al. observed a moderate defect in epithelial cell invasion by the *sap1-3* or *sap4-6* deletion mutants (Dalle et al., 2010). Interestingly, they observed that hyphal invasion decreased significantly only if the fungal cells were pretreated with a protease inhibitor. Additionally, they observed a role for Saps in induced endocytosis as well. The authors suggested that the Saps rather have a role in altering fungal surface in order to activate induced endocytosis.

In the turgor-mediated, forceful penetration mechanism, hyphae are proposed to accumulate enough solute to draw water inside, which will generate enough pressure to invade the underlying surface. Plant pathogenic fungi utilize this mechanism, where they accumulate high levels of glycerol in order to generate turgor required for penetrating a leaf cuticle (Bastmeyer et al., 2002; Wilson and Talbot, 2009). *C. albicans* also accumulates glycerol in response to raised extracellular osmolarity (Fan et al., 2005). The glycerol accumulation occurs via activation of the HOG (**H**igh **o**smolarity **g**lycerol) MAP kinase cascade (Hohmann, 2002). However, it is unknown if the biofilms or invading hyphae accumulate glycerol to attain turgor for invasion as in the plant pathogenic fungi. There is a strong reason to believe that this may be true for *C. albicans* as well since the hyphae were often observed to penetrate abiotic, protease-resistant surfaces of medical devices (Brand, 2012; Leonhard et al., 2010). However, this mechanism for invasion demands experimental substantiation.

## **Biofilm-associated gene expression**

If biofilm cells have unique phenotypic properties, one might expect that biofilm cells express a set of genes that are different from planktonic cells. Several studies have characterized the biofilm transcriptome (Desai et al., 2013; Garcia-Sanchez et al., 2004; Murillo et al., 2005; Nett et al., 2009; Yeater et al., 2007). Although many different growth conditions and comparison conditions were utilized, there is good overall agreement, especially among many of the most highly induced genes in biofilm formation (Desai et al., 2013). Most importantly, these transcriptome studies have provided leads for functional analysis. For example, in the first such study, Garcia-Sanchez et al. found that amino acid biosynthetic genes were consistently up regulated in biofilms grown under diverse conditions (Garcia-Sanchez et al., 2004). That observation led them to assay biofilm formation by a *gcn4Δ/Δ* mutant, which is defective in the general control of amino acid biosynthetic genes. The *gcn4Δ/Δ* mutant produced a biofilm, but its overall biomass and metabolic activity was substantially reduced compared to the wild type. These assays were conducted in a rich medium in which planktonic growth of the wild type and mutant strains were equivalent. Hence the mutant may be defective in retention of cells within the biofilm. Such a mutant phenotype would be difficult to detect in a large in vitro screen; the profiling data clearly pointed in a unique direction for functional analysis. In addition, these findings fit well with the observation made repeatedly that ribosome biogenesis genes are up regulated in biofilm cells compared to planktonic cells. A simple hypothesis is that both amino acid synthesis genes and ribosomal biogenesis genes allow increased protein synthesis in biofilm cells, or perhaps a subset of biofilm cells, that contributes to biofilm stability and cohesion. Given the *gcn4Δ/Δ* mutant phenotype, those protein products may be adhesins or extracellular matrix components that mediate cell-cell adherence.

Broader surveys of mutants defective in biofilm-induced genes have not always yielded many genes that clearly function in biofilm formation, based on mutant phenotype (Bonhomme et al., 2011). One reason for the limited correlation may be functional redundancy of biofilm-associated genes, for which examples are well known (Nobile et al., 2006a; Nobile et al., 2009; Taff et al., 2012).

Because a biofilm is a complex and heterogeneous environment, one might expect that some biofilm-induced genes may be part of response pathways that have little impact on biofilm phenotypes per se. Thus many investigations have sought to prioritize biofilm-induced genes for functional analysis. Perhaps the most elegant prioritization approach was undertaken by Nobile et al. (Nobile et al., 2012), who extended the transcription factor mutant screen (Nobile and Mitchell, 2005) to identify six biofilm regulators. They combined genome-wide expression profiling of the transcription factor mutants with chromatin immunoprecipitation assays to define the transcription factors' direct targets. There were over ~1000 target genes in the overall biofilm network, but only 23 genes were bound by all six regulators. These shared targets may be highly enriched for biofilm-related functions. A second prioritization approach is to focus on genes that are biofilm-induced under diverse conditions, as the d'Enfert group did with a panel of growth conditions (Bonhomme et al., 2011; Garcia-Sanchez et al., 2004) to define common biofilm-induced genes. They later constructed homozygous deletion mutants for a panel of these biofilm-induced genes and screened for biofilm defects, as assayed by reduced biofilm biomass (Bonhomme et al., 2011). Among the 38 genes examined, they identified six to be required for full biofilm biomass accumulation. Such mutants hold promise to identify new biofilm-specific functions. Indeed, the study went on to demonstrate that the Tye7 transcription factor promotes biofilm formation by mediating up-regulation of glycolytic genes in the hypoxic environment created during biofilm maturation.

## **The cell surface and adherence**

The cell wall is the cellular structure that interacts most directly with the substratum or another cell. The *C. albicans* cell wall is primarily made of carbohydrates and glycoproteins (Gow and Hube, 2012). Carbohydrates such as  $\beta$ -glucan and chitin form an inner core of cell wall, responsible for its mechanical strength, and mannoproteins that include adhesins form an outer fibrillar layer (Gow and Hube, 2012). Adhesins are defined by their ability to mediate adherence directly or their structural similarity to proteins that do so (Dranginis et al., 2007). Other cell wall or cell surface proteins may affect adhesin levels, processing, or exposure at cell surface, and thus affect adherence indirectly.

Many adhesins of *C. albicans* have a C-terminal sequence that is used for covalent attachment of a glycosylphosphatidylinositol (GPI) anchor (Chaffin, 2008). This GPI anchor initially tethers the protein on the outer face of the plasma membrane. The GPI anchor is then cleaved; the protein and anchor remnant are transferred to  $\beta$ -1,6-glucan and remain attached to the cell wall (Chaffin, 2008). Adhesins of this class include members of the Als (**A**gglutinin **L**ike **S**equence) family (Hoyer et al., 2008), Eap1 (**E**nhanced **A**dherence to **P**olystyrene 1) (Li and Palecek, 2003), Hwp1 (**H**ypal **W**all **P**rotein 1) (Nobile et al., 2006b; Staab et al., 1999), and Rbt1 (**R**epressed **B**y **T**UP1) (Monniot et al., 2013), all of which are expressed at much higher levels in hyphal cells than in yeast cells. There is an adhesin-like protein expressed at highest levels in yeast cells, Ywp1 (**Y**east **W**all **P**rotein 1), but it seems to function as an anti-adhesin (Granger et al., 2005). There are also proteins that may function as adhesins but lack a GPI anchor, including Mp65 (**M**annoprotein of **65**kDa) (Sandini et al., 2011), Csh1 (**C**ell **S**urface **H**ydrophobicity) (Singleton et al., 2001) and Pra1 (**p**H regulated **a**ntigen) (Chaffin, 2008).

Early approaches to identify adhesins involved analysis of cell wall components that adhered to a surface after the adherent cells were washed away (Chaffin et al., 1998; Tronchin et al., 1989). However, the first studies to define *C. albicans* adhesins functionally relied upon heterologous expression in *Saccharomyces cerevisiae* (Fu et al., 1998; Gaur et al., 1999). Als1 was identified in a screen of a *C. albicans* expression library in *S. cerevisiae* for clones that improved *S.*

*cerevisiae* adherence to epithelial and endothelial cells (Fu et al., 1998). Als5 was identified through a similar approach: its expression in *S. cerevisiae* improved adherence to beads coated with fibronectin, laminin, and collagen (Gaur et al., 1999). Adhesins from this ALS gene family have since been studied in detail (Dranginis et al., 2007; Hoyer et al., 2008). They are organized into four major regions: (1) an N-terminal immunoglobulin-like domain, (2) a threonine-rich region, (3) a series of 36 amino acid tandem repeats, and (4) a highly glycosylated stalk region (Dranginis et al., 2007; Lipke et al., 2012) (All Als proteins have N-terminal signal sequences as well, allowing their entry into the secretion pathway). Initial adherence has been proposed to be mediated by the N-terminal module, which is capable of ligand binding (Hoyer and Hecht, 2001; Klotz et al., 2004; Salgado et al., 2011). These ligands include a broad range of denatured peptides, reflecting the broad specificity of Als proteins (Klotz et al., 2004). The threonine-rich region and the tandem repeat region are required for cell-cell adherence, as demonstrated through heterologous expression of domain deletion mutants in *S. cerevisiae* (Rauceo et al., 2006). The eight different Als proteins seem to have redundant functions in biofilm formation for the most part, because high-level expression of any ALS gene in a biofilm-defective *als1Δ/Δ als3Δ/Δ* mutant restores biofilm formation in vitro and in vivo in the rat venous catheter model (Nobile et al., 2008a). Thus our current understanding is that the Als proteins function as a set of interchangeable adhesins to promote biofilm formation.

Recent studies have addressed a long-standing mystery about the Als proteins and other adhesins: how can proteins with such weak affinities for their ligands mediate stable binding? The answer lies in the ability of the threonine-rich region to form multi-protein aggregates, or amyloids (Lipke et al., 2012). When amyloid formation is initiated (by tugging an Als in an atomic force microscope, for example), it spreads across the cell surface to create a nanodomain. The Als aggregate becomes in essence a multivalent adhesin. Thus even weakly bound ligands are rebound rapidly after they are released (Lipke et al., 2012). Such amyloid-forming regions are found in many other cell surface adhesins, so amyloid formation may be a common mechanism to stabilize ligand-binding interactions.

Several other GPI-linked cell wall proteins function as biofilm adhesins, including Eap1, Hwp1, and Rbt1. Eap1 was identified as a *C. albicans* library clone that enabled adherence to plastic by otherwise nonadherent *S. cerevisiae* strain (Li and Palecek, 2003). Like the Als adhesins, Eap1 has an N-terminal ligand-binding domain followed by serine- and threonine-rich repeats that permit the N-terminal domain to project beyond the cell wall glucan (Li and Palecek, 2008). Eap1 is required for biofilm formation, because an *eap1Δ/Δ* mutant is defective in biofilm formation in vitro and in vivo in the rat venous catheter model (Li et al., 2007).

Hwp1 is structurally distinct from the Als proteins and Eap1. It is in essence a set of short peptide repeats followed by a GPI anchor addition site. Its role in host cell binding is remarkable: it is a substrate for host transglutaminases, which link it covalently to epithelial cell surfaces (Staab et al., 1999). Although it may also serve as a transglutaminase substrate during biofilm formation in vivo, it must function differently in biofilms formed in vitro because *C. albicans* does not make its own transglutaminases (Staab et al., 1999). An *hwp1Δ/Δ* mutant has a moderate-to-severe biofilm defect in vitro and in vivo (Nobile et al., 2006b). Two observations argue that Hwp1 has a distinct and complementary role to that of the Als adhesins in biofilm formation (Nobile et al., 2008a). First, overexpression of *HWP1* does not allow biofilm formation by the *als1Δ/Δ als3Δ/Δ* mutant, in contrast to overexpression of any *ALS* gene. Second, a mixture of biofilm-defective *als1Δ/Δ als3Δ/Δ* cells and biofilm-defective *hwp1Δ/Δ* cells is able to form a biofilm. The mechanism seems likely to be that Hwp1 and Als1/Als3 can interact on cell surfaces to mediate cell-cell binding. This inference comes from the fact that heterologous expression of *HWP1* in *S. cerevisiae* improves its adherence wild-type *C. albicans* cells, and not to *als1Δ/Δ als3Δ/Δ* mutant cells (Nobile et al., 2008a). Hwp1 and Als1/Als3 may thus function analogously to mating agglutinins of *S. cerevisiae* that permit binding of *MATa* and *MATα* cells (Dranginis et al., 2007).

Rbt1 is in the same adhesin family as Hwp1 (Ene and Bennett, 2009; Monniot et al., 2013). An *rbt1Δ/Δ* mutant has a mild biofilm defect in vitro, but shows additive effects with mutations in family members *HWP1* and *HWP2* (Ene and Bennett, 2009). Its N-terminal region promotes surface hydrophobicity and mediates adherence to polystyrene (Monniot et al., 2013). A central

domain is predicted to have high aggregation potential, and amyloid-inhibitor experiments similar to those carried out with Als5 support such a function (Monniot et al., 2013). Although Rbt1 is normally expressed only on hyphal cells, Monniot et al. could create a constitutive *RBT1* allele through fusion to the *TEF1* promoter. Interestingly, this constitutively expressed protein could be recognized by anti-epitope antibodies only on hyphal cell surfaces. Recognition on yeast cell surfaces required mild digestion of the cell wall with zymolyase (Monniot et al., 2013). These observations suggest that there is a fundamental structural difference between yeast and hyphal cell walls that affects the exposure of Rbt1 and, potentially, many other adhesins.

One interesting GPI-anchor containing protein, Ywp1, functions to reduce adherence (Granger, 2012; Granger et al., 2005). *YWP1* is expressed at much higher levels in yeast cells than in hyphae, so it is possible that Ywp1 is critical for dispersion of yeast cells from a biofilm. It is yet not known how Ywp1 exerts its anti-adhesive effects; it may interact with specific adhesins, or it may alter the cell surface to deny access to adhesins. In that context, it would be interesting to see if Ywp1 is required for the inhibition of Rbt1 epitope access on yeast cells observed by Monniot et al. (Monniot et al., 2013).

How is adherence regulated? As mentioned above, many of the major known adhesins are expressed at highest levels on hyphal cells. Their expression is regulated by transcription factors that also govern hyphal development (Biswas et al., 2007; Nobile et al., 2012). In addition, the adherence of yeast cells, which is thought to be the initial step in biofilm formation, appears to be under complex control. Finkel et al. screened for transcription factor mutants with altered adherence to silicone (Finkel et al., 2012), and uncovered 30 transcription factors that are required for adherence in vitro. Expression of all known and predicted cell wall protein genes was assayed in the mutants, which allowed provisional assignment of both regulators and cell wall protein genes to pathways. The value of this approach was supported by positive overexpression-rescue tests of several new pathway relationships. For example, the findings indicated that Snf5 and Ace2 lie in a pathway that governs adherence, biofilm formation, and cell wall integrity (Finkel et al., 2012). In addition, the findings argued that the protein kinase Cbk1

and transcription factor Bcr1 act in the same pathway, and contemporaneous studies revealed that Cbk1 phosphorylates Bcr1 (Gutierrez-Escribano et al., 2012). A simple interpretation is that a large number of transcriptional regulatory pathways govern adherence, but they ultimately impact a small number of response mechanisms. Interestingly, several of the transcription factors were not required for biofilm formation in an in vitro system, but were required in the rat catheter in vivo model (Finkel et al., 2012). This finding emphasizes the limitations of in vitro biofilm models, and the potential that our reliance on in vitro models may cause us to overlook critical functions that act in vivo during infection.

Several upstream regulators that govern adhesin expression have also been identified, thus paving the way to define the actual molecular or physiological signals that govern biofilm formation. As mentioned above, the protein kinase Cbk1 phosphorylates and activates Bcr1, perhaps ensuring that hyphal adhesins are only expressed when Cbk1-dependent cell polarity functions are active (Gutierrez-Escribano et al., 2012). In addition, the Tor1 kinase, a central regulator of ribosome biogenesis and starvation responses, is a negative regulator of adhesin genes *ALS1*, *ALS3*, and *HWP1*. (Bastidas et al., 2009). This relationship may reflect a role for starvation in promoting adherence and biofilm formation. Recent studies have revealed that the stress-responsive MAP Kinase Hog1 mediates this effect of Tor1, and that transcription factor Brg1 may be the direct target of this pathway (Su et al., 2013). Because Hog1 is activated by high osmolarity as well as oxidative stress (Shapiro et al., 2011), these signals may also influence the ability to adhere and form a biofilm. Finally, we note that the cyclic AMP-dependent protein kinase catalytic subunit Tpk1 functions as a negative regulator of adherence and *ALS1* expression (Fanning et al., 2012a), perhaps through effects on the cyclic AMP pathway target transcription factor Efg1 (Shapiro et al., 2011). This pathway governs hyphal morphogenesis, so it seems possible that the response can modulate the adhesin levels on hyphae in a biofilm. Clearly these novel pathway relationships will whet our appetites for dissection of signals and responses in biofilm formation for some time to come.

Many genes that have broad effects on cell wall biogenesis or integrity also affect adherence or biofilm formation. For example, *GAL102* and the *PMT* (**P**rotein **M**annosyl **T**ransferase) gene family govern protein mannosylation (Peltroche-Llacsahuanga et al., 2006; Sen et al., 2011). The impact of respective mutations on biofilm formation may result from altered adhesin glycosylation. Other cell wall proteins that govern adherence but may not be adhesins are Sun41 and Pga1, both of which have roles in cell wall integrity (Finkel et al., 2011; Hashash et al., 2011; Hiller et al., 2007; Norice et al., 2007). However, the fact that a cell wall protein affects cell wall integrity does not rule out the possibility that it is an adhesin. The Als adhesins in particular are famous as multifunctional proteins. Als3 is the best example, with roles in adherence to numerous substrates, host receptor binding, host cell invasion, and iron acquisition (Liu and Filler, 2011). Als2 is a possible bridge between cell wall integrity and adhesin function: it seems to be essential for viability, and changes in *ALS2* gene dosage have profound effects on cell wall thickness and sensitivity to cell wall perturbing agents (Fanning et al., 2012a; Zhao et al., 2005). Thus a known adhesin seems to have a role in overall cell wall architecture and integrity.

Might the cell wall have a sensory function? The transcription of many genes (including adhesin genes) is induced rapidly after the initial adherence step (Yeater et al., 2007). Perhaps surface binding generates a signal that switches the cell growth program from planktonic to biofilm. In fact, several groups have studied contact sensing phenomena and their regulation (Brand et al., 2009; Kumamoto, 2005, 2008; Zucchi et al., 2010). The transmembrane protein Dfi1, through calmodulin binding, regulates the activity of a MAP kinase Cek1. The MAP kinase Mkc1 is also activated after cells interact with semisolid surfaces (Kumamoto, 2005; Puri et al., 2012; Zucchi et al., 2010). Both Cek1 and Mkc1 have roles in biofilm formation (Kumamoto, 2005, 2008; Zucchi et al., 2010). Thus, while the evidence now is fragmentary, a fascinating possibility is that physical changes in the cell wall occur upon substratum binding that activate Cek1 and Mkc1 to promote biofilm formation.

## **Extracellular matrix material**

A mature biofilm shows complex architecture with heterogeneous cell types enmeshed in extracellular matrix. Biofilm matrix was first characterized by the Douglas group (Al-Fattani and Douglas, 2006). They found presence of carbohydrate, protein, hexosamine, phosphorus and uronic acid. Additionally, they observed that treatment with enzymes such as  $\beta$ -1, 3-glucanase, proteinase K, DNase I, chitinase and  $\beta$ -N-acetylglucosaminidase compromised biofilm cohesion (Al-Fattani and Douglas, 2006). A good portion of the glucose initially detected by the Douglas group is found in soluble  $\beta$ -glucan (Nett et al., 2007), which Nett and colleagues have shown to be a key matrix determinant of antifungal drug resistance (see below). Thus the *C. albicans* biofilm matrix functions in both biofilm integrity and drug resistance.

Matrix production can vary considerably with growth conditions. For example, there is less matrix production when biofilms are grown statically than with shaking (Hawser et al., 1998). Also, matrix production is greater in RPMI medium than in Spider medium (Daniels et al., 2013), both of which are commonly used by many investigators. A further complication is that matrix composition has not been dissected under these varied growth conditions. Given the broad functional roles of matrix components, it may be useful to develop some standardized procedures for analysis of biofilm properties.

The most well understood role of a matrix component is the function of  $\beta$ -1, 3 glucan in biofilm azole resistance. Nett et al. manipulated the essential *FKS1* gene, which is responsible for cell wall  $\beta$ -1, 3 glucan synthesis (Nett et al., 2010a). They showed that decreased or increased *FKS1* expression or activity results in a corresponding change in amount of biofilm matrix (soluble)  $\beta$ -1, 3 glucan. Hence matrix  $\beta$ -1, 3 glucan follows the same biosynthetic pathway as cell wall  $\beta$ -1, 3 glucan. Remarkably, the strains with reduced *FKS1* activity produced biofilms in vitro and in vivo that were exquisitely sensitive to fluconazole, while during planktonic growth there was no change in fluconazole sensitivity (Nett et al., 2010a). These observations showed that  $\beta$ -1, 3-glucan synthesis is required for a biofilm-specific drug resistance mechanism. In fact, addition of isolated biofilm matrix to planktonic cells conferred fluconazole resistance. Direct binding assays were

used to show that drug sequestration is the mechanism by which  $\beta$ -1, 3 glucan confers biofilm fluconazole resistance (Nett et al., 2010a). In order to understand the biogenesis of matrix  $\beta$ -1, 3 glucan, Taff et al. created null mutant strains in candidate glucan modification genes that were up-regulated in vivo during biofilm development (Taff et al., 2012). They found three genes, two that encode glucan transferases Bgl2 and Phr1, and one that encodes exoglucanase Xog1, to affect matrix  $\beta$ -1, 3-glucan production and fluconazole susceptibility. Because the glucan modification pathway is extracellular, it seems like an excellent target for anti-biofilm therapeutics.

Proteins and DNA also constitute an integral part of the matrix material. The protein component has been characterized through a proteomic approach by Lopez-Ribot and colleagues (Thomas et al., 2006). Many of the most abundant proteins found in matrix were similar to the proteins found in supernatants of planktonic cultures. In addition, a large proportion of the matrix proteins are annotated as cytoplasmic. DNA is also a functional matrix component, as indicated by the finding that DNase I treatment compromises biofilm integrity (Al-Fattani and Douglas, 2006). Moreover, addition of DNA improves biofilm formation as indicated by increased biomass (Martins et al., 2010). It seems possible that cell lysis may be a major source of the cytoplasmic proteins and DNA in the biofilm matrix.

There have several been approaches to identify the regulators of biofilm matrix production. An unusual biofilm morphology led Nobile et al. to identify the zinc acquisition regulator Zap1 as a negative regulator of matrix  $\beta$ -1, 3- glucan (Nobile et al., 2009). Transcriptomic and ChIP assays followed by functional analysis revealed the key Zap1 targets to include two glucoamylases (Gca1 and Gca2) and three alcohol dehydrogenases (Csh1, lfd6 and Adh5) (Nobile et al., 2009). Although Gca1 and Gca2 may act directly on matrix polysaccharides, it seems likely that Csh1, lfd6 and Adh5 act indirectly, perhaps through effects on quorum sensing molecule production (Ganguly et al., 2011). Recently, the Soll lab identified a role for Bcr1 in regulating the impenetrability of MTL-heterozygous biofilms to dyes and polymorphonuclear leukocytes, which are likely to be matrix-associated traits. Through a series of Bcr1 target gene overexpression assays, they found that the extracellular CFEM (Common in several Fungal Extracellular

**M**embrane proteins) proteins promote this matrix function (Srikantha et al., 2013). The CFEM proteins were shown previously to be required for biofilm formation, but their role in matrix properties was not anticipated (Perez et al., 2006). It remains to be determined whether the CFEM proteins (Weissman and Kornitzer, 2004) are themselves matrix components, or if they act more indirectly through effects on signaling or nutrient acquisition.

The studies of Zap1 and Bcr1 seem to have defined pathways that do not affect *FKS1* regulation (see (Taff et al., 2012) in particular). However, a candidate gene approach based on *S. cerevisiae* orthologous function identified Smi1 as a regulator that acts upstream of *FKS1* (Nett et al., 2011). Specifically, a *smi1Δ/Δ* mutant had decreased biofilm fluconazole resistance, β-glucan production, and *FKS1* RNA accumulation. Moreover, increased expression of *FKS1* caused increased fluconazole resistance in the *smi1Δ/Δ* mutant. Current evidence indicates that Smi1 acts through the transcription factor Rlm1 to govern *FKS1* expression (Nett et al., 2011). In addition, the chaperone Hsp90 is required for matrix β-glucan production (Robbins et al., 2011). This role for Hsp90 is independent of its regulatory interactions with the known client proteins calcineurin and Mkc1. Hsp90 may affect *FKS1* expression or activity, perhaps through the Smi1-Rlm1 pathway.

## **Biofilm metabolism**

A central theme that has emerged from transcriptome studies is that the mature *C. albicans* biofilm presents a hypoxic environment. The first general indication of biofilm hypoxia came from the observation that glycolytic genes are up regulated in biofilms (Bonhomme et al., 2011; Garcia-Sanchez et al., 2004). This response might be expected if energy from hexoses in biofilms derives from fermentative reactions, which are much less efficient than respiration. Indeed, the Butler group set out to do a comparison of gene expression during biofilm growth and during hypoxia with the species *Candida parapsilosis* (Rossignol et al., 2009). A set of 60 genes was common to the two responses, representing mainly genes involved in glycolysis or in synthesis of fatty acids and ergosterol. In addition, a recent metabolomic comparison of biofilm and planktonic cells revealed that biofilms contain lower levels of succinate, fumarate, citrate and malate (Zhu et al., 2013). This outcome probably reflects diminished flux through the tricarboxylic cycle, as expected if respiration rates are lower in biofilm cells than in planktonic cells. The overall hypoxic metabolism of biofilm cells is functionally significant, based on properties of the transcription factor Tye7. This transcription factor is an activator of glycolytic genes, and its function is critical for growth when respiration is blocked (Askew et al., 2009). Bonhomme et al. found that a *tye7Δ/Δ* mutant had greatly reduced ability to form a biofilm, in keeping with the hypothesis that the biofilm environment is hypoxic (Bonhomme et al., 2011). In addition, the mutant biofilm contained an excess of filamentous cells, and observations with metabolic inhibitors argued that hyperfilamentation was a result of decreased glycolytic flux and ATP synthesis (Bonhomme et al., 2011). This study leads to two interesting conclusions. First, hypoxic or fermentative carbon metabolism is critical for biofilm formation. Second, it is generally appreciated that biofilm growth leads to abundant hyphal formation in media that induce planktonic hyphae poorly (see (Chandra et al., 2001; Richard et al., 2005) for example); it seems possible that hypoxia may be the signal that induces hyphal formation during biofilm growth.

The transcription factor Efg1, a central regulator of biofilm formation and hyphal formation (Finkel and Mitchell, 2011; Shapiro et al., 2011), may have a pivotal role in coordinating hyphal formation and hypoxic metabolism. Stichernoth and Ernst explored this connection through examination of

Efg1-responsive genes under hypoxic conditions (Stichternoth and Ernst, 2009). Interestingly, many of the same genes that were activated rapidly by Efg1 corresponded to metabolic genes activated during biofilm formation. In fact, the *TYE7* gene is a direct target of Efg1 (Nobile et al., 2012). Therefore, the metabolic genes that respond to Efg1 during hypoxia may do so through their activation by Tye7.

If fermentation is necessary for biofilm physiology, one might expect biofilms to accumulate increased levels of fermentation products such as ethanol compared to planktonic cells. However, ethanol is not more abundant in biofilms (Mukherjee et al., 2006; Zhu et al., 2013), and in fact inhibition of ethanol production leads to increased biofilm formation (Mukherjee et al., 2006). These observations can be reconciled with the metabolic inferences discussed above if *C. albicans* uses alternate electron acceptors, thus yielding reduced products other than ethanol. For example, hypoxic growth induces the genes involved in sulfur assimilation and methionine and cysteine biosynthesis (Stichternoth and Ernst, 2009). These genes were also found to be up-regulated in biofilms (Garcia-Sanchez et al., 2004; Murillo et al., 2005; Nett et al., 2009; Stichternoth and Ernst, 2009; Yeater et al., 2007). It is possible that, when oxygen is scarce such as in biofilms, the sulfur assimilation pathway, with its multiple reduction involving steps, provides additional means to balance the reducing equivalents arising from glycolysis.

Many metabolic products have impact on *C. albicans* cell properties that affect the structure or integrity of the biofilm. The most intensively studied example is the quorum sensing molecule farnesol, which functions as an inhibitor of hyphal morphogenesis and of biofilm formation (Hornby et al., 2001; Ramage et al., 2002b) through its action on the Ras1-cyclic AMP pathway (Lindsay et al., 2012). Additionally, farnesol has recently been shown to block Nrg1 degradation (Lu et al., 2014), and Nrg1 can promote cell dispersion from biofilms (Lu et al., 2014). Although the biofilm environment may modify responses to quorum sensing molecules (Ganguly et al., 2011), the simplest generally accepted model at this time is that farnesol and other quorum sensing molecules promote release of yeast cells from mature biofilms.

## **Biofilm drug resistance**

*C. albicans* biofilm cells are much more resistant than planktonic cells to a spectrum of antifungal drugs. As described above, drug sequestration by matrix  $\beta$ -1, 3- glucan is one major resistance mechanism (Nett et al., 2010a). However, the, extracellular DNA of biofilm matrix contributes to resistance to amphotericin B, as DNase treatment increases antifungal susceptibility of biofilm cells (Martins et al., 2012). Several additional processes further contribute to drug resistance. For example, the drug efflux pump genes *CDR1*, *CDR2* and *MDR1* are up regulated in biofilms, and contribute to fluconazole resistance of early, though not mature, biofilms (Mukherjee et al., 2003; Ramage et al., 2002a). A decrease in ergosterol levels is observed in intermediate and mature biofilms, so there is potentially less target available for amphotericin B (Mukherjee et al., 2003). Additionally, persister cells have been observed for *C. albicans* biofilms as they have for bacterial biofilms (LaFleur et al., 2006). LaFleur et al. identified these phenotypic variants from biofilms as survivors after amphotericin B treatment (LaFleur et al., 2006). There has been exciting progress recently in defining the genetic determinants of persister cell formation: The Thevissen group has shown that reactive oxygen species generated by miconazole treatment induce expression of the superoxide dismutase (*SOD*) gene family. They linked this response to generation of persisters by showing that chemical superoxide dismutase inhibition, or a genetic deletion affecting the major cell surface family members Sod4 and Sod5, causes a severe reduction in the level of persisters (Bink et al., 2011). The authors note that this mechanism may be specific to miconazole. The challenge in analysis of persisters reflects in part a broader knowledge gap: we do not understand at this time the extent of heterogeneity among fungal biofilm cells (Stewart and Franklin, 2008), nor have we developed the tools to dissect subpopulations. In any case, it is clear that biofilm drug resistance is a multifactorial phenomenon. The most effective therapeutic strategies will probably be those that prevent biofilms from forming, rather than those that attempt to eliminate them once they have formed.

# Regulatory role of glycerol in *Candida albicans* biofilm formation

## Work disclaimer

Shantanu Ganguly initiated the work of biofilm transcriptome profiling. He, along with Ronald Stamper and Elizabeth Hill made the mutant strains and carried out the phenotypic assays. I analyzed the data, as tabulated in Table 5. A figure was constructed using the same data as shown in Figure 1(B). I carried out the rest of the work described in this chapter.

## Introduction

*C. albicans* biofilms are commonly found on surfaces of implanted devices such as venous catheters, voice prostheses, dentures, and urinary catheters (Donlan, 2001, 2002). In addition, *C. albicans* can infect mucosal surfaces, producing a growth state that has similarity to abiotic surface biofilms in both architecture and genetic control (Ganguly and Mitchell, 2011).

Biofilm formation is thought to begin with the adherence of individual cells to a surface. Growth into a biofilm then requires cell-cell adherence, so that the surface is populated. Mature biofilms display biofilm-specific phenotypes that distinguish them from cells grown in liquid suspension culture, called planktonic cells. These biofilm phenotypes include accumulation of extracellular matrix material and acquisition of drug resistance (Kumamoto and Vines, 2005; Nett et al., 2011). In the case of *C. albicans*, resistance is notable in particular to azole antifungals, which are frontline therapeutics (Ramage et al., 2002a). Cell heterogeneity, a signature feature that contributes to biofilm properties, is quite apparent for *C. albicans* biofilms because two major cell types, yeast (blastospores) and hyphae, are present. The balance of yeast and hyphal cells in a biofilm is influenced by diffusible signals in the form of quorum sensing molecules (Ganguly et al., 2011). Yeast cells can be released from a biofilm, and thus can cause disseminated infection. Hyphae express numerous adhesins and are probably responsible for biofilm integrity, since

every known hypha-defective mutant is also defective in biofilm production (Finkel and Mitchell, 2011).

One approach to understanding key functions in biofilm formation is to identify mutants unable to form biofilms, or those that form biofilms with altered properties. For *C. albicans*, this kind of approach has been implemented with random insertion mutants as well as mutants representing prioritized classes of gene products (Finkel et al., 2012; Nobile and Mitchell, 2005). The approach has also been combined with expression profiling to examine mutants in genes that are preferentially expressed in biofilm cells, compared to planktonic cells (Garcia-Sanchez et al., 2004; Murillo et al., 2005; Nobile et al., 2012; Yeater et al., 2007). In the foundational *C. albicans* study of this kind, Garcia-Sanchez et al. (Bonhomme et al., 2011) relied upon diverse comparisons between biofilm and planktonic growth conditions to arrive at a core set of biofilm-induced genes. Later, homozygous deletion mutants were constructed for a panel of these genes and screened for biofilm defects, as assayed by reduced biofilm biomass (Bonhomme et al., 2011). Among the 38 genes examined, six were required for full biofilm biomass accumulation yet had no defect in formation of hyphae. Such mutants hold promise to identify new biofilm-specific functions. Indeed, the study went on to demonstrate that the Tye7 transcription factor promotes biofilm formation by mediating up-regulation of glycolytic genes in the hypoxic environment created during biofilm maturation.

In this chapter, I describe our work where we have taken the work of Bonhomme et al. (Bonhomme et al., 2011) as inspiration, but have modified several features in order to extend the approach. First, we have used RNAseq profiling in order to acquire a comprehensive view of biofilm-associated gene expression changes. Second, we used two different *C. albicans* clinical isolates, SC5314 and WO-1, in order to focus on conserved biofilm regulatory responses. Third, we have broadened the phenotypic screen to examine several biofilm-related phenotypes. We find that the majority of biofilm-responsive genes that we could disrupt have a measurable role in biofilm properties. We examined the biofilm-related function of one gene, *RHR2*, in detail. This gene specifies glycerol 3-phosphate phosphatase, and we confirm the findings of Bonhomme et

al. that *rhr2* mutants have a mild biofilm defect when grown *in vitro* (Bonhomme et al., 2011). We trace this defect not to a direct consequence of glycerol metabolism, but rather to the regulatory impact of this metabolic pathway. Our findings are particularly striking because of the severity of the requirement for Rhr2 to form biofilms *in vivo*, in a catheter model of biofilm infection. Our results emphasize the pivotal role that metabolic pathways can play, not only in physiology, but also in regulation.

## **Results**

### Biofilm-responsive gene expression and function

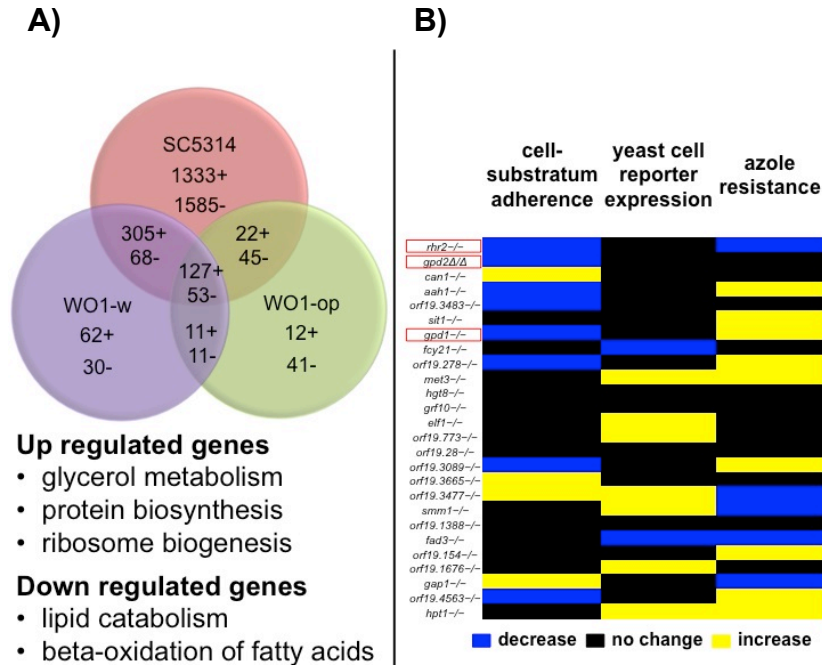
We used gene expression as a basis to identify genes that may function in biofilm formation. Prior biofilm profiling studies have used strains derived from SC5314, the first sequenced *C. albicans* isolate. We extended those findings by examining a second sequenced isolate, WO-1, alongside SC5314, through RNASeq profiling. Strain WO-1 can exist in both white and opaque states, and we thus used both WO-1 white cells, and WO-1 opaque cells, and SC5314 cells as independent inocula. We defined biofilm-regulated genes as those differentially expressed in biofilm-grown cells versus planktonic cells, each of which had been grown for 48h in Spider medium. We found a total of 165 genes with significantly altered expression between biofilm and planktonic samples for all three inocula. As shown in Figure 1(A), 112 of them were significantly up regulated, and 47 were significantly down regulated. The biofilm up-regulated genes represented functions in ribosome biogenesis, protein synthesis, glycerol metabolism, and amino acid transport. The biofilm down-regulated genes represented functions in lipid catabolism and beta-oxidation of fatty acids. Many of our findings are in agreement with previous studies (a detailed table showing comparisons is under Table S3 in (Desai et al., 2013)).

We created insertion mutants in order to screen up-regulated genes for functions related to biofilm formation. We selected the 62 most highly up-regulated genes for this analysis. We were able to obtain homozygous insertion mutants for 25 genes. The remaining genes may be essential under our growth conditions, or may have been difficult to disrupt for technical reasons.

We conducted a panel of assays to determine whether these genes govern any phenotypes related to biofilm formation. For many genes, we had multiple mutant isolates so that consistency of any phenotypic alteration could be assessed. We assayed for overall biofilm formation, activation of a co-cultured "yeast reporter" strain in biofilms, germ-tube formation, adherence to silicone and sensitivity to fluconazole. The results are summarized in Appendix. We found none of the mutants to be defective in germ-tube formation. However, we found 9 mutants to alter

*YWP1* expression in a co-cultured reporter strain, as shown in Figure 1(B). This suggests that the mutations alter production of a quorum-sensing molecule. We also found 14 mutants with altered sensitivity towards fluconazole and 10 mutants with altered adherence to silicone, as shown in Figure 1(B). Overall, these findings suggest that the majority (20/25) of biofilm-regulated genes have some measurable impact on biofilm properties.

**Figure 1: Biofilm gene expression and phenotypic screen for insertion mutants in biofilm up-regulated genes.**



(A) A Venn diagram showing the distribution of number of genes that were up- or down-regulated in biofilms of the strains: SC5314, WO1-white and WO1-opaque. These genes belong to the functional categories that are mentioned under the Venn diagram.

(B) A phenotypic heatmap showing phenotypes for the mutants in biofilm up regulated genes. The biofilm-related properties: substrate adherence, yeast-cell reporter expression and fluconazole sensitivity were assayed. The assays were performed as described under methods. For each assay, multiple isolates were tested and the changes were quantified relative to the wild-type strain. The mutants for which multiple isolates showed a statistically significant ( $p \leq 0.05$ ) unidirectional change relative to wild type are marked with blue and yellow bars for a decrease and an increase, respectively. The mutants with no significant change or where the independent isolates behaved differently are marked in black.

## Rhr2 function in adherence and biofilm formation

We found 6 mutants with significantly decreased adherence and 3 mutants with significantly increased adherence as compared to the wild-type strain (Figure 1B). Among the adherence defective mutants, *rhr2*<sup>-/-</sup> was particularly interesting because *RHR2* is the most highly biofilm up-regulated gene. *RHR2* encodes an enzyme, glycerol-3-phosphatase, which acts at the terminal step in glycerol biosynthesis (Fan et al., 2005). Despite the fact that Rhr2 biochemical function is well established, there was no obvious reason that Rhr2 should govern adherence.

To verify Rhr2 function, we constructed an *rhr2* $\Delta/\Delta$  deletion mutant and an *rhr2* $\Delta/\Delta$ +*pRHR2* complemented strain. The *rhr2* $\Delta/\Delta$  mutant was defective in adherence, and the complementation with a copy of *RHR2* rescued the adherence defect, as shown in Figure 2(B-i). Therefore, Rhr2 has a positive role in adherence.

We quantified glycerol levels in biofilms and planktonic cells to verify Rhr2 function. Wild-type biofilms accumulate glycerol at levels 5-fold higher than planktonic cells, as shown in Figure 2(B-ii). The *rhr2* $\Delta/\Delta$  mutant had ~50% reduction in biofilm glycerol accumulation when compared to the wild type. Complementation with a wild-type copy of *RHR2* improved glycerol accumulation. These measurements verify that glycerol accumulates at high levels in biofilms, in parallel with the high-level expression of *RHR2*.

Prior studies showed that *RHR2* is required for efficient biofilm formation, because biofilms produced by an *rhr2* $\Delta/\Delta$  mutant had 2-fold reduced biomass in a minimal medium (Bonhomme et al., 2011). We confirmed the mutant defect in our standard biofilm medium, Spider medium. In this medium, the *rhr2* $\Delta/\Delta$  mutant biofilm biomass was reduced substantially compared to the wild type and complemented strains, as shown in Figure 2(A). In addition, confocal imaging revealed that the depth of the *rhr2* $\Delta/\Delta$  mutant biofilm was greatly diminished compared to the wild type and complemented strains, as shown in Figure 2(C). Apical-view images indicate that the mutant biofilm consists primarily of a basal layer of yeast-form cells with few interspersed hyphae. If a defect in glycerol production is the cause of the mutant biofilm defect, then exogenous glycerol

may restore biofilm formation by the mutant. We tested this hypothesis by assaying biofilm formation in Spider-glycerol medium, in which glycerol replaces mannitol as the carbon source. As shown in Figure 2(D), spider-glycerol medium supported biofilm formation by the wild-type strain, though overall depth and biomass were reduced slightly compared to biofilms formed in Spider medium. These properties likely reflect the reduction in growth rate in Spider-glycerol, compared to Spider medium (data not shown). Importantly, in Spider-glycerol medium the *rhr2Δ/Δ* mutant strain formed biofilms similar in structure and biomass to that of the wild type and complemented strains (Figure 2(A) and (D)). These results confirm that Rhr2 is required for biofilm formation, and that its biofilm function derives from its role in glycerol synthesis.

**Figure 2: *RHR2* is required for biofilm formation in vitro through its role in glycerol biosynthesis.**

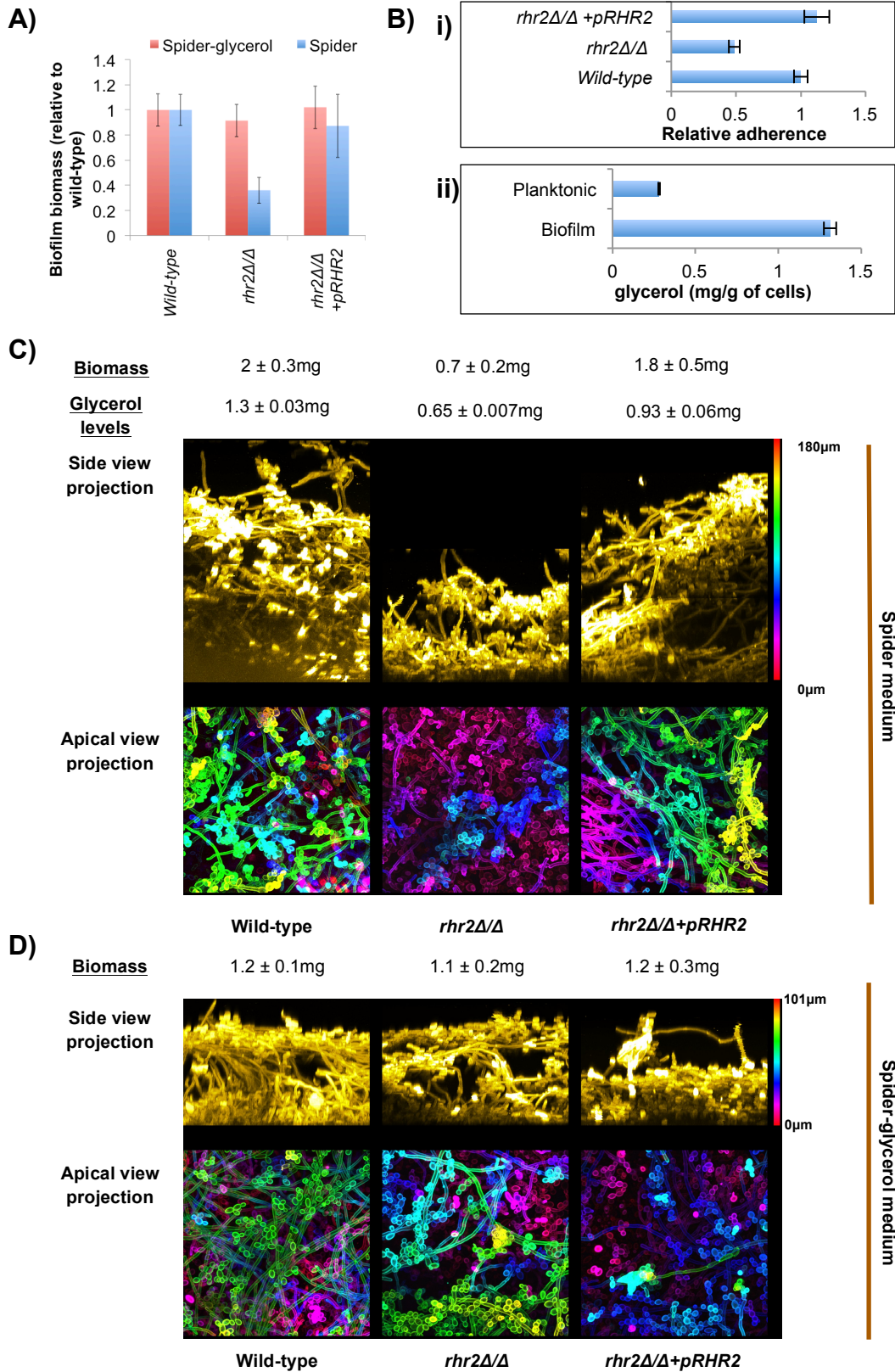


Figure 2: (A) Biofilm biomass. Biofilms, grown in spider or spider-glycerol media for 48 hours, were dried for 2 days and the average dry weight was measured (n=5). Relative biomass was calculated by taking ratio of the average biofilm biomass for the mutant or complemented strains to the average biomass of wild-type strain. The strains used were DAY185 (wild-type), JVD005 (*rhr2Δ/Δ*) and JVD006 (*rhr2Δ/Δ+pRHR2*)

(B) i. Adherence assay for the strains: DAY185 (wild type), JVD005 (*rhr2Δ/Δ*) and JVD006 (*rhr2Δ/Δ+pRHR2*). ii. Biofilm vs. planktonic glycerol estimates for the wild-type strain (DAY185). Glycerol was quantified enzymatically as described under methods. The quantified glycerol levels were normalized against total cell weight.

(C) and (D) Confocal imaging of biofilms. 24 h biofilms of *wild type*, *rhr2Δ/Δ* and *rhr2Δ/Δ+pRHR2*, were used. Side-view projections were computed by re-slicing the intensity corrected serial image stack from bottom to top. The re-sliced stack was then used for maximum intensity projection. The displayed apical view projections were pseudocolored to aid in visualization of biofilm depth. The color calibration bar is displayed on top right corners, displaying the colors in a spectrum as a function of biofilm thickness in microns. The color calibration bars were kept different for two different growth media for comparative purpose, as the wild-type biofilm was thinner in spider-glycerol medium as compared to the wild-type biofilm in spider medium. Scale-bars correspond to 15μm.

The clear environmental influence on Rhr2-dependence of biofilm formation leads to the question of whether Rhr2 is required for biofilm formation *in vivo*. We addressed this question with two biofilm infection models, a rat central venous catheter model (Andes et al., 2004) and a mouse oropharyngeal candidiasis model (Kamai et al., 2001). In the venous catheter model, biofilm formation within the catheter lumen was assessed by scanning electron microscopy. The *rhr2Δ/Δ* mutant was severely defective in biofilm formation, as shown in Figure 5, yielding a catheter lumen virtually devoid of *C. albicans* cells. Biofilm formation was restored in the complemented strain. In the mouse oropharyngeal candidiasis model, biofilm formation was assessed by fungal burden on the tongue. In this model, the mutant showed no defect compared to the wild type and complemented strains (data not shown). Therefore, Rhr2 is not required for biofilm infection of the oral mucosa, but it is required for biofilm formation on a central venous catheter. Rhr2 biological function is contingent upon the environment *in vivo*, as it is *in vitro*.

### Rhr2 impact on biofilm gene expression

It seemed possible that the impact of Rhr2 on adherence and biofilm formation might be a result of effects on gene expression. To explore that possibility, we compared the mutant and complemented strain through whole-genome expression profiling using RNAseq (Figure 3 (A), full data: Table S1 in (Desai et al., 2013)), with confirmation by nanoString and RT-qPCR assays. The two strains were grown under planktonic conditions for profiling to avoid indirect effects of differences in biofilm formation ability. We observed that many genes with functional roles in biofilm formation were down regulated in the *rhr2Δ/Δ* mutant (Figure 3), including the adhesin genes *ALS1*, *ALS3*, and *HWP1*. In fact, the genes down-regulated in the *rhr2Δ/Δ* mutant were almost up-regulated in wild-type biofilm cells compared to planktonic cells; the genes up-regulated in the *rhr2Δ/Δ* mutant are almost all down-regulated in wild-type biofilm cells compared to planktonic cells, as shown in the heatmap in Figure 3(A). As shown in Figure 3(B), providing glycerol to the *rhr2Δ/Δ* mutant through growth in Spider-glycerol medium led to increased *ALS1* and *HWP1* expression. On a larger scale as well, providing glycerol rescued the gene expression defect arising due to glycerol-deficit, as shown in Figure 3(C). Taken together, these observations suggest that the high level expression of *RHR2* and glycerol in biofilm cells may be required for a substantial portion of the biofilm-associated gene expression profile.

Figure 3: Glycerol is required for biofilm gene expression response.

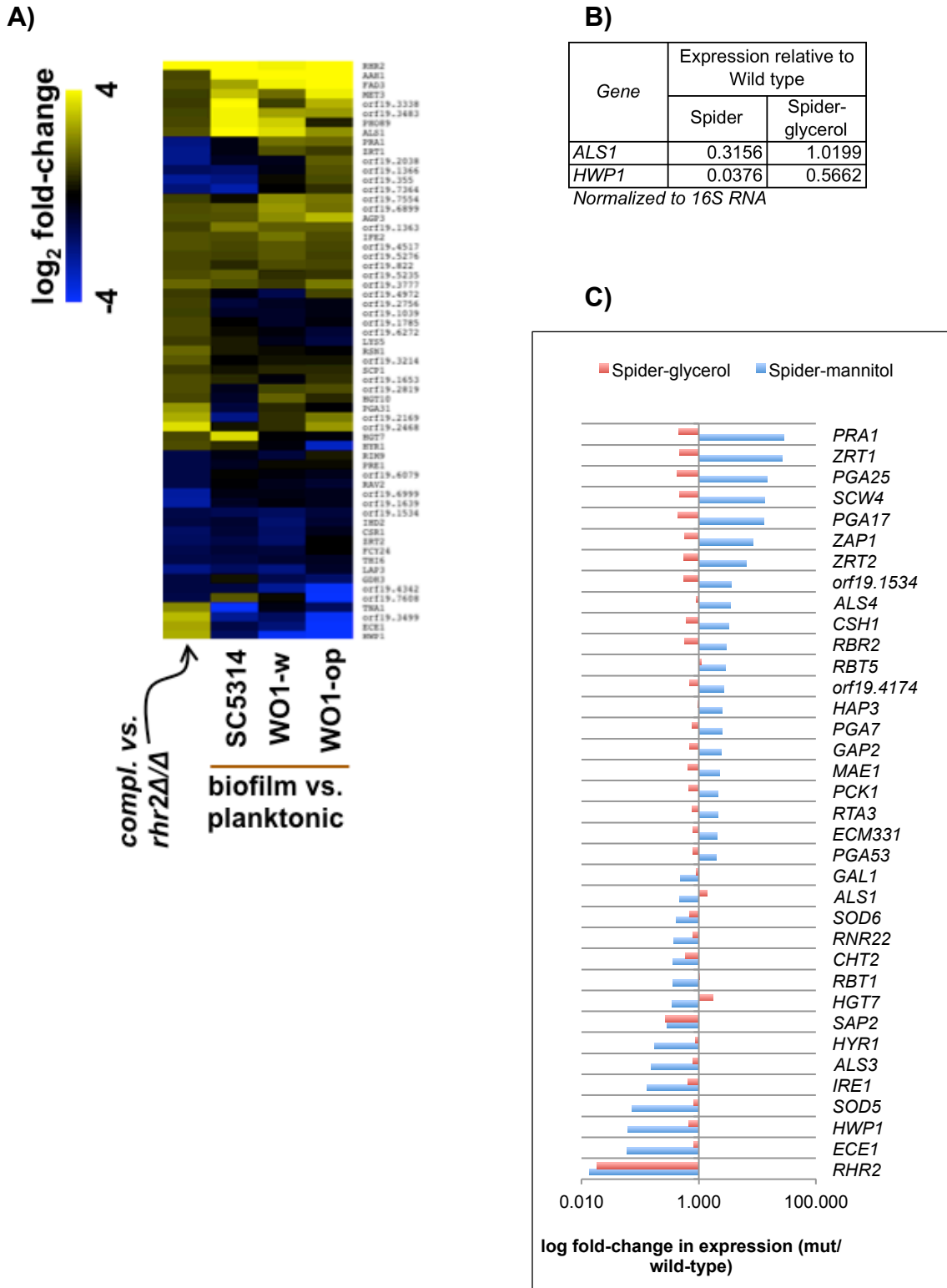


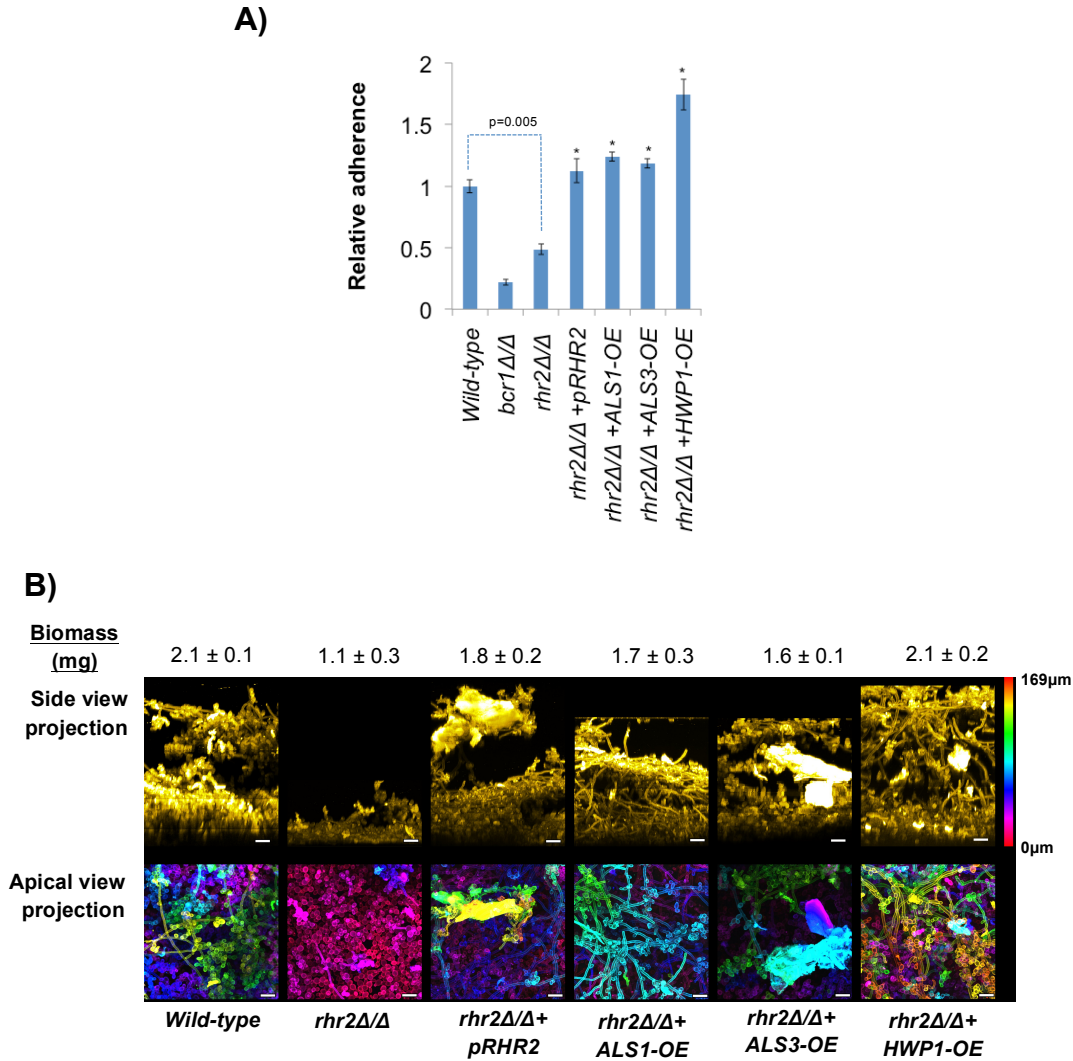
Figure 3: (A) Gene expression heatmap. RNAseq expression data values for *rhr2Δ/Δ+pRHR2* (JVD006) complement were divided by expression data values of the *rhr2Δ/Δ* (JVD005) mutant to calculate fold-change values. Genes with fold-change  $\geq 1.5$  or  $\leq 0.67$  are shown. The heatmap also displays the fold-change in expression in biofilm vs. planktonic conditions for three wild type inocula. Yellow is used for up-regulated genes and blue indicates genes down-regulated.

(B) & (C) Glycerol rescues the biofilm gene expression defect of *rhr2Δ/Δ*. Overnight cultures grown in YPD/YP-glycerol were used to inoculate Spider/Spider-glycerol media and cells were grown for additional 8 hours. RNA extracted from *wild type* and *rhr2Δ/Δ* was used to quantify gene expression via RT-qPCR as shown in (B) or the nanoString platform, as shown in (C).

### Functional basis of the *rhr2Δ/Δ* mutant biofilm defect

The gene expression profile of the *rhr2Δ/Δ* mutant suggested the simple hypothesis that diminished adhesin gene expression might be the cause of the mutant defects in adherence and biofilm formation. To test that hypothesis, we created *rhr2Δ/Δ* mutant derivatives with restored high-level expression of each adhesin gene – *ALS1*, *ALS3*, and *HWP1* – and assessed their capacity for adherence and biofilm formation. Increased expression of each adhesin improved adherence of the *rhr2Δ/Δ* mutant to levels comparable to the wild-type strain, as shown in Figure 4(A). In addition, increased of each adhesin restored biofilm formation ability of the *rhr2Δ/Δ* mutant *in vitro*, as determined by both biomass measurements and confocal imaging (Figure 4(B)). We also assessed biofilm formation ability of these strains *in vivo* with the rat venous catheter biofilm model (Figure 2.5). Increased expression of *ALS1*, *ALS3*, or *HWP1* in the mutant led to biofilm formation *in vivo*, with increased *ALS3* expression causing the most extensive biofilm formation. These findings indicate that Rhr2 is required for biofilm formation *in vitro* and *in vivo* because of the regulatory consequences of altered glycerol synthesis.

**Figure 4: The function of *RHR2* in adhesin gene expression is required for silicone adherence and biofilm formation in vitro.**



(A) Adhesin overexpression rescues the substrate adherence defect of *rhr2*Δ/Δ. Cell-wall adhesin genes were overexpressed using the constitutive *TDH3* promoter in *rhr2*Δ/Δ background. Substrate adherence was quantified as described in methods. ‘\*’ at top of bars indicate p-value < 0.05 with respect to *rhr2*Δ/Δ

(B) Adhesin overexpression rescues biofilm formation of *rhr2*Δ/Δ. The adhesin over-expression strains were used to analyze biofilm formation. The biofilm biomass assay and confocal imaging of biofilms were performed as outlined under methods and Figure 2(B). Scale-bars correspond to 15μm. The strains used were: wild type (DAY185), JVD006 (*rhr2*Δ/Δ+pRHR2), JVD005 (*rhr2*Δ/Δ), JVD018 (*rhr2*Δ/Δ+ALS1-OE), JVD020 (*rhr2*Δ/Δ+HWP1-OE) and JVD025 (*rhr2*Δ/Δ+ALS3-OE) respectively.

**Figure 5: The function of *RHR2* in adhesin gene expression is required for biofilm formation in vivo.**

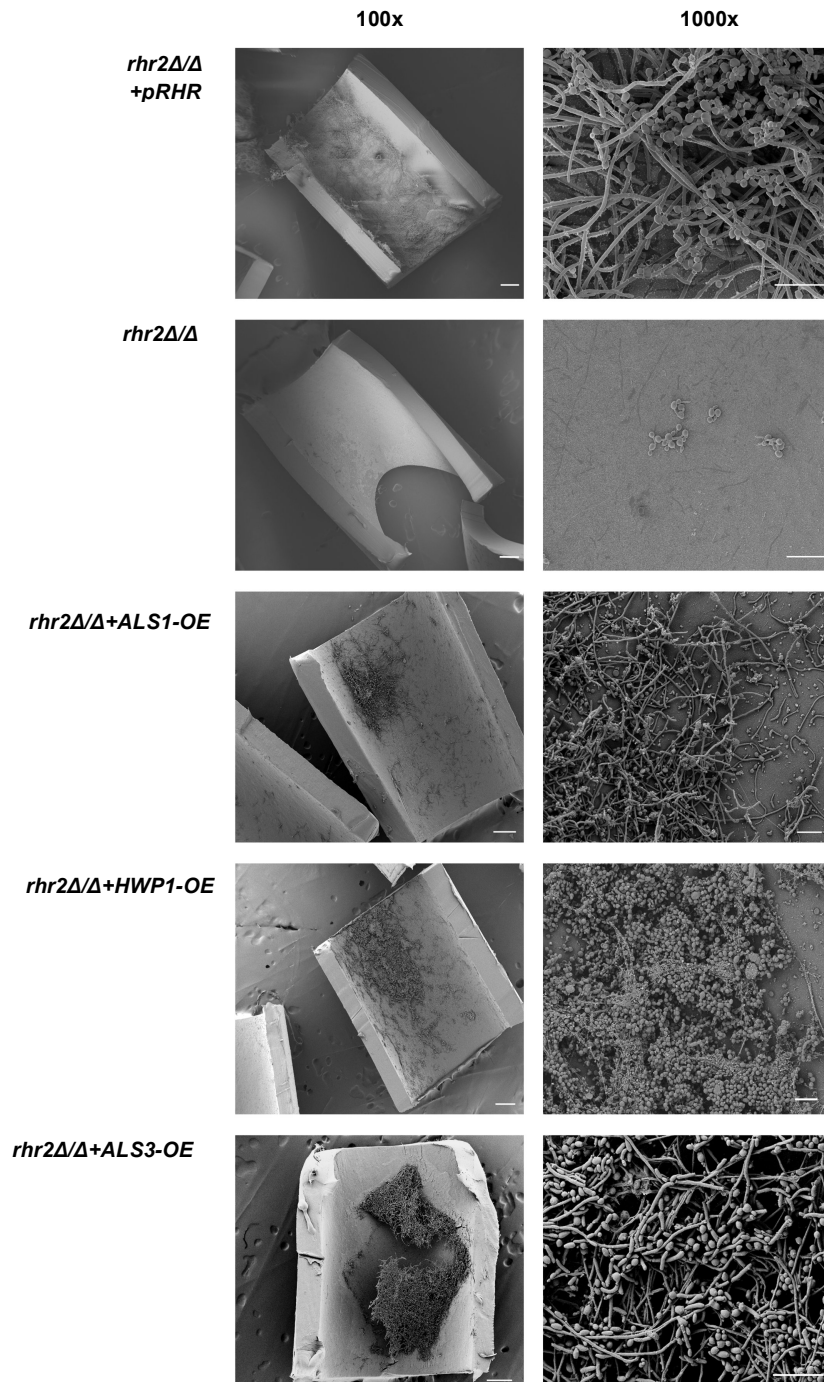


Figure 5: The strains were inoculated to the catheter lumen and the resulting biofilms were imaged using scanning electron microscopy. The shown images are 100x- and 1000x-magnification views of the biofilms. The strains used were: JVD006 (*rhr2Δ/Δ*+*pRHR2*), JVD005 (*rhr2Δ/Δ*), JVD018 (*rhr2Δ/Δ*+*ALS1-OE*), JVD020 (*rhr2Δ/Δ*+*HWP1-OE*) and JVD025 (*rhr2Δ/Δ*+*ALS3-OE*) respectively.

## Glycerol and biofilm gene-regulation

How does glycerol influence gene expression? One hypothesis is related to the well-established role of glycerol in maintaining intracellular osmotic pressure (turgor) (Hohmann, 2002). Turgor is sensed by a phosphorelay system (Hohmann, 2002) that ultimately activates the MAP kinase Hog1 under low-turgor conditions (Kaserer et al., 2009), thus affecting target gene expression (Bahn, 2008). A simple model is that loss of Rhr2 mimics the effect of high external osmolarity and causes elevated Hog1 activity, which in turn causes the *rhr2 $\Delta/\Delta$*  gene expression alterations. Two observations argue against this model. First, Hog1 is constitutively activated by mutation of the phosphorelay gene *SLN1*, but a *sln1*<sup>-/-</sup> insertion mutation does not cause the biofilm defect predicted by this hypothesis, as shown in Figure 6(A). Second, an amino acid substitution in the phosphorelay component Ssk1 (D513K) causes constitutive Hog1 activation and a defect in hypha formation (Menon et al., 2008; Menon et al., 2006). However, the *rhr2 $\Delta/\Delta$*  mutant has no defect in hypha formation. Therefore, we have no evidence that the Hog1 pathway mediates the biofilm-related defects of the *rhr2 $\Delta/\Delta$*  mutation.

We favor a second model in which glycerol levels may be sensed by one or several transcription factors that are required for adherence or biofilm formation (Finkel et al., 2012; Nobile et al., 2012). *RHR2* appears to be integrated into the biofilm regulatory network, because most transcription factors (TF) that are required for biofilm formation are required for *RHR2* RNA accumulation. If *RHR2* indeed functions downstream of any of the biofilm-regulatory TFs, then its forced overexpression under a specified TF mutant background should restore the biofilm defect for that particular TF mutant. It is, however, not that straightforward, as many of these TFs are also required for RNA accumulation of two other glycerol biosynthetic genes *GPD1* and *GPD2* (Finkel et al., 2012; Nobile et al., 2012). These genes encode orthologous enzymes that produce glycerol-3-phosphate by reduction of dihydroxyacetone phosphate (DHAP), a substrate for Rhr2 in glycerol biosynthesis. Thus under the TF mutant backgrounds where *GPDs* and *RHR2* are co-regulated, the *RHR2* overexpression, to probe a functional relationship, would be futile. In order to avoid this, we grew the mutant biofilms in the glycerol medium where we

observed a restored biofilm formation by the *rhr2Δ/Δ* mutant (Figure 2(D)). As shown in Figure 6(B), however, none of the tested mutants had a rescued biofilm-growth in glycerol medium. This still does not rule out a possibility that the TF genes for these mutants act downstream of the glycerol signal. We reasoned that overexpression of the transcription factors, if downstream, would improve biofilm formation by *rhr2Δ/Δ* mutant. As shown in Figure 6(C), the known biofilm regulators: *BCR1*, *BRG1* and *EFG1* rescue biofilm formation by *rhr2Δ/Δ* mutant. We also overexpressed *UME6*, a hyphal regulator (Banerjee et al., 2008), as its expression was reduced (fold-change =  $0.5 \pm 0.1$ ), in *rhr2Δ/Δ* mutant. As shown in Figure 6(C), *UME6* overexpression also leads to an improvement in biofilm formation by *rhr2Δ/Δ* mutant. A possibility cannot be denied where these transcription factors can be thought to act independently of glycerol levels. We, however, still favor the possibility that they act downstream of *RHR2*. In that case, the question arises; what is the signal that the transcription factors are relaying? We hypothesized that the role of glycerol in maintaining plasma-membrane stretch to normalcy, through its role in turgor maintenance, is somehow relayed through these transcription factors. A normally stretched membrane would maintain the membrane-tethered sensory protein(s) in place. In *C. albicans*, Dfi1 is one such protein that is membrane-tethered and spans the cell wall (Davis et al., 2013; Zucchi et al., 2010). It is responsible for relaying changes in cell wall to intracellular compartments in the kinase, Cek1-dependent manner (Zucchi et al., 2010). We therefore considered a simple model, as shown in Figure 6(F), where turgor-deficit would lead to sensory-deficit, hence hypersensitivity to cell-wall perturbing agents as caspofungin. Figure 6(D) shows that, similar to *dfi1Δ/Δ*, *rhr2Δ/Δ* is sensitive to caspofungin treatment, as determined using multiple mutant isolates. Additionally, we observed that the *rhr2Δ/Δ* had significantly thinner cell wall as compared to the wild type and complemented strains. Figure 6(D) shows the images and quantification. These experiments provide a preliminary support to our argument; however, further experiments are still required to prove if this is indeed the case.

**Figure 6: A hunt for the possible regulator(s) that mediate the biofilm gene expression response of glycerol.**

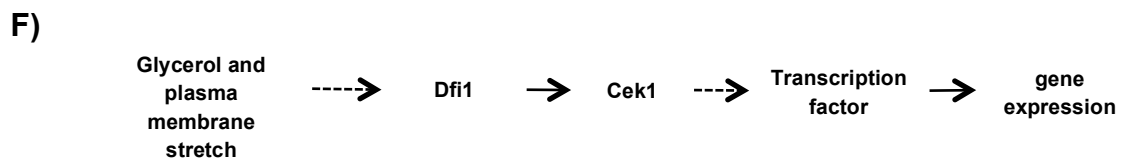
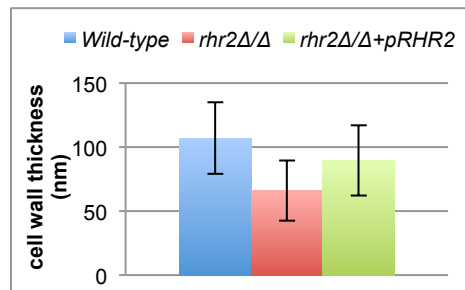
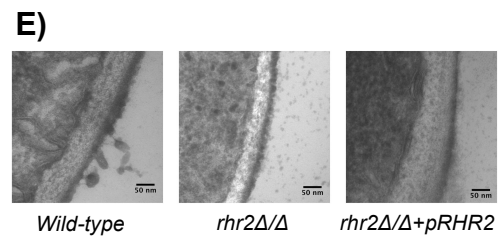
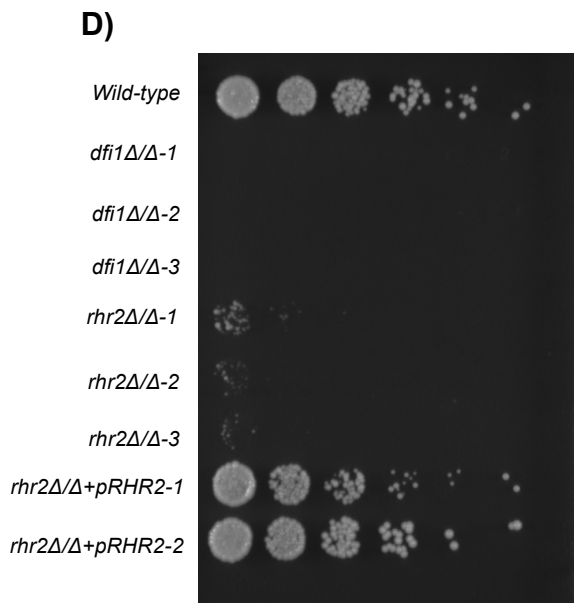
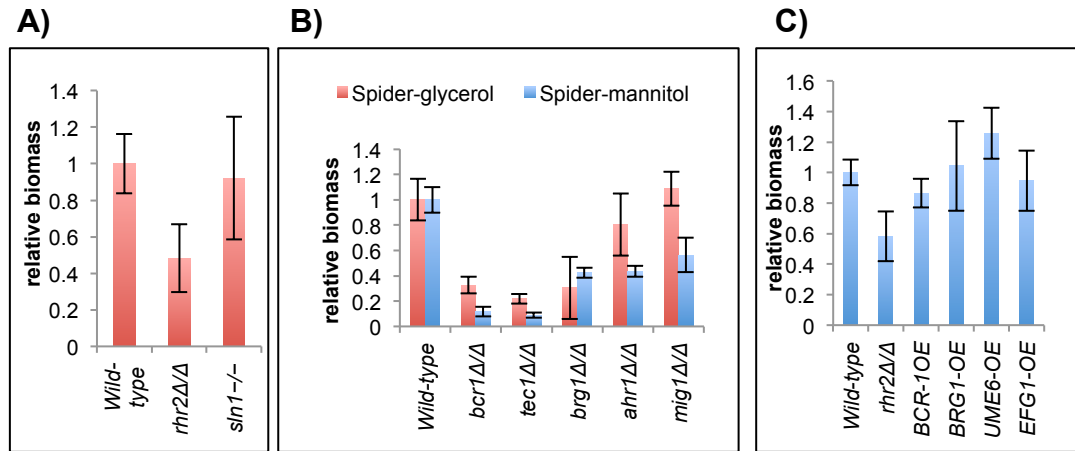


Figure 6 (A), (B), & (C) Biofilm biomass assay. The genotypes of the assayed strains are mentioned in plots. Similarly the different growth conditions, if applicable, are mentioned in the legend. The error bars show standard deviation values. Strains used: *sln1*<sup>-/-</sup> (SF40, SF40a), the TF mutants and a marker matched wild-type were from the Homann deletion collection (Homann et al., 2009).

(D) Caspofungin sensitivity assay. The assay was performed as described under methods. The image shown here is the digital photograph of the YPD-agar plate containing caspofungin. The genotypes of the strains are marked on left. Strains used were: *dfi1* $\Delta/\Delta$  (TA12, TA15 and TA18), *rhr2* $\Delta/\Delta$  (JVD005, JVD022-23) and *rhr2* $\Delta/\Delta$ +*pRHR2* (JVD006, JVD008).

(E) Cell-wall thickness analysis. The cell-wall depths were analyzed via transmission electron microscopy (TEM). The microscopy and sample preparation was carried out as described by Fanning et al. (Fanning et al., 2012a). The images shown here were acquired using sectioned cells. These images were used to quantify the cell-wall thickness. The plot shows average thickness (nm) with error-bars showing standard deviation values. Strains used were:wild type (DAY185), *rhr2* $\Delta/\Delta$  (JVD005) and *rhr2* $\Delta/\Delta$ +*pRHR2* (JVD006). The result represents analysis from a single experiment. Further attempts are required for substantiation to this initial observation.

(F) Proposed model for glycerol-mediated biofilm regulation. The dashed arrows mark proposed relationships while the solid arrows mark the relationship that has already been established.

## **Discussion**

It has been understood for some time that *C. albicans* biofilm formation depends upon cell surface adhesins (Finkel and Mitchell, 2011; Finkel et al., 2012). There has been considerable progress in identification of the transcription factors that control adhesin gene expression (Desai et al., 2013). However, the environmental and physiological signals that govern adhesin expression, especially those that function *in vivo* during infection, are more poorly defined. Here we started with a well-established strategy based on differential gene expression and found that glycerol biosynthesis is critical for a substantial portion of the biofilm-associated gene expression profile, including adhesin gene expression.

Several prior studies have examined the biofilm transcriptome, using a range of profiling methods and growth platforms (Garcia-Sanchez et al., 2004; Murillo et al., 2005; Nobile et al., 2012; Yeater et al., 2007). Our study is unique in a sense that we employed two different *C. albicans* strains under similar growth conditions for delineating a common biofilm gene expression response. For strain WO-1, we used separate white and opaque cell inocula, but because our growth temperature of 37° induces conversion to white cells, we expected the white and opaque biofilms to yield similar expression profiles. They did. However, we were surprised at the extent of similarity between SC5314 and WO-1 biofilm transcriptomes, given that these strains represent different clades and mating types. In addition, the genes we find to be up-regulated in both SC5314 and WO-1 biofilms have previously been identified as up-regulated in other biofilm vs. planktonic comparisons (Garcia-Sanchez et al., 2004; Murillo et al., 2005; Nobile et al., 2012; Yeater et al., 2007). The parallels among these datasets suggest that we have a reliable and robust definition of the mature biofilm transcriptome.

The overall results of our mutant analysis argue that up-regulated genes function in biofilm development, because 20 insertion mutants among the 25 genes sampled caused measurable alterations in biofilm properties. Our findings contrast with the pioneering study of Bonhomme et al. (Bonhomme et al., 2011), who examined deletion mutants of biofilm up-regulated genes. They

identified biofilm defects in only nine of the 38 mutants examined. This difference between our findings may reflect the fact that Bonhomme et al. used one assay for biofilm formation, biofilm biomass, whereas we have used a panel of biofilm-associated phenotypes. The diversity of genes and phenotypes we have found opens the door for many future functional studies.

Our focus on *RHR2*, which specifies glycerol 3-phosphatase, was based on four features. First, it is the most highly up-regulated gene in biofilms compared to planktonic cells in our comparison. Second, it has been identified as a biofilm-associated gene in several other profiling studies (Garcia-Sanchez et al., 2004; Yeater et al., 2007). Third, foundational work from the d'Enfert lab has shown that an *rhr2ΔΔ* mutant produces a biofilm with reduced biomass *in vitro*, which we confirmed (Bonhomme et al., 2011). Hence while the mutant defect seems only partial, it is robust. Finally, the mutant had an adherence defect, a phenotype that we have studied in some detail, and yet one with no obvious connection to glycerol metabolism. Our analysis reveals that, on the one hand, the relationship is fairly simple: Rhr2 is required for RNA accumulation from the major adhesin genes *ALS1*, *ALS3*, and *HWP1*. Prior studies have shown that these adhesins are required for biofilm formation *in vitro* and *in vivo* (Nobile et al., 2006a; Nobile and Mitchell, 2005; Nobile et al., 2006b), and we showed here that increased expression of any one of those adhesins can restore biofilm formation, *in vitro* and *in vivo*, in an *rhr2ΔΔ* mutant background. These observations argue strongly that Rhr2 is required for biofilm formation primarily to promote expression of key adhesin genes.

The regulatory impact of Rhr2 extends well beyond adhesin gene expression. Under the planktonic growth conditions in which we compared the mutant and complemented strain, almost 400 genes were differentially expressed. Strikingly, the expression alteration in the *rhr2ΔΔ* mutant for many of these genes correlates inversely with their expression alteration in response to biofilm growth (Figure 3). These results suggest that glycerol metabolism is a major signal that drives biofilm-associated gene expression. In fact, the *rhr2* insertion mutant also displayed a significant sensitivity to fluconazole under biofilm growth conditions; a phenotype that may also reflect altered expression of biofilm-associated Rhr2-responsive genes.

If glycerol synthesis generates a biofilm-promoting signal, one might expect all glycerol biosynthetic mutants to have similar biofilm defects. Indeed, all three glycerol biosynthetic genes (*GPD1*, *GPD2* and *RHR2*) were among the most highly induced genes in biofilms. *GPD1* and *GPD2* encode NADH-dependent glycerol-3-phosphate dehydrogenases that probably have redundant functions; *RHR2* encodes a glycerol-3-phosphatase that acts at the final step in the pathway (Fan et al., 2005; Pahlman et al., 2001). Although Rhr2 is the sole predicted glycerol-3-phosphatase in *C. albicans*, null *rhr2Δ/Δ* mutants can still accumulate some glycerol. It seems reasonable that this glycerol derives from phospholipase action on phospholipids, and perhaps promiscuous phosphatases that may act on glycerol-3-phosphate. We included two independent *gpd1*<sup>-/-</sup> insertion mutants in our screen, and both displayed reduced adherence, as expected. We were unable to construct a *gpd2*<sup>-/-</sup> insertion mutant, but a *gpd2Δ/Δ* mutant in the Noble collection has reduced adherence as well. Thus our observations with *gpd1* and *gpd2* mutants are consistent with the hypothesis that internal glycerol has a positive role in adherence.

What governs the expression of biofilm genes in response to glycerol? Our observations suggest that the expected HOG (**H**igh **O**smolarity **G**lycerol) pathway does not relay the glycerol signal for biofilm gene expression. Our preliminary observations show that glycerol levels impact the cell-wall integrity. These observations prompted us to propose that glycerol's function to maintain a turgid-stretch in plasma membrane impacts the biofilm-gene expression. At least two models can be put forth. In the first model, an impact of turgor on trafficking can be considered. In the fission yeast, turgor plays an important role in endocytosis where a decrease in turgor leads to an increased endocytosis (Basu et al., 2014). An opposite can be proposed for exocytosis, which is required for delivery of cell-wall proteins, important for biofilm formation as well as signaling. Thus, it is possible that the impact of turgor on delivery of cell-wall components affects the biofilm gene expression. In our second model, we propose that a normally stretched plasma membrane is required to place a membrane-tethered, cell-wall-spanning sensory protein, such as Dfi1 (Davis et al., 2013; Zucchi et al., 2010), that ultimately drives the biofilm gene expression. Further experiments are warranted to substantiate any of these claims.

Why might internal glycerol levels be a regulatory signal that is required for biofilm formation?

One possible reason has to do with the need for glycerol in biogenesis of glycosylphosphatidylinositol (GPI) anchor. These glycolipid structures are used to generate the tethers that hold adhesins and other mannoproteins to the cell surface. Thus it may benefit the cell to take inventory of its glycerol stores before embarking on a growth pathway that relies upon functional adhesin biogenesis. A second possible reason has to do with one niche for *C. albicans* biofilm formation: mucosal surfaces. It is possible a mucosal biofilm serves as a stepping-stone toward surface invasion. If that is the case, then it may benefit the cell to ensure that glycerol is available to support turgor generation necessary for tissue penetration.

## **Methods**

### Media and Strain Construction

*C. albicans* strains were grown on yeast extract-peptone-dextrose (YPD) or YP-glycerol (2% Bacto Peptone, 2% dextrose/glycerol, 1% yeast extract) media, supplemented with 80µg/ml uridine. For biofilm assays, Spider medium (1% nutrient broth, 1% mannitol and 0.2% K<sub>2</sub>HPO<sub>4</sub>) or Spider-glycerol medium (1% nutrient broth, 1% glycerol and 0.2% K<sub>2</sub>HPO<sub>4</sub>) media were used. During mutant strain construction, prototrophs were selected on synthetic defined medium (2% dextrose, 6.7% yeast nitrogen base with ammonium sulfate and complete synthetic mixture [CSM] lacking uridine, arginine or histidine).

All the strains used in this study are described in Table 2. The insertion mutant strains used for the initial adherence screen were constructed as described previously (Nobile and Mitchell, 2009). The *rhr2Δ/Δ* deletion strain (JVD005) was constructed in BWP17 strain background using a method described previously (Wilson et al., 1999). Briefly, gene-disruption cassettes for transformation were amplified using 120bp primers and the plasmids, pRS-ARG4 (Wilson et al., 1999) or pGEM-URA3 (Wilson et al., 1999), which contain *ARG4* and *URA3* for PCR-directed integration. The forward primer was designed to have homology to 100bp sequence upstream of the *RHR2* start codon while the reverse primer had homology to the 100bp sequence following the stop-codon. Both the primers were flanked by a 20bp sequence homologous to the plasmids, as mentioned above. Sequential transformations of these gene-disruption cassettes into *C. albicans* BWP17 strain yielded the deletion strain JVD005. The gene-complemented strain for *rhr2Δ/Δ* was constructed by a common complementation protocol as described previously. Briefly, a gene-complementation cassette was generated by amplifying *RHR2* fragment from *C. albicans* genomic DNA by PCR, using primers to incorporate flanking regions homologous to a plasmid pDDB78 (Ma et al., 1987). The linearized plasmid and the complementation cassette were co-transformed into *S. cerevisiae* for homologous recombination to obtain a plasmid, a derivative of pDDB78 containing *RHR2*. This plasmid after amplification in *E. coli* was linearized with Nru1 and transformed into *C. albicans* to direct integration at the *HIS3* locus.

The overexpression strains under specific gene-deletion background were constructed by transformation with the gene-overexpression cassettes. These cassettes were amplified from the plasmid pCJN542 (Nobile et al., 2008b) using a forward primer having 100bp homologous sequence to the 500bp upstream of the gene of interest and a reverse primer having 100bp homologous sequence exactly ending at the start codon of the gene. The amplified fragment (gene-overexpression cassette) was transformed into appropriate *C. albicans* strain and the transformants were selected by growth on YPD+ 400µg/mL nourseothricin (clonNAT) plates.

#### RNA sample preparation for RNAseq analysis

For isolating RNA from biofilms, cells were grown in 50 ml of spider medium in 150-cm<sup>2</sup> polystyrene tissue culture flasks (Corning- tissue culture treated; catalog number 430823) in order to maximize the surface area of biofilm growth and permit extraction of ~250µg total RNA for RNA-Seq. The strains WO1-white and WO1-opaque were selected on YPD + Phloxine B (5µg/ml [Sigma-Aldrich P2759-25G]) plates for ~5 days at 24°C (Slutsky et al., 1987). One white colony was picked for WO1-white strain and one opaque colony was picked for WO1-opaque strain for overnight growth in YPD for growth in biofilm and planktonic conditions. Biofilms were grown as follows: Cells from overnight cultures of SC5314, WO1-white and WO1-opaque in YPD were added to each tissue-culture flask at a final optical density at 600 nm (OD<sub>600</sub>) of 0.5 in 50 ml spider medium. Cell adherence to the flasks was for 90 min at 37°C with 35 rpm agitation in the incubator. After the cell adherence step, the flasks were washed with phosphate-buffered saline (PBS), and 50 ml of fresh spider medium was added to the flasks. The flasks were then incubated for 48 h at 37°C with 35 rpm agitation during which biofilms grow. For planktonic condition, cells from the same overnight cultures of SC5314, WO1-white and WO1-opaque in YPD were each added conical flasks at a final OD<sub>600nm</sub> of 0.2 in 50 ml spider medium. Cells were grown for 48 hours at 37°C with 225 rpm agitation in the incubator.

For RNA extraction, the biofilms were harvested by scraping the bottoms of the flasks using a cell scraper and filtering the cell slurry on a vacuum manifold. The planktonic cells were harvested similarly by vacuum filtration. The filters were flash frozen immediately after harvesting each

sample. The cells were kept frozen on filters at  $-80^{\circ}\text{C}$  until RNA extraction. RNA was extracted using a RiboPure-Yeast kit (Ambion) following the manufacturer's instructions as described previously (Blankenship et al., 2010; Ganguly et al., 2011). Briefly, cells were resuspended from filters with 3 ml ice-cold distilled water, followed by 15 to 30 s of vigorous vortexing. For biofilm and planktonic samples, the slurry was very thick so each sample was split into two for RNA extraction to enable efficient disruption of harvested cells, thereby optimizing RNA yields. The resuspended cells were transferred to a 1.5-ml tube and spun down according to the manufacturer's protocol. During the cell disruption step, the cells were beaten with a Next Advance Bullet Blender for 3 min at  $4^{\circ}\text{C}$  for cell lysis. Post extraction procedure, for biofilm and planktonic samples, the RNA for the same sample was combined and dried together for deep sequencing.

For gene expression analysis of *rhr2 $\Delta/\Delta$* , the strains (wild-type-DAY185, *rhr2 $\Delta/\Delta$* -JVD005, and *rhr2 $\Delta/\Delta$ +pRHR2*-JVD006) were grown overnight in YPD/YP-glycerol medium at  $30^{\circ}\text{C}$ . Cells from overnight cultures in YPD/YP-glycerol medium were added to 50 ml Spider/Spider-glycerol medium at a final  $\text{OD}_{600\text{nm}}$  of 0.2. Cells were grown for additional 8 hours at  $37^{\circ}\text{C}$  with 225 rpm agitation in the incubator and harvested in a similar fashion as described above. RNA extraction was also done similarly as described above.

#### Yeast-cell reporter expression assay in mixed biofilms

The mixed biofilms were grown as described previously (Ganguly et al., 2011). Briefly, the strains under analysis were grown overnight in YPD at  $30^{\circ}\text{C}$ . The overnight cultures were used to inoculate 4 mL Spider medium, contained in wells of 6-well polystyrene plates (Costar 3736 6-well untreated plates; catalog number 07201588) pretreated overnight with fetal bovine serum (FBS). For mixed biofilms, wild-type (DAY185), *zap1 $\Delta/\Delta$*  (CJN1201, positive control) and the mutants under study were inoculated at  $\text{OD}_{600}$  of 0.4 while the reporter strain (SGH281) was inoculated at  $\text{OD}_{600}$  of 0.1. The cells were allowed to adhere to wells for 90 minutes in an incubator-shaker at 35 rpm and  $37^{\circ}\text{C}$ . After 90 minutes the cells not adhering were washed off

with phosphate buffer saline (PBS). Fresh Spider medium was then added to each well and incubation was continued for additional 48 hours, which resulted in biofilm formation. Biofilms were harvested by scraping the bottoms using a cell scraper and the cell-suspensions were then filtered using a vacuum manifold. The filters containing cells were immediately transferred to -80°C until used for RNA extraction. RNA was extracted using the Ambion kit as described above.

#### Fluconazole sensitivity assay

Overnight cultures grown in YPD (30°C) were diluted to  $1 \times 10^6$ /mL (using haemocytometer) in RPMI+MOPS+Histidine medium and seeded into wells (100µL/well) of 96-well plate. Biofilms were grown stationary for 6 hours at 37°C. Biofilm supernatant was aspirated, and wells were washed thrice with 100µL 1xPBS. Fluconazole or control RPMI+MOPS+HIS was added (100µL/well) and incubated stationary at 37°C for 24 hours. Supernatant was aspirated and XTT solution (0.25mg/mL in RPMI+MOPS+HIS) was added to each well and incubated for 30 minutes at 37°C without shaking. Absorbance values were then measured on TECAN plate reader at 450nm (XTT) and 690nm (background, as per Sigma instructions)

#### RNA sequencing and differential expression analysis

For comparison of biofilm and planktonic growth in the wild type strains, the RNAseq libraries (strand-specific, single read) were prepared exactly as described by Bruno *et al.* (Bruno and Mitchell, 2004) and 30-nt of sequence was determined from one end of each cDNA fragment using the Illumina GA2 platform (Bentley *et al.*, 2008). For the comparison of *rhr2Δ/Δ* and complemented strains, the RNAseq libraries (non-strand-specific, paired end) were prepared with the TruSeq RNA Sample Prep kit (Illumina, San Diego, CA) per manufacturer's protocol and 100-nt of sequence was determined from both ends of each cDNA fragment using the Hiseq 2000 platform (Illumina, San Diego, CA) per the manufacturer's protocol.

The sequencing reads were aligned to the *C. albicans* reference genomes (SC5314 or WO-1) using TopHat (Trapnell *et al.*, 2009) allowing up to two mismatches per 30bp segment and

removing reads that aligned to more than 20 locations. The alignment files from TopHat were then utilized to calculate the RPKM (reads per kilobase per million mapped reads) for each gene for each sample (Mortazavi et al., 2008). The fold change for each gene was calculated using the normalized RPKM values and the differentially expressed genes were determined after applying a minimum read count cut-off of 10 and minimum fold change of 2X. Differentially expressed gene sets were then compared across experimental replicates to identify groups of that were reproducibly up or down regulated.

#### NanoString data collection and analysis

RNA extracted from the cells harvested after 8 hours planktonic growth in Spider medium was used for NanoString analysis. The data collection was carried out as described previously (Geiss et al., 2008). Data were normalized using *TDH3* expression as a control. The fold-expression change (*rhr2Δ/Δ* vs. *rhr2Δ/Δ+pRHR2*) was calculated for 134 different genes for which hybridization probes were present on the NanoString probeset.

#### Quantitative RT PCR

RNA extracted from the mixed biofilms as well as from the cells harvested after 8 hours planktonic growth in Spider/Spider-glycerol medium was used for NanoString analysis. 10 µg RNA was rendered DNA-free using a kit (Ambion). The DNA-free RNA was then used to synthesize cDNA using the AffinityScript multiple temperature cDNA synthesis kit (Stratagene). A control reaction was included, in which reverse transcriptase was omitted to ensure the absence of DNA contamination. 2X iQ SYBR Green Supermix (Bio-Rad), 1 µl of first-strand cDNA reaction mixture, and 0.1 µM of primers were mixed in a total volume of 25µl per reaction. Real-time PCR was performed in triplicate using a CFX Connect Real-Time System (Bio-Rad). The program for amplification had an initial denaturation step at 95°C for 5 min, followed by 40 cycles of 95°C for 45 s and 58°C for 30 s. Product amplification was detected using SYBR Green fluorescence at the end of the 58°C step. Gene expression was determined using Bio-Rad iQ5 software ( $\Delta\Delta CT$  method), with *TDH3* and *16S RNA* expression used for normalization.

### Adherence analysis

The different mutant strains were analyzed for their ability to adhere to an abiotic silicone substrate as described by Finkel et al (Finkel et al., 2012). Briefly, the Fluxion Bioflux 200, equipped with a microscope, was used for adherence analysis. This set-up allows a constant flow of cells through microfluidic channels. The strains under analysis were grown overnight in YPD medium at 30°C and after dilution to an OD<sub>600nm</sub> of 0.2 they were loaded for the assay. After 30 minutes of flow through microfluidic channels, cells adhered to the silicone substrate in channels were visualized with microscope. Two photographs per channel were taken and the number of adhered cells was quantified. Average values from two channels (per strain) were computed. For different mutant strains, these values were compared with the values obtained for control strains (Wild type strain-DAY185 as a positive control and *bcr1Δ/Δ*-CJN702 as a negative control). A ratio of average number of adhered cells for mutant vs. wild type was calculated and plotted for comparative analysis.

### Confocal imaging of biofilms

The strains under analysis were grown overnight in YPD/YP-glycerol media at 30°C. The overnight cultures were used to inoculate 2 mL spider/spider-glycerol media at OD<sub>600</sub> of 0.5, containing silicone square (1.5sqcm) pretreated overnight with fetal bovine serum (FBS). The cells were adhered to silicone by incubating for 90 minutes in an incubator-shaker at 60 rpm and 37°C. After 90 minutes the cells not adhering to substrate were washed off with phosphate buffer saline (PBS) and the squares were then placed in fresh spider/spider-glycerol media. After incubation for 24 hour at 37°C with 60 rpm agitation, the medium was aspirated out and the formed biofilms were fixed by placing the squares in 4% formaldehyde for 30 minutes. The fixed biofilms were stained with 25µg/mL of Alexa594-fluor conjugated ConcanavalinA in PBS for 60 minutes in dark with gentle agitation. The fixed, stained biofilms were then analyzed via confocal microscopy. For the purpose of confocal imaging on an inverted microscope, a dish had been designed to contain a cover glass fused at center with double-sided tapes spaced about 1.3cm

apart from each other. This arrangement allowed spacers (tapes) to hold the silicone square with the grown biofilms facing towards cover-glass, without any significant perturbation to the three dimensional architecture. The biofilms were imaged with a Zeiss LSM 510 Meta/DuoScan inverted spectral confocal microscope using a 40x/1.2NA-water immersion objective with the laser line at 561 nm. The Zen 2009 software was used to obtain the desired Z-stack images. For thick biofilms where attenuation of signal due to light scattering was significant at greater depths, the Z-stacks were collected in multiple parts with higher laser power and gain-settings. The serial image stacks were processed in FIJI (<http://rsbweb.nih.gov/ij/>) for correction of intensity loss due to light scattering in thick biofilm samples. The shown apical view projections were computed from the intensity corrected image stacks using temporal color code plugin. For computing side-view projections, the intensity corrected serial image stacks were resliced from bottom to top and then maximum intensity projection method was used under the Z-project command provided by FIJI (<http://rsbweb.nih.gov/ij/>).

#### Virulence assay

The virulence for different strains was assayed using the mouse oropharyngeal candidiasis (OPC) model (Kamai et al., 2001). Briefly, 5 days post infection, the mice were euthanized and the tongue tissues were removed. The tissues were homogenized and analyzed to determine colony-forming units. For histopathological analyses, tissue samples were fixed with formalin and embedded in paraffin for thin sectioning. The tissue sections were then stained with periodic acid Schiff (PAS) for further analysis.

#### In vivo biofilm assay

For *in-vivo* analysis of biofilm formation, the rat venous catheter model was used (Andes et al., 2004). Briefly, 24 hours post inoculation, the catheters were removed and the biofilms formed in the lumen of catheters were imaged via scanning electron microscopy. Final images were assembled in FIJI (<http://rsbweb.nih.gov/ij/>).

### Biofilm biomass estimation

Biofilms were grown as described above with an exception that they were allowed to grow for 48 hours instead of 24 hours. After 48 hours, medium was aspirated out and the silicone squares containing biofilms were gently washed with PBS. After washing, the squares were placed in wells of a new plate at slightly slanted position for drying. The biofilms containing silicone squares were dried for 48 hours and weighed individually for estimation of biomass.

### Glycerol assay

The strains (Wild type, *rhr2Δ/Δ* and *rhr2Δ/Δ+pRHR2*) were grown overnight in YPD at 30°C. The overnight cultures were used to inoculate 4 mL Spider medium, contained in wells of 6-well polystyrene plates (Costar 3736 6-well untreated plates; catalog number 07201588) pretreated overnight with fetal bovine serum (FBS). The strains were inoculated at OD<sub>600</sub> of 0.5. The cells were allowed to adhere for 90 minutes in an incubator-shaker at 35 rpm and 37°C. After 90 minutes the cells not adhering to the well bottom were washed off with phosphate buffer saline (PBS). Fresh Spider medium was then added to each well and incubation was continued for additional 48 hours, which resulted in biofilm formation. Biofilms were harvested by scraping the bottoms using a cell scraper. The cell suspensions from six wells were combined together and then filtered on Millipore filters using a vacuum manifold. The filters containing cells were immediately transferred to boiling 0.5M Tris-HCl (2mL) for glycerol extraction as described previously [138]. The boiling continued for 10 minutes. The suspension was then centrifuged at 5000rpm for 1 minute. The supernatant was collected for glycerol measurements, while the pellet was saved for weighing to normalize glycerol levels across different samples. Glycerol quantification was performed using the glycerol assay kit (Boehringer Mannheim 10 148 270 035), as per the manufacturer's instructions.

### Caspofungin sensitivity assay

Overnight cultures were grown in YPD media at 30°C. The following day the OD<sub>600</sub> was measured for all the strains and cultures were diluted to an OD of 1 in sterile water. The OD = 1 stock was then used to prepare five different, 1:5 serial dilutions. Volumes of 3 µL were spotted on YPD plates containing 125 ng/mL caspofungin. Growth was continued for 48h, after which the plates were digitally photographed.

# Active penetration by *Candida albicans* hyphae

## Introduction

The commensal *Candida albicans* is responsible for diverse mucosal, systemic and disseminated infections. The cylindrical, filamentous hyphal cells contribute significantly to *Candida*'s pathogenic potential. These hyphae express numerous adhesins on their surface, which mediate adherence to epithelial, endothelial and abiotic surface (Finkel and Mitchell, 2011; Zhu and Filler, 2010). Adherence is the first step towards establishing a foothold for biofilm formation and invasion. Hyphae from biofilms, whether mucosal or abiotic, invariably invade the underlying surface (Brand, 2012). For *C. albicans*, invasion has been investigated by growing fungi in contact with epithelial cell monolayers or with reconstituted human epithelium (Wachtler et al., 2012; Zhu and Filler, 2010). These studies have revealed two modes of hyphal invasion. The first, which has been examined in detail, is the passive way in which *C. albicans* hypha induces its own endocytosis via the surface invasins, Als3 and Ssa1 (Phan et al., 2007; Sun et al., 2010; Zhu and Filler, 2010). These invasins activate the actin-mediated endocytic pathway via engaging in interactions with E-cadherin and EGFR/HER2 on epithelial surface (Phan et al., 2007; Zhu et al., 2012). The second mechanism is an active mechanism where *C. albicans* hyphae actively invade via combined actions of force exertion and lytic enzyme secretion. This mechanism of invasion has remained incompletely understood. For active invasion, the role of lytic enzymes, such as the **S**ecreted **a**spartyl **p**roteinases (**Saps**), has been assessed by observing epithelial invasion for the null mutants in single or multiple genes of the *SAP* family (Correia et al., 2010; Lermann and Morschhauser, 2008) (Dalle et al., 2010). Altogether these studies have revealed that the *SAP* mutants have defects in some in vitro models but not others (Dalle et al., 2010; Lermann and Morschhauser, 2008). Additionally, Dalle et al. observed that the epithelial cell invasion defect for the *sap4-6* triple deletion mutant persists even for the killed hyphae (Dalle et al., 2010). Based on this observation they suggested a role for *SAP4-6* in

passive invasion as well. Thus, the exact contribution of *SAP* genes in active invasion has still remained unclear.

Unlike the lytic invasion, the forceful mechanism of turgid invasion has not been examined in detail. This mechanism for invasion is clearly operational in *C. albicans* as, in addition to the mucosal invasion, the hyphal invasion was observed in the abiotic surfaces of medically implanted devices as well (Brand, 2012; Leonhard et al., 2010). This mode of invasion has been well studied in *Magnaporthe oryzae*, the pathogenic fungus responsible for rice blast disease (Almeida et al., 2009; Bastmeyer et al., 2002). This fungus forms a special melanized cell structure called “appressorium” which, upon adherence to the surface, initiates invasion when fresh water is provided. The appressorium generates enormous turgor via glycerol accumulation that drives a penetration peg through an underlying leaf surface. Although a similar mechanism has been suggested for *C. albicans*, it has not been characterized in detail (Brand, 2012).

In this chapter, I address the mechanism of forceful hyphal invasion. I first provide a theoretical model for hyphal invasion. I then used elastic polyacrylamide hydrogels for invasive biofilm growth to validate the predictions made by our theoretical model. Using this assay, I established a role for glycerol-mediated turgor in invasion. In order to further probe the genetic requirements for invasion, I used a panel of transcription factor mutant strains to identify mutants defective in invasion, which revealed several processes that play roles in invasion. I further dissected roles of turgor, substrate adherence, biofilm formation and hyphal morphology in invasion using a panel of genetically engineered strains.

## Results

### Theoretical modeling for hyphal invasion in an infinite elastic solid

We can assume the substratum for hyphal invasion as an infinite elastic solid of elastic modulus **G**. Let us suppose the radius of an invading hypha is  $r_0$ . In that case we can consider hyphal invasion as a procedure that makes and expands a borehole. If we consider the borehole expansion, in an infinite elastic solid, from a finite radius  $R_0$  to  $r_0$  to occurs under pressure **P**, then the relation for expansion is as given below (contributed by Lanni, F.):

$$r_0 = R_0 \left( \sqrt{\frac{G}{G - P}} \right) \quad \dots(1)$$

where,  $r_0$

= internal radius of the substratum material points demarcating the borehole after expansion

$R_0$  = internal radius of the substratum material points after expansion

$G$  = elastic modulus of the substratum

$P$  = pressure applied for expansion

This equation shows that, for any nonzero radius  $R_0$  and any pressure less than the modulus **G**, a finite expansion will take place. Additionally, this equation shows that an expansion to the full hyphal radius from  $R_0 = 0$ , i.e. invasion initiation, is possible for  $P = G$ . This suggests that if a mechanism exists to generate turgor equivalent to the elastic modulus of substratum, invasion is possible (Lanni, F.).

If we consider the hypha as a cylinder with an elastic cell wall of elastic modulus  $E_{cw}$ , then hyphal growth can be explained by plastic deformation at the tip, similar to plant cells (Lockhart, 1965; Proseus et al., 1999) and fission yeast growth models (Minc et al., 2009). In this case, the turgor above a critical value,  $P_c$ , deforms the plastic wall irreversibly for tip-extension. For invasive

growth, the hypha has to expand against the elastic material of modulus,  $G$ . Under this condition, the invasive growth rate depends on the effective turgor pressure  $P_{eff}$ , where,

$$P_{eff} = P - (P_c + G) \quad \dots(2)$$

where,  $P$  = total turgor

$P_c$  = critical stress above which plastic extension of the cell wall takes place

$G$  = elastic modulus of the substratum

Similar to the plant cell growth models proposed by Lockhart (Lockhart, 1965) and Ortega (Proseus et al., 1999), the rate of growth:

$$\frac{1}{V} \frac{dV}{dt} = \phi P_{eff} + \frac{1}{E_{cw}} \frac{dP_{eff}}{dt} \quad \dots(3)$$

where,  $\frac{1}{V} \frac{dV}{dt}$  = relative rate of volumetric growth

$\phi$  = cell wall extensibility, describing the irreversible extension for  $P > P_c + G$

per unit pressure per unit time

$E_{cw}$  = cell wall elastic modulus

$\frac{dP_{eff}}{dt}$  = change in pressure with time.

In the case when the cell maintains constant osmolarity during growth, the second term of equation (3) is zero. Additionally, we can rewrite the equation for axially tip growing hypha, in terms of hyphal cell length, as given below:

$$\frac{1}{\pi r_0^2 L} \frac{\pi r_0^2 dL}{dt} = \phi P_{eff}$$

...(4)

where  $r_0$  and  $L$  are hyphal radius and length respectively.

$$\frac{dL}{dt} = L \phi P_{eff}$$

...(5)

Upon rearrangement and integration we get the following:

$$L_t = L_0 e^{(\phi P_{eff} t)}$$

...(6)

Our observations with invading hyphae show that the invading hyphae have septa, thus they would have undergone mitosis. We can assume that while invading, the tip extends, then stops, undergoes mitosis and septates. The new tip cell then continues the growth process. Under our tacit assumption, all the cells in a hyphal chain, except the one at the tip, go to  $G_0$  state. Hence, the growth curve for a single hyphal chain would contain a series of exponential “spurts”, each of the duration  $T_{cc}$ , the cell-cycle period. An overall plot of hyphal length vs. time would look similar to a series of exponential “spurts” arranged in tandem. The mean slope would represent the change in hyphal length per  $T_{cc}$ , which is the speed of invasion,  $v_i$ .

$$v_i = \frac{L_{t_{cc}} - L_0}{T_{cc}}$$

...(7)

where,  $L_0 =$  effective initial length of a new cell at tip

$T_{cc} =$  cell cycle period

Substituting  $L_{t_{cc}}$  using a form of equation (6),

$$v_i = \frac{L_0(e^{(\phi T_{cc})} - 1)}{T_{cc}}$$

...(8)

The exponential part can be linearized, considering  $e^{(\phi T)}$  is not too large.

Hence,  $e^{(\phi P_{eff} T_{cc})} = 1 + (\phi P_{eff} T_{cc}) + \dots$

Taking the first two terms,

$$v_i = L_0 \phi P_{eff}$$

...(9)

At time  $t$ , an average overall hyphal length,  $L_h$ :

$$L_h = v_i t = L_0 \phi P_{eff} t$$

...(10)

Substituting  $P_{eff}$  from equation (2) and rearranging yields,

$$L_h = L_0 \phi t (P - P_c - G)$$

...(11)

If the experimental variable is the substratum elastic modulus:  $G$ , equation (11) can be put in a form of an equation of line:

$$y = c + mx; \text{ where } c = L_0 \phi t (P - P_c) \text{ and } m = -L_0 \phi t$$

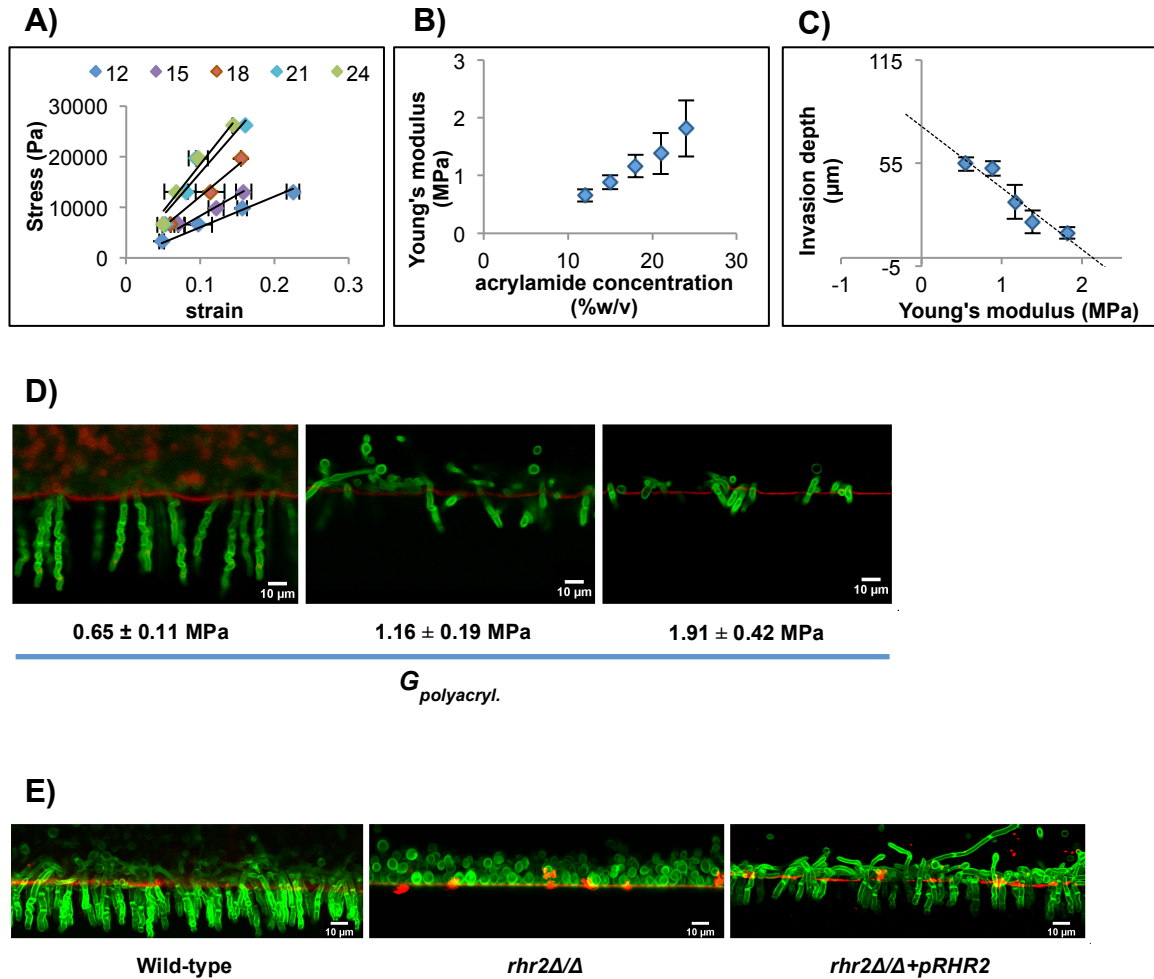
...(12)

Thus, at a specified time,  $t$ , the invasion depth,  $L_h$ , decreases linearly with an increase in elastic modulus of substratum ( $G$ ).

In order to verify this experimentally, we employed polyacrylamide hydrogel as an elastic substratum to analyze invasion. We varied the elastic modulus of polyacrylamide by varying acrylamide concentration with a constant concentration of bisacrylamide. We assessed elastic moduli by measuring strain in response to the tensile stress applied by hanging weight on strips of polymerized gel. These yielded linear stress-strain curves as shown in Figure 7(A). The moduli were in range of 0.6-1.9 MPa for gels with acrylamide concentrations ranging from 12%-24%, as shown in Figure 7(B). We then grow biofilms on these gels and optically determined hyphal invasion depth. In order to correctly assess the invasion depth, we marked the gel surface layer with fluorescent microparticles, as shown in red in Figure 7(D). We then measured the hyphal invasion depth from the fluorescently marked surfaces. According to our model, Figure 7(C) represents a linear decrease in the hyphal invasion depth with an increase in substrate elastic modulus, which suggests that invasive growth essentially depends on the effective hyphal turgor. Additionally, the line showing linear fit to the data in Figure 7(C), can be extrapolated to the horizontal axis. The value of this intercept yields the maximum turgor a hypha can attain. Our plot shows that the hyphae attain at least 2 MPa (20 atm).

Which osmolyte accounts for turgor in hyphae? Glycerol is an obvious candidate, as many plant pathogenic fungi employ glycerol to generate turgor while forcing a penetration peg through an underlying leaf cuticle (Bastmeyer et al., 2002). *C. albicans* accumulates significantly higher glycerol while growing on surfaces as a biofilm (Desai et al., 2013; Zhu et al., 2013) and hyphae in biofilms often invade the underlying surface (Brand, 2012). To examine a role for glycerol in invasion, we used *rhr2Δ/Δ*, which accumulates significantly less glycerol than the wild-type strain in biofilms. The *rhr2Δ/Δ* strain was completely defective in invading polyacrylamide, as shown in Figure 7(E). Reintegrating one copy of the *RHR2* back in *C. albicans* restores the invasion, implying a gene-specific role.

**Figure 7: *Candida albicans* hyphae employ turgor to invade an elastic substratum.**



(A) Stress-strain curves for the four different polyacrylamide hydrogel substrates. Four different hydrogels were polymerized where acrylamide was used at 12, 18, 21 and 24% w/v while bisacrylamide was used at a constant concentration of 0.5%w/v. The legend on right shows markers corresponding to different hydrogels made by using different % of acrylamide. The horizontal error-bars mark standard deviation in strain values.

(B) Young's moduli for the four different hydrogels. Young's moduli were computed as the stress/strain ratios from the data displayed in Figure 7(A). The error-bars mark standard deviation in moduli values.

(C) Depth of hyphal invasion with respect to substrate's modulus of elasticity. The hyphal invasion depths were measured from the collected images. Such images are shown in Figure 7(D), where linear distances from the substrate surface to invading hyphal end were measured using FIJI (<http://fiji.sc/Fiji>). The error-bars mark standard deviation values from at-least 5 different images obtained from different hydrogel discs. The dotted line is a linear best fit.

Figure 7 (D) Confocal micrograph of *C. albicans* invasive growth into elastic hydrogels of increasing modulus of elasticity ( $G_{polyacryl.}$ ). The circular polyacrylamide discs, containing *C.*

*albicans* biofilms, were fixed with 4% formaldehyde and subsequently co-incubated with 0.185 mg/mL Calcofluor white and 0.05% green FluoSpheres in 1x PBS. Roughly 1-2 mm sized strips were then cut across the disc diameter, with a sharp razor and the strip is laid over a cover-glass, housed within a culture dish. Single images were taken for each specimen using 405 and 488nm laser lines. The images were compiled in ImageJ and pseudo-colored green and red, for Calcofluor stained cell wall and FluoSpheres-marked surface, respectively. The numbers at bottom mark  $G_{polyacryl}$  for the different hydrogels. The scale-bars are shown at bottom right.

(E) Glycerol deficit results in complete invasion defect. Biofilms of the indicated strains were grown on polyacrylamide, polymerized with 18%/0.5% (acryl./bis.). The gel specimens for imaging were prepared as described above. Serial stacks of images were acquired for specimens indicated at the bottom of images. The image stacks were then processed in ImageJ and the maximum intensity projections from equally thick stacks were computed for display. The scale-bars are displayed at the bottom of each image panel.

### Genetic control of invasive growth

In order to determine which cellular processes play important roles in invasive biofilm growth, we screened a panel of 150 transcription factor mutant strains of *C. albicans* (Homann et al., 2009). Our rationale behind using transcription factor mutants was straightforward. The transcription factors regulate a common set of redundant genes involved in a diverse array of processes. Many of these processes have been associated with specific transcription factors for their regulation. Thus transcription factor mutants can help to uncover the processes important for biofilm invasive growth. Using this screen we uncovered 9 TF mutants to be defective in invasion, as described under Table 1. Among these: *BRG1*, *NDT80*, *EFG1*, *TEC1* and *ROB1* are known regulators of biofilm formation, hyphal formation and virulence (Finkel and Mitchell, 2011; Fox and Nobile, 2012; Ramage et al., 2002a). Although not surprising, these results validate the role of active invasion in virulence. One other mutant, *dpb4Δ/Δ* was also severely defective in biofilm formation and invasion. It has been shown recently that *DPB4* has roles in mitochondrial DNA maintenance, ribosome biosynthesis, and other indirect roles in alternate carbon source utilization (Khamooshi et al., 2014). It is, however, not clear if it plays any role in biofilm formation. The remaining three mutants: *sfl2Δ/Δ*, *upc2Δ/Δ* and *lys14Δ/Δ*, were not defective in biofilm formation, but they had severe to moderate defects in invasion. *UPC2* has roles in regulating genes involved in ergosterol biosynthesis and hypoxic growth (Synnott et al., 2010). It is possible that polyacrylamide may impose hypoxia, and thus *upc2Δ/Δ* may have a defect in invasive growth. The defect showed by *lys14Δ/Δ* was moderate, both for biofilm formation and invasion. It has been shown recently that Lys14 binds to promoters of several cell-surface localizing proteins/enzymes' encoding genes (Perez et al., 2013). It is possible that alterations in cell wall are responsible for the observed defects.

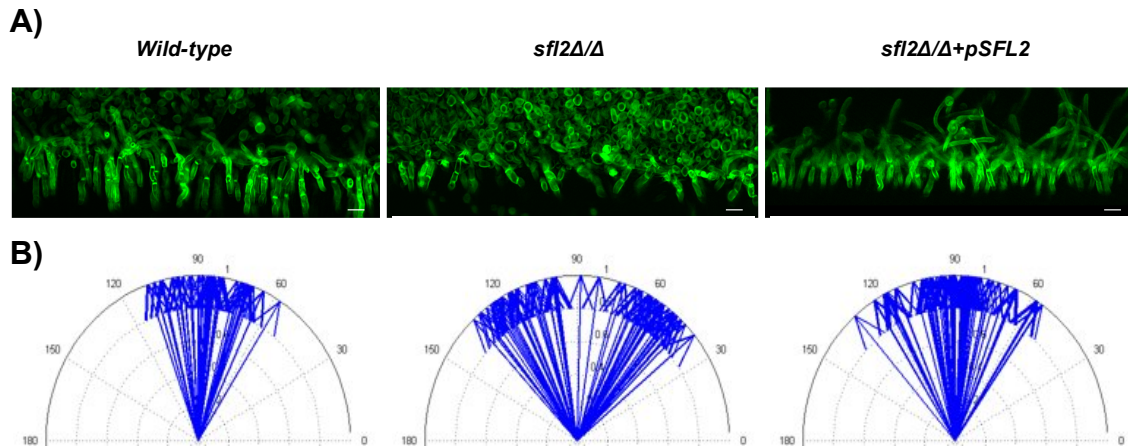
*SFL2* has a role in normal hyphal morphogenesis (Znaidi et al., 2013). The invasion defect shown by its mutant, *sfl2Δ/Δ* was extremely interesting. The hyphae were invading at minimal depth with random penetration orientations, as shown in Figure 8A). We therefore measured invasion angle from substrate surface for the wild type, mutant and complemented strains. As shown in Figure 8(B), the invasion angles show a very wide distribution for the mutant, as

compared to the narrower distribution, centered around 90°, for wild-type. The complemented strain showed restoration to the wild-type phenotype. Hyphal orientation depends on Ca<sup>2+</sup> signaling (Brand and Gow, 2009). Under normal circumstances, it is possible that invading hypha secretes some repellent small molecule that acts through the Ca<sup>2+</sup> signaling components and maintains negative autotropism (the mutual separation of invasive hyphae). The *sfl2Δ/Δ* may either have a defective reception for this hypothetical repellent molecule or it may have defects in generating or secreting the molecule. It may also be possible that the mutant has defects in thigmotropism. These hypotheses remain to be tested.

**Table 1: Transcription factors encoding genes that have a role in hyphal invasion.**

<b>Gene</b>	<b>Mutant phenotype</b>	<b>Functional description from the <i>Candida</i> genome database</b>
<i>BRG1</i>	Complete defect in biofilm formation and invasion	Transcription factor; recruits Hda1 to hypha-specific promoters; <b>Tn mutation affects filamentation</b> ; Hap43-repressed; Spider and flow model biofilm induced; <b>required for Spider biofilm formation</b> ; Bcr1-repressed in RPMI <i>a/a</i> biofilms
<i>EFG1</i>	Complete defect in biofilm formation and invasion	bHLH transcription factor; required for white-phase cell type, <b>RPMI and Spider biofilm formation, hyphal growth</b> , cell-wall gene regulation; roles in adhesion, virulence; Cph1 and Efg1 have role in host cytokine response; binds E-box
<i>TEC1</i>	Complete defect in biofilm formation and invasion	TEA/ATTS transcription factor; white cell pheromone response, <b>hyphal gene regulation; required for Spider and RPMI biofilm formation</b> ; regulates <i>BCR1</i> ; Cph2 regulated transcript; alkaline, rat catheter, Spider, flow model biofilm induced
<i>NDT80</i>	Complete defect in biofilm formation and invasion	Ortholog of Ndt80; meiosis-specific transcription factor; activator of <i>CDR1</i> induction by antifungal drugs; required for wild-type drug resistance and for <b>Spider biofilm formation</b> ; transcript induced by antifungal drug treatment
<i>ROB1</i>	Complete defect in biofilm formation and invasion	Zn(II)2Cys6 transcription factor; <b>required for Spider model biofilm formation</b> ; mutant displays abnormal colony morphology and invasive growth; caspofungin repressed; flow model biofilm induced; rat catheter biofilm repressed
<i>DPB4</i>	Complete defect in biofilm formation and invasion	Putative DNA polymerase epsilon subunit D; null mutant is viable but slow-growing and displays abnormal invasive growth on SD and YPD media; Spider biofilm repressed
<i>SFL2</i>	Moderate defect in biofilm formation. Hyphal penetration to minimal depth with randomly oriented invasive hyphae unlike the exclusive parallel invasive phenotype of the wild-type strain.	Transcription factor involved in regulation of morphogenesis; <b>required for filamentous growth</b> , for virulence in reconstituted human epithelium (RHE) model but not in mice; induced upon RHE infection but <i>C. dubliniensis</i> ortholog is not; Spider biofilm induced
<i>UPC2</i>	Moderate defect in biofilm formation with complete defect in invasion	Zn2-Cys6 transcript factor; regulator of ergosterol biosynthetic genes and sterol uptake; binds <i>ERG2</i> promoter; induced by ergosterol depletion, by azoles, anaerobicity; macrophage/pseudohyphal-repressed; flow model biofilm induced
<i>LYS14</i>	Moderate defect in biofilm formation with decreased hyphal invasion depth	Zn(II)2Cys6 transcription factor; binds to promoters of several cell surface localizing proteins or enzymes with cell-wall modifying activities; <b>decreased fitness in systemic infection model</b>

**Figure 8: SFL2 functions in invasive hyphal orientation.**



(A) Invasion defect of *sfl2Δ/Δ*. Imaging of invading hyphae was performed as described under Figure 7's captions.

(B) Invasion angle quantification. The angles of invasions were measured using ImageJ for at least 30 hyphae, from at least 3 different hydrogel specimens. The compass plots shown here indicates individual hyphal angle with a single arrow. These were constructed in MATLAB by converting the Cartesian angle data for each hypha to polar coordinates with unit vector length.

### Biofilm formation and filamentation are necessary, but are not sufficient for invasion

As discussed above, biofilm formation and hyphal morphogenesis are important determinants for invasion. In the physical context, the biofilm serves as an adherent structure that provides an unyielding mechanical support for the buried hyphal cells, priming them for turgid invasion, as shown in Figure 9(A). If this is true, non-turgid cells should not invade, even if they are hyperadherent or constitutively filamentous. The glycerol-deficient mutant, *rhr2Δ/Δ*, provides us a valuable strain to address the question. I overexpressed a set of genes in *rhr2Δ/Δ* background to yield strains with aforementioned properties. *ALS1* encodes a cell-surface adhesin and its overexpression in *rhr2Δ/Δ* is known to yield a strain that has restored substrate adherence and biofilm formation (Desai et al., 2013). In our system the *ALS1* overexpression rescued biofilm formation, as shown in Figure 3.3(B). Overexpression of the biofilm regulator, *BRG1* (Nobile et al., 2012) and the hyphal regulator *UME6* (Carlisle et al., 2009), in *rhr2Δ/Δ* leads to constitutive hyphal formation by the resultant strains. As shown in Figure 9(B), these strains formed confluent biofilms, possibly resulting from up regulation of adhesins and hyphal genes. Consistent with our idea, these adhesins were up regulated, as shown in Figure 9(C). Overexpression of *BCR1*, however, did not rescue biofilm-formation. Bcr1 regulates expression of *ALS3*, *HWP1* and other adhesins (Nobile and Mitchell, 2005). In *rhr2Δ/Δ*, however, *BCR1* overexpression does not induce *ALS3* and *HWP1* expression, as shown in Figure 9(C). Hence, it is possible that the activity of Bcr1 is dependent upon intracellular glycerol, however it requires further examination.

Together, the overexpression strategy provided us an arsenal of strains, which were possibly less turgid (due to defect in glycerol accumulation), yet hyper-adhesive and constitutively filamentous. When tested for invasion in polyacrylamide, consistent with our expectation, they showed none to minimal invasion. As shown in Figure 9(D), neither the adhesin- nor the TF- overexpression strains restored the invasion. These data support our model that biofilm provides a mechanical support for the buried hypha to invade, if and only if it can generate enough turgor.

**Figure 9: Biofilm hyphae defective in glycerol accumulation cannot invade.**

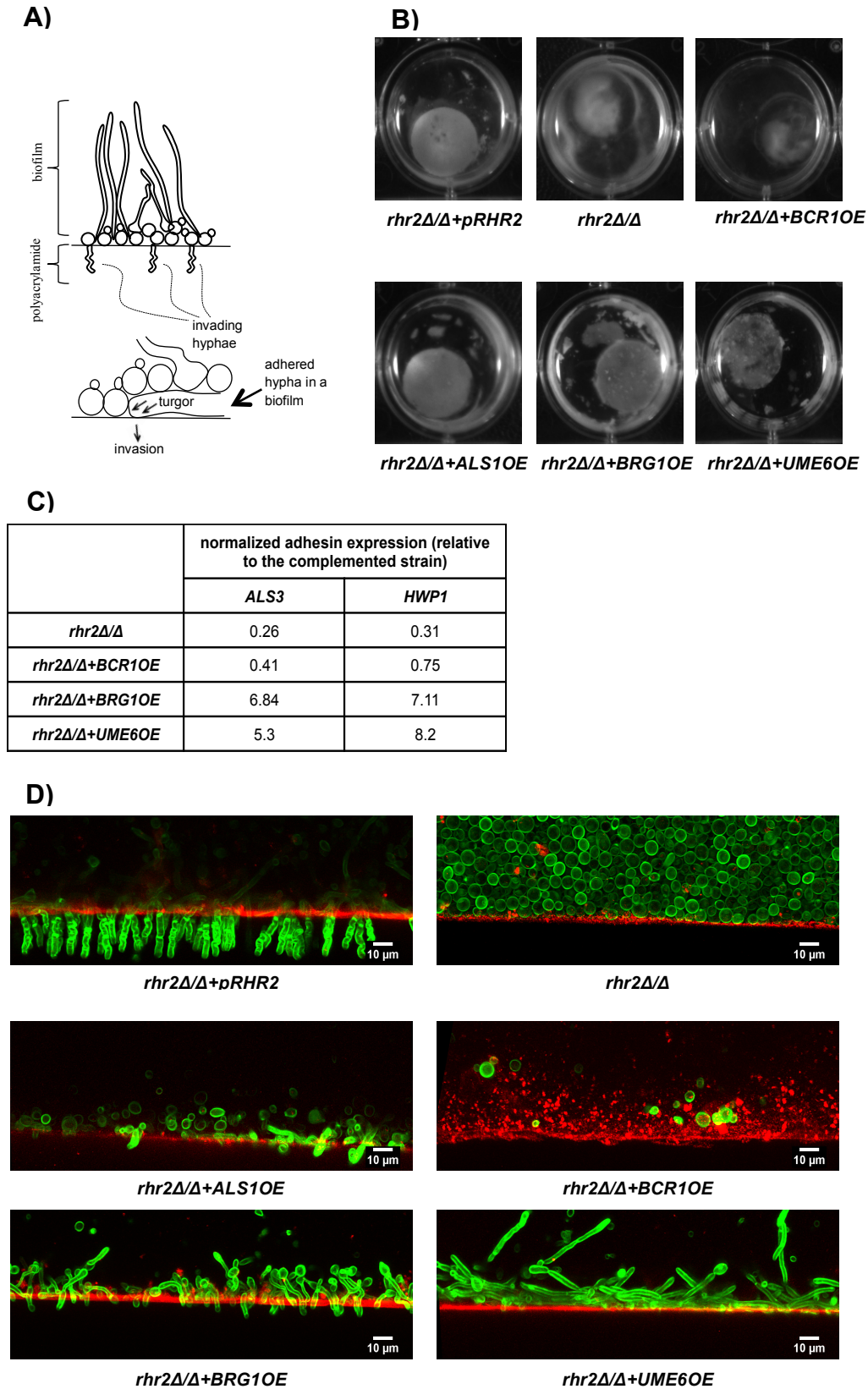


Figure 9 (A) Schematic representation of hyphal invasion in a biofilm.

(B) Biofilm formation on polyacrylamide discs. Biofilms for the indicated strains were grown on 18%/0.5% (acryl./bisacryl.) polyacrylamide gel discs. After 48h of growth the biofilms were photographed.

(C) Gene expression analysis. Cells were grown in YPD with 10% fetal bovine serum for the indicated strains for 8 hours. These cells were harvested for RNA isolation. RT-qPCR was performed to determine relative expression. Data were normalized using *TDH3* expression as normalization standard. The normalized data were then used to compute expression changes relative to the *RHR2* complement.

(D) Confocal micrographs of invading hyphae. Biofilms of the indicated strains were grown on polyacrylamide, polymerized with 18%/0.5% (acryl./bis.). The gel specimens for imaging were prepared as described under captions for Figure 7. Serial stacks of images were acquired for specimens, obtained by growing the *C. albicans* strains indicated at the bottom of images. The image stacks were then processed in ImageJ and the maximum intensity projections from equally thick stacks were computed for display. The scale-bars are displayed at the bottom of each image panel. The strains used were: wild type (DAY185), JVD006 (*rhr2Δ/Δ+pRHR2*), JVD005 (*rhr2Δ/Δ*), JVD018 (*rhr2Δ/Δ+ALS1-OE*), JVD039 (*rhr2Δ/Δ+BCR1-OE*) and JVD051 (*rhr2Δ/Δ+UME6-OE*), JVD065 (*rhr2Δ/Δ+BRG1-OE*) respectively.

## **Discussion**

We have described the forceful mode of hyphal invasion for *C. albicans*. We show that glycerol provides a way for hyphae to invade. The hyperadherent hyphae in biofilms, if defective in glycerol accumulation, cannot invade. In order to probe the significance of the turgid-invasion mechanism in context of disease, we employed the mouse intraabdominal candidiasis model. We observed that turgor is necessary to precipitate intra-abdominal candidiasis as well (Cheng, S., personal communication). In vivo, however, the requirement of glycerol and turgor in causing disease seems to be niche-specific and highly dependent on the host cell-type. For example, at the intestinal epithelia, turgid invasion should be the primary mechanism for causing disease, as the epithelium-lining enterocytes do not endocytose the hyphae (Dalle et al., 2010). Additionally, the turgid invasion should be glycerol-dependent as the glycerol-biosynthetic gene- *GPD1* was highly up regulated in the intra-abdominal infection model (Cheng et al., 2013). Indeed, our preliminary data support the role of glycerol-mediated forceful hyphal invasion to precipitate intra-abdominal infection. On the other hand, the oral epithelial cells support induced-endocytosis of *C. albicans* hyphae. Thus, at oral epithelia, forceful invasion should be underplayed by *Candida* (Dalle et al., 2010). Indeed, it has been observed that the *rhr2Δ/Δ* mutant was not defective in virulence in the mouse OPC model (Desai et al., 2013).

*C. albicans* can avoid glycerol for turgid invasion at some niches where it can obtain other osmolytes from the environment. For example, in kidney, the osmolyte glycerophosphocholine is abundantly available. Thus in kidney, *C. albicans* should not require glycerol biosynthesis for invasion. Indeed, during disseminated infection to the kidney, the glycerol-biosynthetic genes are the most down-regulated genes (Xu, W. unpublished data). Additionally, a mutant lacking the glycerophosphocholine transporter, *GIT1*, is defective in virulence in the disseminated infection model (Bishop et al., 2013), supporting our view of niche-specific requirement of turgor and glycerol in causing diseases

How much turgor is required for invasion? The theoretical model and invasion data with a stiff substrate suggest that the invading hypha has to accumulate effective turgor of at-least ~2 MPa

or 20 atm in order to penetrate the stiff gels used in our study. This value is higher than turgor needed for free growth in the fission yeast (Minc et al., 2009). It is possible that *C. albicans* hyphae accumulate higher turgor while invading than free growth. Indeed, *C. albicans* biofilms accumulate higher glycerol than the planktonic cells (Desai et al., 2013; Zhu et al., 2013) and hyphae, if present in biofilms, are prone to invade. A direct experimental turgor measurement is, however, required.

Our observations with *rhr2Δ/Δ* and invasion-defective transcription factor mutants suggest that biofilm formation and hyphal morphology are required for invasion. The correlation between defects in biofilm-formation and invasion is expected, as a defect in biofilm-formation leads to lesser number adherent-cells, hence lesser invasion. Similarly, the invading cells are always hyphae, therefore a correlation between hyphal defect and invasion is expected as well. The hyphae, however, cannot invade, even when enmeshed in a biofilm if they cannot accumulate glycerol. Our experiments with strains overexpressing the biofilm-regulator (*BRG1*), hyphal-regulator (*UME6*) and an adhesin (*ALS1*) support this argument.

The additional determinants for invasion include the proteins affecting cell wall structure at invading hyphal-tip such as, the cell wall modifying enzymes, the vesicle delivery system and regulators of both of these (Sudbery, 2011). According to the theoretical model, all these components can affect the cell wall extensibility ( $\phi$ ), which has a major impact on invasion. Our approach provides an easy way to reveal the mutants/pharmacological treatments having an impact on extensibility ( $\phi$ ). The approach would simply require analyzing the invasion depth vs. substrate elastic moduli profiles.

In summary, we have provided insights into the forceful invasion mechanism of *C. albicans*, using biophysical approaches, molecular genetics and an animal disease model.

## **Methods**

### Media and Strain Construction

*C. albicans* strains were grown on yeast extract-peptone-dextrose (YPD) medium. For biofilm assays, YPD with 10% fetal bovine serum (FBS) was used. The overexpression strains were constructed as described under the “Methods” section of Chapter 2.

### RNA sample preparation

For gene expression analysis of the strains (wild-type-DAY185, *rhr2Δ/Δ*-JVD005, and *rhr2Δ/Δ+pRHR2*-JVD006, *rhr2Δ/Δ+BCR1OE*-JVD039, *rhr2Δ/Δ+UME6OE*-JVD051 and *rhr2Δ/Δ+BRG1OE*-JVD065) were grown overnight in YPD medium at 30°C. Cells from overnight cultures in YPD medium were added to 50 ml YPD+10%FBS at a final OD<sub>600nm</sub> of 0.2. Cells were grown for additional 8 hours at 37°C with 225 rpm agitation in the incubator. The cells were harvested by filtering the cell suspension on a vacuum manifold. The filters were flash frozen immediately after harvesting each sample. The cells were kept frozen on filters at -80°C until RNA extraction. RNA was extracted using a RiboPure-Yeast kit (Ambion) following the manufacturer’s instructions as described previously (Desai et al., 2013). Briefly, cells were resuspended from filters with 1.5 ml ice-cold distilled water, followed by 15 to 30 s of vigorous vortexing. The resuspended cells were transferred to a 1.5-ml tube and spun down according to the manufacturer’s protocol. During the cell disruption step, the cells were beaten with a Next Advance Bullet Blender for 3 min at 4°C for cell lysis. Post extraction procedure, the RNA was stored -80°C until further use.

### Quantitative RT PCR

10 µg RNA was rendered DNA-free using a kit (Ambion). The DNA-free RNA was then used to synthesize cDNA using the AffinityScript multiple temperature cDNA synthesis kit (Stratagene). A control reaction was included, in which reverse transcriptase was omitted to ensure the absence of DNA contamination. 2X iQ SYBR Green Supermix (Bio-Rad), 1 µl of first-strand cDNA reaction

mixture, and 0.1  $\mu\text{M}$  of primers were mixed in a total volume of 25 $\mu\text{l}$  per reaction. Real-time PCR was performed in triplicate using a CFX Connect Real-Time System (Bio-Rad). The program for amplification had an initial denaturation step at 95°C for 5 min, followed by 40 cycles of 95°C for 45 s and 58°C for 30 s. Product amplification was detected using SYBR Green fluorescence at the end of the 58°C step. Gene expression was determined using Bio-Rad iQ5 software ( $\Delta\Delta\text{CT}$  method), with *TDH3* and *16S RNA* expression used for normalization.

#### Polyacrylamide gel preparation

Stock solutions of acrylamide (Bio-Rad) and bisacrylamide (Bio-Rad) were prepared at concentrations of 35% and 2.5%w/v, respectively. The required volumes were withdrawn and mixed together. Gelatin powder (Sigma) was added at a final concentration of 0.1%w/v to the water, required to make up the final volume. Gelatin was dissolved by heating the gelatin-water suspension in a microwave for ~5-10 seconds. The gelatin solution was then added to the acrylamide-bisacrylamide mixture. To this mixture of acrylamide-bisacrylamide and gelatin, 10x PXS was added such that the final concentration of PBS is 1x. Thus prepared mixture in 1xPBS was then transferred to a petri dish for degassing. Degassing under vacuum was performed in a standard degassing chamber for 30 minutes. After degassing, the polymerization catalysts: TEMED (tetramethylethylenediamine) and APS (ammonium persulfate) were added at concentrations of 0.05%w/v each. The petri dish was swirled gently to mix the contents uniformly. Immediately, the unpolymerized mixture was poured between two glass plates. The glass plates yielding 1.5mm thick gels were utilized. A layer of water-saturated butanol was applied by putting ~500 $\mu\text{L}$  atop the gel. Polymerization was continued for 30mins-1h. The polymerized gels were removed from the molds and washed with distilled water by swirling at low speed on an orbital shaker (5x). These were later trimmed for either biofilm growth or elasticity analysis.

#### Elastic modulus measurement

For elastic moduli measurement, gel strips were cut to 10mm width with a sharp razor. The cut strip was then glued to rectangular pieces of glass slides at both of its ends along the long axis,

using Superglue (cyanoacrylate cement). With the help of paper clips, the gel strip with the glass slides was suspended under gravity. Tensile stress was applied at the free end of the suspending gel-strip by hanging weights from the lower piece of glass. The strain was then measured by recording a change in gel extension in response to two different weights:  $m_1$  and  $m_2$ . The initial length  $L_1$  was recorded with a digital Vernier caliper when the weight  $m_1$  was suspended to stretch the gel. The final length  $L_2$  was recorded the same way when  $m_2$  was suspended to stretch the gel. The strain was calculated as the difference:  $L_2 - L_1$ . At least three strain values were determined for at least three different applied stresses. The resulting data were then used to plot stress-strain curves. The ratio: stress/strain is the Young's modulus.

$$E = (m_2 - m_1)gL_1/A(L_2 - L_1) \quad \dots(13)$$

where,  $E = \text{Young's modulus}$

$(m_2 - m_1) = \text{weight difference}$

$(L_2 - L_1) = \text{strain}$

$A = \text{cross - sectional area of the hydrogel strip}$

$g = \text{gravitational rate constant, } 9.8 \text{ m/s}^2$

### Confocal imaging of invasion

The strains under analysis were grown overnight in YPD at 30°C. The overnight cultures were used to inoculate 2 mL YPD+10%FBS at OD<sub>600</sub> of 0.5 in wells, containing polyacrylamide discs pretreated overnight with fetal bovine serum (FBS). The cells were adhered to polyacrylamide by incubating for 90 minutes in an incubator-shaker at 60 rpm and 37°C. After 90 minutes the cells not adhering to substrate were washed off with phosphate buffer saline (PBS) and fresh YPD+10%FBS was then placed in each well. After an incubation for 48 hour at 37°C with 60 rpm agitation, the medium was aspirated out and the circular polyacrylamide discs, containing C.

*albicans* biofilms, were fixed with 4% formaldehyde (30 minutes) and subsequently co-incubated with 0.185 mg/mL Calcofluor white and 0.05% green FluoSpheres in 1x PBS (1 hour). Roughly 1-2 mm sized strips were then cut across the disc diameter, with a sharp razor and the strip was laid over on its side on a cover-glass, housed within a culture dish. Serial stacks of images were acquired with a Zeiss LSM 510 Meta/DuoScan inverted spectral confocal microscope using a 40x/1.2NA-water immersion objective with the laser lines at 405nm and 488 nm. The Zen 2009 software was used to obtain the desired Z-stack images. The serial image stacks were processed in FIJI (<http://rsbweb.nih.gov/ij/>). The apical view projections were computed from the intensity corrected image stacks. For invasion depth and angle analysis, the standard tools provided by FIJI were employed.

#### Glycerol assay

The strains (Wild type, *rhr2Δ/Δ* and *rhr2Δ/Δ+pRHR2*) were grown overnight in YPD at 30°C. The overnight cultures were used to inoculate 4 mL Spider medium, contained in wells of 6-well polystyrene plates (Costar 3736 6-well untreated plates; catalog number 07201588) pretreated overnight with fetal bovine serum (FBS). The strains were inoculated at OD<sub>600</sub> of 0.5. The cells were allowed to adhere for 90 minutes in an incubator-shaker at 35 rpm and 37°C. After 90 minutes the cells not adhering to the well bottom were washed off with phosphate buffer saline (PBS). Fresh Spider medium was then added to each well and incubation was continued for additional 48 hours, which resulted in biofilm formation. Biofilms were harvested by scraping the bottoms using a cell scraper. The cell suspensions from six wells were combined together and half of the volume was then filtered on Milipore filters using a vacuum manifold. The filters containing cells were immediately transferred to boiling 0.5M Tris-HCl (2mL) for glycerol extraction as described previously (Desai et al., 2013). The boiling continued for 10 minutes. The suspension was then centrifuged at 5000rpm for 1 minute. The supernatant was collected for glycerol measurements, while the pellet was saved for weighing to normalize glycerol levels

across different samples. Glycerol quantification was performed using the glycerol assay kit (Boehringer Mannheim 10 148 270 035), as per the manufacturer's instructions.

The other half of the cell suspension was used to estimate cytosolic volume. The cell suspension was mixed uniformly and then aliquoted to 900 $\mu$ L volumes. To these aliquots, 100  $\mu$ L 1% Blue dextran was added. Similar volume was added to a tube containing just the buffer/medium without the cells. After uniform mixing, the cells were centrifuged at maximum speed for a minute. The supernatant was collected and its absorbance was read at 620nm ( $A_{cells}$ ). An increase in absorbance for Blue dextran in samples containing cells is indicative of the lesser void volume available for Blue dextran ( $V_{Total} - V_{cells}$ ). This void volume was determined using the Beer's equation using  $E^{1\%}$  of 8.9 for dextran blue. The absorbance values of samples not containing cells were also recorded ( $A_{no\ cells}$ ). This value was used to calculate the cytosolic volume:

$$V_{cells} = V_{Total}(1 - A_{no\ cells}/A_{cells})$$

...(14)

# Adhesin-dependent regulation of biofilm maturation

## Introduction

Adhesins are integral to biofilm development in *C. albicans*. In the early phase of biofilm development, adhesins mediate cellular adherence to an underlying substrate (Dranginis et al., 2007; Finkel et al., 2012; Hoyer et al., 2008). As the biofilm matures with appearance of confluent layers of hyphae and extracellular matrix, these adhesins mediate cell-cell adherence (Dranginis et al., 2007; Garcia et al., 2011; Nobile et al., 2008a). Als1 was the first adhesin to be identified, through a heterologous expression screen in *Saccharomyces cerevisiae*, by its ability to confer adherence to the otherwise nonadherent yeast (Fu et al., 1998). Since then many members of the *ALS*-gene family were uncovered to function as adhesins (Hoyer et al., 2008).

Several observations point towards a close functional association between the *ALS*-gene family members and biofilm development. First, many *ALS* genes are up regulated in biofilms (Chandra et al., 2001; Desai et al., 2013; Garcia-Sanchez et al., 2004; Nobile et al., 2012). Second, overexpression of individual *ALS* genes improves biofilm formation by the biofilm defective mutants (Desai et al., 2013; Nobile et al., 2006a; Nobile et al., 2012; Zhao et al., 2006). Third, a strain with both copies of *ALS1* and *ALS3* deleted was defective in biofilm formation in the rat catheter model in vivo (Nobile et al., 2006a). Additionally, a redundant function for the different members of *ALS* members can be proposed as overexpression of any one of them can restore the biofilm formation by *als1Δ/Δ als3Δ/Δ* double mutant (Nobile et al., 2008a).

In addition to their functions in adherence, several other roles have been discovered for many *ALS*-family members. For example, Als3 mediates epithelial and endothelial receptor binding to induce hyphal endocytosis (Liu and Filler, 2011; Phan et al., 2007). It also functions in iron acquisition (Liu and Filler, 2011). Als2, on other hand, serves vital functions in cell wall integrity and viability (Zhao et al., 2005). Additionally, Als2 and Als4 have impacts on cell morphology, as it was observed that the conditional and null mutants in *ALS2* and *ALS4*, respectively, had slower kinetics of hyphal morphogenesis (Zhao et al., 2005).

In this chapter, we focus on the role of Als1. Through comprehensive studies of gene expression under diverse conditions with a set of mutant and genetically engineered strains, Fanning, S. characterized that during *C. albicans* biofilm development, Als1 promotes expression of several maturation-associated genes through the transcription factor, Brg1. My assistance through biofilm imaging provided further substantiation to the argument for the role of Als1 in biofilm maturation. We further proved that the biofilm regulator Bcr1 functions upstream of the maturation-associated Als1-Brg1 pathway.

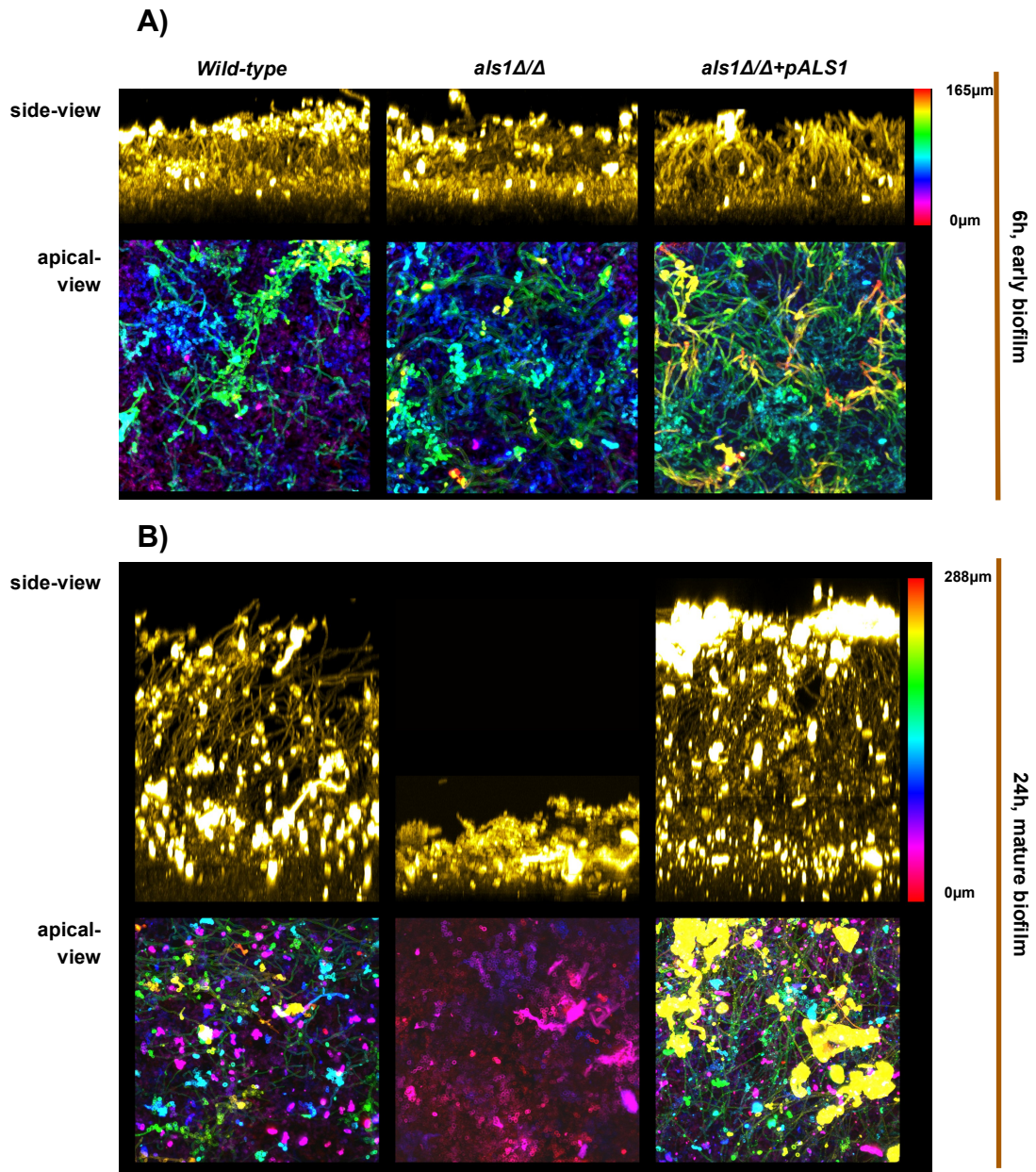
## **Results**

### Role of Als1 in biofilm maturation

As mentioned above, several transcriptomic studies identified higher levels of *ALS1* mRNA in biofilms. The impact of *ALS1* was, however, subtle as determined using null mutants (Nobile et al., 2008a). A possibility cannot be denied where other functionally redundant *ALS* genes may obscure the impact of *ALS1* deletion on biofilm formation. Fanning et al. reported that, in comparison to all the *ALS* genes, *ALS1* mRNA levels were significantly higher in biofilms grown in YPD medium (Fanning et al., 2012a; Fanning et al., 2012b). Therefore, YPD was used to grow biofilms to assay an impact of *ALS1* deletion on biofilm formation. Two different time points were chosen to assess *ALS1* function: 6h and 24h. At 6h, all the strains: the wild type, mutant and complement, formed biofilms to a similar extent. The gross morphologies were similar, as can be seen from the fluorescence micrographs shown in Figure 10(A). As apparent from the side-view projections, the biofilms were of similar thickness. The axial views, pseudo-colored for depth, indicated similar hyphal content with no apparent presence of extracellular matrix. At 24h, however the mature biofilms were significantly different, as shown in Figure 10(B). The biofilms formed by wild type and complemented strains showed the usual morphology of a mature biofilm, i.e. confluence of hyphae and extracellular matrix as well as increased thickness. All these attributes were absent in the *als1Δ/Δ* biofilm. It showed no considerable presence of hyphae and similar was true for the extra cellular matrix. The absence of hyphae was biofilm specific as the *als1Δ/Δ* was capable in hyphal formation under planktonic conditions (Fanning, S.). In order to probe reasons behind the observed impact of *ALS1* on biofilm maturation, Fanning, S. carried out a comprehensive transcription profiling study. Her work demonstrated a novel role for *ALS1* in stimulating expression of several biofilm-related genes, for which induction was previously described at intermediate or mature stage of biofilm development (Desai et al., 2013; Nett et al., 2009). In order to further decipher if the observed transcriptional stimulation by *ALS1* overexpression is *ALS1*-specific, Fanning, S. overexpressed other cell-surface proteins in wild-type. These proteins included: an *ALS* family member (*ALS4*), a highly divergent adhesin

(*HWP1*), and a non-adhesive cell-wall protein-encoding gene (*EXG2*). When examined for gene expression response, the two adhesin-overexpressing strains showed a very similar transcription profile as the *ALS1* overexpression strain. On the other hand, *EXG2* overexpression did not have any stimulatory impact on transcription. Through these experiments, Fanning, S. uncovered a novel phenomenon where adhesin expression switched on the transcription of genes associated with biofilm maturation.

Figure 10: *ALS1* is required for a mature biofilm formation in YPD medium.

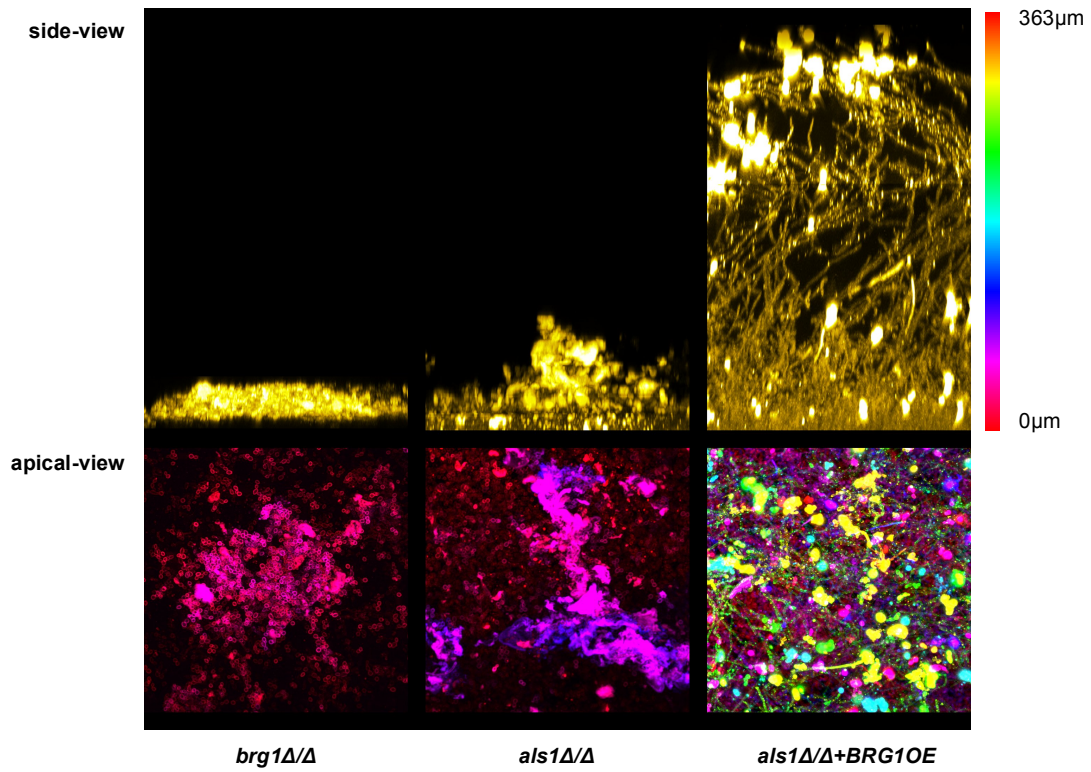


(A) & (B), apical and side-view projections of early-phase biofilms. Confocal imaging was performed on embedded biofilm specimens as described under Methods. The scale bars on left indicate total thickness values.

### Involvement of Brg1 in adhesin-dependent gene expression response

*BRG1* transcription was highly stimulated upon overexpression of all three adhesins. A possibility was considered where *ALS1* stimulated Brg1 activity which, being a positive auto-regulator (Nobile et al., 2012), stimulated its own mRNA accumulation and hence the other biofilm-related genes. If this is true than *als1Δ/Δ* and *brg1Δ/Δ* should phenocopy each other. In order to see that biofilms were grown for *brg1Δ/Δ* in YPD, under similar conditions as *als1Δ/Δ*. As shown in Figure 11, *brg1Δ/Δ* had similar looking biofilm as *als1Δ/Δ*: rudimentary thin biofilm with little to no hyphae and insignificant extracellular material. Additionally, if Brg1 functions downstream of *ALS1* then overexpression of *BRG1* in absence of *ALS1* should form a normal biofilm. We indeed observed the same. As shown in Figure 11, overexpression of *BRG1* in *als1Δ/Δ* significantly improved biofilm formation by the otherwise biofilm defective *als1Δ/Δ*. The biofilm improved significantly in thickness with a confluent layer of hyphae and copious extracellular matrix. These data are in total agreement with the transcription data where overexpression of *BRG1* rescues the transcription defects observed for *als1Δ/Δ* (Fanning, S.).

**Figure 11: Functional connections between *ALS1* and *BRG1*.**

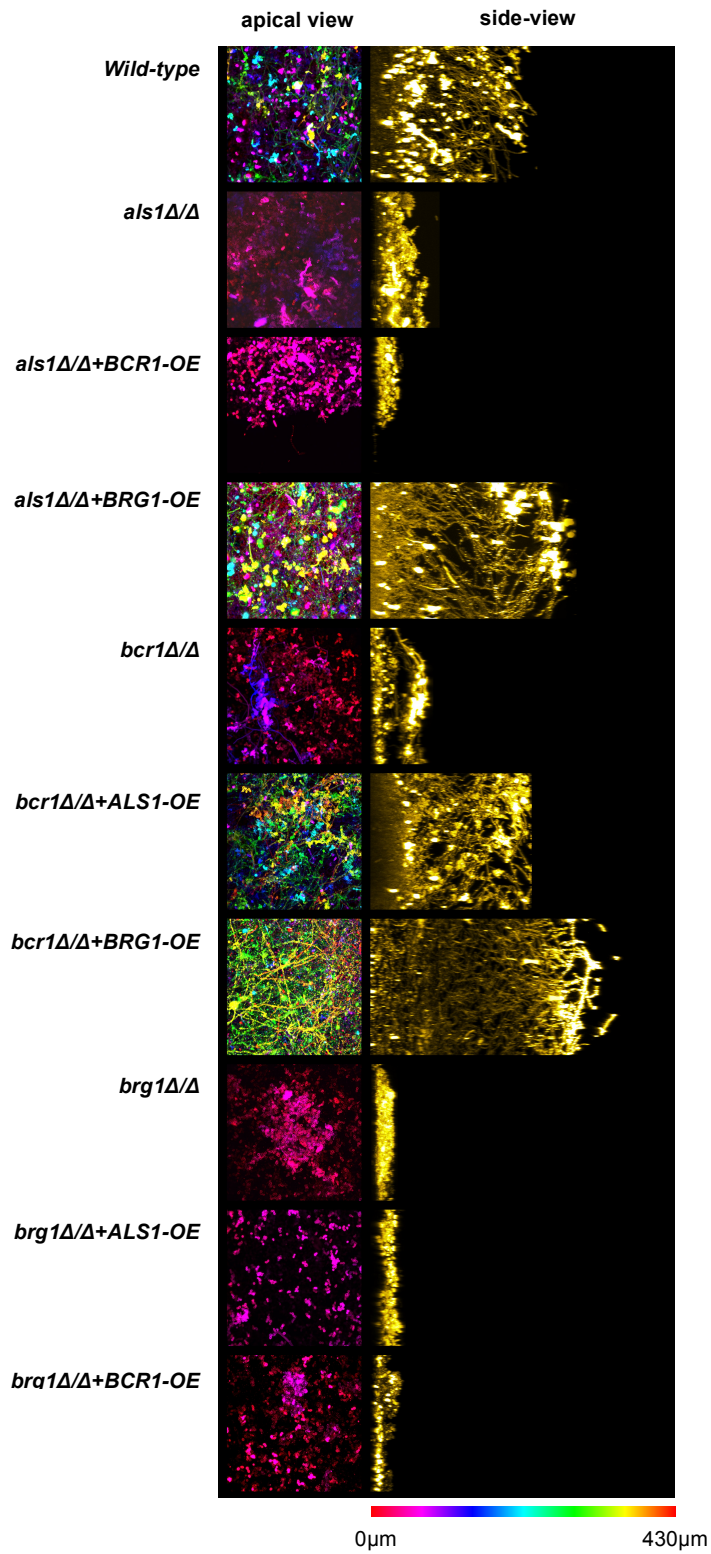


Side- and apical-view projections of biofilms grown in YPD for 24 hours at 37°C

### Functional relationship between Bcr1, Als1 and Brg1

Bcr1 was the first characterized regulator of biofilm formation in *C. albicans* (Nobile and Mitchell, 2005). It regulates several cell-surface adhesins and *BRG1* (Nobile et al., 2012; Nobile and Mitchell, 2005). This raises an obvious question if the Als1-Brg1 module functions downstream of Bcr1 to precipitate their effects on biofilm formation. If this is true then both the downstream targets, *ALS1* and *BRG1*, when overexpressed, should rescue biofilm formation by *bcr1Δ/Δ*. On the other hand, *BCR1* should not improve biofilm formation by *als1Δ/Δ* or *brg1Δ/Δ*. In order to determine if this is indeed the case, we grew biofilms of the three mutants and the mutants harboring overexpression alleles. As shown in Figure 12, the relationship holds true where Bcr1 functions upstream of Als1-Brg1 pathway. As shown in Figure 4.3, the *bcr1Δ/Δ* is defective in development of a mature biofilm. The mutant, however, produced a normal looking mature biofilm with confluence in hyphae and extracellular material, when *ALS1* and *BRG1* were overexpressed. The *als1Δ/Δ*, however, remained defective, even if the *BCR1* levels were boosted up via overexpression. Only the *BRG1* overexpression could make the *als1Δ/Δ* to form a normal mature biofilm. The *brg1Δ/Δ*, on other hand, remained defective in all circumstances. Neither *BCR1* nor *ALS1* could rescue biofilm formation by *brg1Δ/Δ*, when overexpressed.

Figure 12: Functional relationship between *BCR1*, *ALS1* and *BRG1*.



Side- and apical-view projections of biofilms grown in YPD for 24 hours at 37°C.

## **Discussion**

Numerous studies have already established an importance for adhesins in biofilm development through their roles in cell-substrate and cell-cell adherence (Finkel and Mitchell, 2011; Hoyer et al., 2008; Nobile et al., 2006a). Our experiments suggest a novel role for these adhesins in biofilm maturation. Specifically, the adhesins were found to stimulate Brg1 activity to stimulate transcription of biofilm maturation-associated genes. Thus, adhesin accumulation during biofilm initiation subsequently drives biofilm maturation.

We observed that, despite high divergence, *ALS1* and *ALS4* both stimulated Brg1 activity. Thus, it is likely that any of the 9 *ALS* genes can induce the similar response (Fanning, S., unpublished). This holds high functional significance in terms of *Candida*'s ability to form biofilms at diverse host-niches. We can easily picture a situation where the different environmental conditions imposed on *Candida* leads to differential accumulation among *ALS* genes. Any of these can bind to suitable ligands on surface to initiate yeast-form adherence and subsequently the Als accumulation will stimulate Brg1 activity to promote biofilm maturation. Functional redundancy, thus, drives adaptability for *C. albicans* to form biofilms at diverse host niches.

In the light of our experiments, we can now reinterpret several previous studies where it was observed that overexpression of *ALS1* restored biofilm formation by the otherwise biofilm-defective mutants (Desai et al., 2013; Nobile et al., 2006a). For example, the strains lacking *BCR1* and *EFG1* produced rudimentary biofilms (Nobile et al., 2006a; Ramage et al., 2002c), however, their biofilm formation ability was restored when *ALS*-related genes were overexpressed (Nobile and Mitchell, 2005; Zhao et al., 2006). It was assumed previously that the rescue was due to the rescue of adherence. Through our experiments, we suggest that Bcr1 and Efg1 are required for activation of Als1-Brg1 pathway.

Our experiments raise a question as how the adhesin levels stimulate a transcription factor? One possibility is that the overactive secretory pathway, required for adhesin delivery on surface, or increased dwell-time for Als1 at the plasma membrane are somehow sensed. A second model is

that the cell wall containing more adhesins is somehow sensed by a plasma membrane tethered cell wall spanning protein. The second model seems more favorable as there is a known surface-sensing pathway (Kumamoto, 2008), which has the same functional output as the Als1-Brg1 pathway. Further experiments will be carried out to validate the hypotheses.

## **Methods**

### Biofilm embedding for microscopy

Biofilms were grown for 24 hours in YPD medium at 37°C with 60 rpm agitation on medical grade silicone. After 24 hours, the medium was aspirated and biofilms were fixed by placing the squares in 4% formaldehyde for 1-3h. Fixed biofilms were stained with 25µg/ml of Alexa594-fluor conjugated ConcanavalinA in PBS for 60 minutes in the dark with gentle agitation. The fixed and stained biofilms were put in 50% glycol methacrylate (GMA) for 40 minutes. The biofilms were then put in 97% GMA activated with benzoyl peroxide for 20 hours. These steps ensured uniform GMA impregnation within biofilms. After 20 hours the biofilms were inverted on a well formed by 300-um thick Swinnex gasket (Milipore), mounted atop coverglass. About 40-60 ul activated GMA was put in the well before inverting the biofilm sample on top of the well. The coverglasses containing the mounted biofilm specimens were placed in a UV-transparent box and deoxygenated for 3 hours by flowing argon. The GMA impregnated biofilms were UV irradiated using long-wavelength (365 nm) UV light box. The UV irradiation initiates GMA polymerization. This is continued for 30 minutes, after which the irradiation was discontinued and complete GMA polymerization is continued overnight with flowing argon at room temperature. The resulting GMA embedded biofilms were transparent and were imaged using a Zeiss LSM 510 Meta/DuoScan inverted spectral confocal microscope using a long working distance, 40x/0.85NA-oil immersion objective with the laser line at 561 nm. Zen 2009 software was used to obtain the desired Z-stack images. For thick biofilms where attenuation of signal due to light scattering was significant at greater depths, the Z-stacks were collected in multiple parts with higher laser power and gain-settings. The serial image stacks were processed in FIJI (<http://rsbweb.nih.gov/ij/>) for correction of intensity loss due to light scattering in thick biofilm samples. The plugins for processing are described in Appendix. The apical view projections shown were computed from the intensity corrected image stacks using temporal color code plugin. For computing side-view projections, the intensity corrected serial image stacks were resliced from bottom to top and then maximum intensity projection method was used under the Z-project command provided by FIJI.

# Functional role of a ribose biosynthetic gene *SHB17* in biofilm development

## Introduction

As described under introduction, the “omics” approaches have aided greatly in understanding biofilm physiology. A central theme that has emerged from these studies is that the *C. albicans* biofilm exhibits a hypoxic environment. This is supported by the fact that glycolytic genes are up regulated in *C. albicans* biofilms (Bonhomme et al., 2011; Garcia-Sanchez et al., 2004).

Glycolytic up-regulation is expected, as under hypoxia the cells will take the less efficient fermentative route for ATP production and thus will increase the flux through glycolysis. The increased glycolytic flux is required for efficient biofilm formation by *C. albicans* as its inhibition, either genetically or pharmacologically, leads to fragile biofilms (Bonhomme et al., 2011). Further support to the biofilm hypoxia argument comes from a recent metabolomics study, where Zhu et al. reported that biofilm accumulates significantly lesser amounts of TCA cycle intermediates (Zhu et al., 2013).

Another consistent observation was biofilm up-regulation of genes involved in ribosome biogenesis (Desai et al., 2013; Garcia-Sanchez et al., 2004). This imposes a high demand for the sugar-phosphate, ribose-5-phosphate (R5P) on biofilm cells. The growing cells can produce this essential nucleotide component either from glucose or from the glycolytic intermediates. R5P production from glucose occurs through the pentose phosphate pathway (PPP), which produces NADPH and R5P. R5P production from glycolytic intermediates occurs non-oxidatively, without a production of NADPH. The protein, Shb17 having an activity of sedoheptulose-1,7-bisphosphatase has been recently described by the Caudy group to function in the nonoxidative pathway of R5P synthesis (Clasquin et al., 2011). They described that Shb17 catalyzes the committed step in riboneogenesis, where in concert with other enzymes of non-oxidative PPP, such as the transketolases and ribose phosphate isomerase, it functions in R5P synthesis from glycolytic intermediates. It has been shown in yeast that when the ribonucleotide demands are

high such as during ribosome biogenesis, *SHB17* and other genes of riboneogenesis pathway shows a coordinated expression. This coordinated expression closely follows the expression of ribosome biogenesis genes. On the other hand, the oxidative PPP genes show an anticorrelated expression.

We hypothesized that the riboneogenesis pathway through Shb17 should play a significant role in biofilm development by *C. albicans* because of two main reasons: First, the biofilms show up-regulation of genes involved in ribosome biogenesis (Desai et al., 2013; Garcia-Sanchez et al., 2004), hence high demands of R5P; Second, an abundance of glycolytic intermediates (Zhu et al., 2013), hence a facilitated flux through Shb17. According to the Candida Genome Database, in *C. albicans* there are two orthologs with the same putative function of Shb17. I, hence, constructed strains where one or both of the orthologous *SHB17* genes were deleted from the genome.

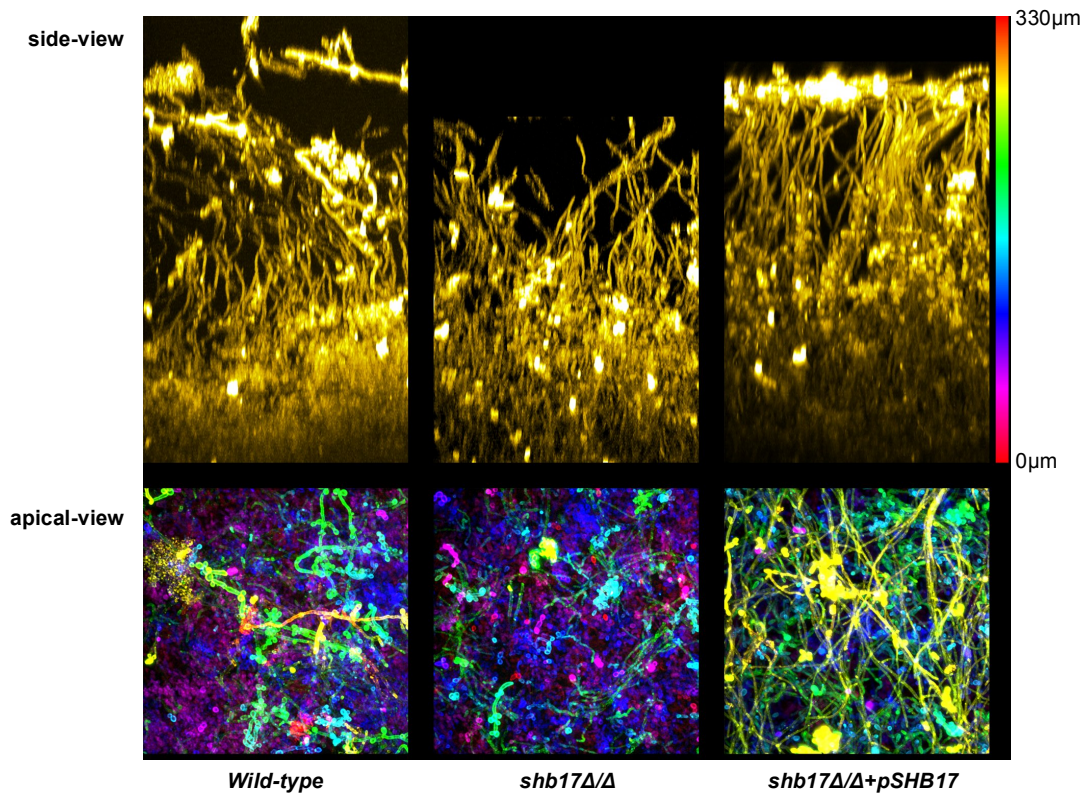
When examined for biofilm formation the mutants showed a very moderate defect in overall biofilm architecture and biomass. However, the mutant had defects in hyphal morphology, which were specific for the hyphal cells in a biofilm. Additionally, I observed that *SHB17*'s role in biofilm hyphal morphology was due to its function in ribose synthesis.

## **Results**

### Function of *SHB17* in biofilm development

There are two orthologous genes, *ORF19.1889* and *ORF19.2202*, which are annotated to the sedoheptulose-1,7-bisphosphatase activity of *S. cerevisiae* Shb17 (scShb17). When searched for *SHB17* in the Candida Genome Database, the *ORF19.1889* comes up as the best hit. Hence I will refer to the Orf19.1889 as Shb17, while other ortholog by its ORF ID. In agreement with our hypothesis of an important role of Shb17-mediated ribose production in biofilm development, I observed biofilm up-regulation of *SHB17* in our previously published data. In this instance, the transcriptional up-regulation in biofilms can be significant. Taking this as a positive sign, I deleted both copies of *SHB17* from the *C. albicans* genome and analyzed the resultant mutant, *shb17Δ/Δ*, for biofilm formation. As shown in Figure 13, the mutant had a very mild defect in biofilm formation. The overall biofilm architecture seems very similar to the wild type and complemented strain's biofilm. All the biofilms showed basal layer consisting of round yeast-form cells while hyphae occupying the rest. There was, however, a remarkable difference in hyphal morphology for the *shb17Δ/Δ* biofilms. As it is shown in the apical view projections, the hyphae of the mutant biofilms looked slender. These slender hyphae were not observed for wild type and the complemented strain.

**Figure 13: Function of *SHB17* in *C. albicans* in biofilm development.**



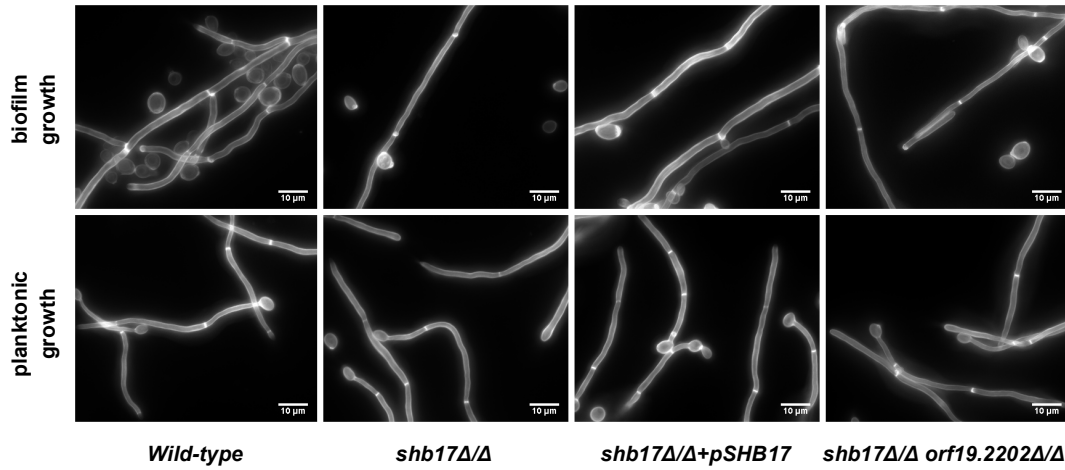
Confocal microscopy was performed on embedded biofilm specimens as described in previous chapter. Shown images are the side- and apical-view projections, computed from the serial image stacks acquired using a confocal microscope.

SHB17 functions to maintain a normal hyphal morphology in biofilms.

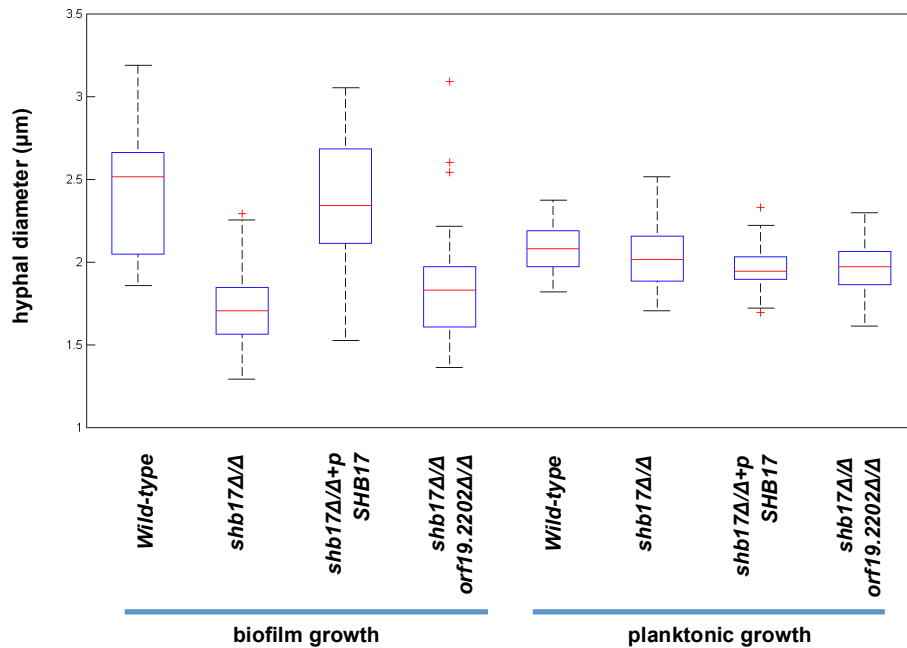
The biofilm images showed slender hyphae in *shb17Δ/Δ* biofilm. Our imaging protocol involves glycol methacrylate plastic embedding of biofilm specimens. In order to see if the observed phenotype is not an embedding artifact, I analyzed the hyphal morphology without plastic embedding. For that, the biofilms were disrupted after growth and the resulting cell suspension was analyzed microscopically to assess hyphal morphology. As shown in Figure 14(A), the hyphae were thinner for *shb17Δ/Δ*. The wild type and complemented strain's biofilm hyphae looked normal. I then sought to analyze if the phenotype is biofilm-specific. For that, I grew planktonic cultures using the same conditions as used for biofilms and analyzed the hyphal cells microscopically. As shown in Figure 14(A), the planktonic hyphae looked similar for all the strains. Surprisingly, the planktonic hyphae were thinner than the biofilm hyphae for all three strains. This is remarkable as it can be proposed that the biofilm environment alters the hyphal morphology in some way. Regardless, it is evident that the mutant hyphae were similar in diameter as the wild type for planktonic conditions. Figure 14(B) shows quantification of hyphal diameter for all three strains grown under biofilm and planktonic conditions. The box plots show a significant decrease ( $p = 10^{-11}$ ) in hyphal diameter for *shb17Δ/Δ* when it was grown under biofilm but not planktonic condition. In order to see if the second ortholog, *ORF19.2202*, has a similar role, I analyzed the *shb17Δ/Δ orf19.2202Δ/Δ* double mutant for biofilm-hyphal morphology. As shown in Figures 14(A) & (B), the hyphae were thinner to a similar extent as they were for the single mutant, *shb17Δ/Δ*.

Figure 14: *SHB17* functions to maintain a normal biofilm hyphal morphology.

A)



B)



(A) Microscopic analysis of disrupted biofilms. The disrupted biofilm cells were fixed and stained with the cell-wall stain, Calcofluor white. Serial images were collected with focus increment of 0.5 microns using an epifluorescence microscope. The shown images are the maximum intensity projection images computed from the image stacks. The scale bars are shown at bottom-right corner.

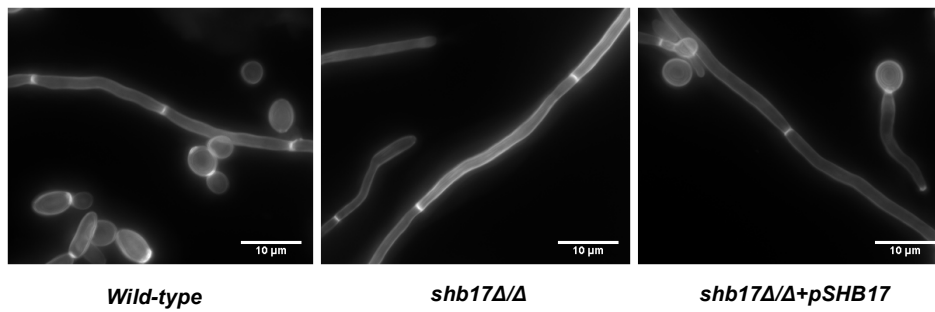
(B) Box plots showing hyphal diameter distributions for the four strains grown under biofilm and planktonic conditions. The plots were constructed by measuring diameter values for >50 random hyphae using FIJI.

*SHB17*'s function in hyphal morphology depends on its role in ribose biosynthesis.

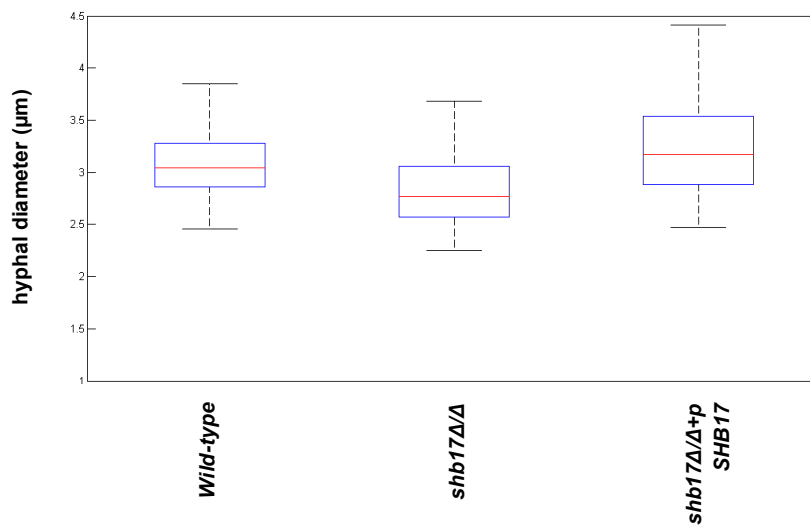
After establishing that *SHB17* functions in maintaining the normal non-slender hyphae in biofilms, I asked if the enzymatic activity of Shb17 in ribose synthesis is responsible for its role in hyphal morphology. In order to assess that, I replaced ribose, in place of mannitol, as a carbon source in our biofilm growth medium. I reasoned that ribose would minimize the flux through Shb17 and hence dampen the phenotype observed for *shb17* $\Delta/\Delta$ . The mutant, indeed, showed what was expected. As shown in Figure 15(A), the hyphae from biofilms of all the three strains looked similar. The quantification, as shown in Figure 15(B), shows that there is no significant difference in hyphal diameter between the different strains.

**Figure 15: *SHB17*'s function to maintain normal biofilm-hyphal-morphology depends on its metabolic role in ribose biosynthesis.**

**A)**



**B)**



(A) Microscopic analysis of disrupted biofilms, grown in the ribose growth medium.

(B) Box plots showing hyphal diameter distributions for wild type, *shb17Δ/Δ* and *shb17Δ/Δ+pSHB17*.

## **Discussion**

Here I show that the biofilm metabolic state affects hyphal morphology. This is supported by the observation that the planktonic hyphae were thinner than the hyphae in biofilm. Additionally, I have discovered that the enzymatic activity of Shb17 in ribose biosynthesis, specifically in biofilms, plays a role in maintaining the biofilm hyphal morphology. Two observations support this argument: first, the *shb17Δ/Δ* biofilm-hyphae were thinner than the wild-type hyphae and second, the biofilm did not show the phenotype of hyphal thinning when grown under ribose as a carbon source.

These observations raise several perplexing questions. First, How does Shb17 function in biofilm-specific manner to maintain a normal hyphal morphology? A simple answer can be put forth: the biofilm metabolic state. It is established that *C. albicans* biofilm presents hypoxia (Bonhomme et al., 2011). Additionally, ribosome biogenesis is significantly up regulated in biofilms (Desai et al., 2013; Garcia-Sanchez et al., 2004). Under these circumstances, when the ribose demands are high due to high ribosome biogenesis, there should be a significant ribose biosynthetic flux through the Shb17-riboseogenesis pathway, as the pentose phosphate pathway (PPP) is down regulated under hypoxia (Celton et al., 2012). The increased flux through Shb17 should also be facile as the substrates feeding into this pathway are abundantly available due to an increased glycolytic flux in biofilms.

In addition to the ribose demands, the cellular NADPH demand also regulates flux through Shb17. Again, the PPP is the major supplier for NADPH. Cells need NADPH for anabolic processes such as amino acid biosynthesis, nucleic acid base synthesis, lipid and sterol biosynthesis. Several observations with the biofilm gene expression, however, suggest that cells in biofilm environment do not require substantial amounts of NADPH. First, the biofilm transcriptomic data show a down-regulation of lipid catabolic processes (Desai et al., 2013). Second, as shown in Table 2, the data also show that many amino acid transporters, nucleoside and nucleic acid base transporters are up regulated (Desai et al., 2013). This suggests that the cells in a biofilm are rewiring from anabolic biosynthesis to a facilitated transport or uptake.

Altogether, these observations suggest that the cells in a biofilm are less demanding for NADPH, which should further increase the flux through Shb17. The up-regulation of sulfate assimilation is, however, counterintuitive. It has been proposed that the multiple reduction steps involved in conversion of sulfate to sulfite help in balancing reducing equivalents arising through increased glycolysis. The sulfate assimilation requires NADPH. In biofilms glycerol production is up regulated (Desai et al., 2013; Garcia-Sanchez et al., 2004; Nett et al., 2009; Zhu et al., 2013). It is possible that the required NADPH is supplied through the glycerol-DHA (dihydroxy acetone) cycle (Celton et al., 2012).

**Table 2: Transporter encoding genes, up-regulated in a *C. albicans* biofilm.**

Transporter genes	ORF ID	Fold change (bio/plank)	Functional description
<i>AGP2</i>	<i>orf19.4679</i>	46.02	Amino acid permease
<i>CAN1</i>	<i>orf19.97</i>	4.10	Basic amino acid permease
<i>CNT</i>	<i>orf19.4118</i>	34.96	CNT family H(+)/nucleoside symporter;
<i>FCY21</i>	<i>orf19.1357</i>	8.09	High affinity, high capacity, hypoxanthine-adenine-guanine-cytosine/ H+ symporter
<i>GAP1</i>	<i>orf19.4304</i>	9.97	Amino acid permease
<i>MUP1</i>	<i>orf19.5280</i>	4.55	Putative high affinity methionine permease
<i>PTR2</i>	<i>orf19.6937</i>	20.52	Putative oligopeptide transporter

Another important question that arises from our observations is about the cell biological phenomenon that gives rise to the observed biofilm hyphal morphology. We propose that the cellular NADPH levels play a role in observed biofilm hyphal morphology. In several fungi, NADPH-dependent reactive oxygen species production has been proven to function in axial tip extension. Although, it is unknown if a similar mechanism exists in *C. albicans* as well, but if proven then the mechanism can justify the observed biofilm-specific phenotype.

## **Methods**

### Growth media and strain construction

Overnight cultures were grown in YPD or YP-ribose, where dextrose was replaced with ribose at same concentration as glucose, i.e. 2%w/v. Similarly, for biofilm growth, spider or spider-ribose media were used. The mannitol was replaced with ribose at the same concentration, i.e. 1%w/v.

The single mutant and complemented strains were constructed as described under Methods in Chapter 2. For the construction of *shb17Δ/Δ orf19.2202Δ/Δ*, the modified URA-blaster method was employed for disrupting ORF19.2202 first (Ganguly and Mitchell, 2012). This yielded a strain that was auxotrophic w.r.t. all the markers along with deletion of *ORF19.2202*. This strain was then used to disrupt *SHB17* alleles as described in Chapter 2.

### Biofilm growth and microscopy

Biofilms were grown as described in Chapter 2 and 4. The microscopy of intact embedded biofilm specimens was performed as described in Chapter 4. For disrupting the biofilms, three silicone squares containing biofilms of a specific strain were dumped in a 50mL conical tube containing 5 mL of 1x PBS. After vortexing the cell suspension was used for microscopy after fixing with 4% formaldehyde and staining with 0.185 mg/mL of Calcofluor white. For analyzing planktonic hyphal morphology, the cultures were grown for 48 hours in 50 mL of spider media in conical flasks at 37°C with constant shaking at 225 rpm. The cells were treated the same way as the cells from biofilms and microscopy was performed using a standard epifluorescence microscope.

## Appendix

### Table of the strains.

**Table 3: Strains used in this disserataion.**

Strain	Genotype	Source
SC5314	Wild type clinical isolate	(Gillum et al., 1984)
BWP17	<u><i>ura3Δ::λimm434 arg4::hisG his1::hisG</i></u> <i>ura3Δ::λimm434 arg4::hisG his1::hisG</i>	Mitchell Lab
DAY286	<u><i>ura3Δ::λiimm434 ARG4::URA3::arg4::hisG his1::hisG</i></u> <i>ura3Δ::λiimm434 arg4::hisG his1::hisG</i>	Mitchell Lab
DAY185	<u><i>ura3Δ::λiimm434 HIS1::his1::hisG ARG4::URA3::arg4::hisG</i></u> <i>ura3Δ::λiimm434 his1::hisG arg4::hisG</i>	Mitchell Lab
EMH141	<u><i>ura3Δ::λimm434 arg4::hisG his1::hisG orf19.3089::Tn7-UAU1</i></u> <i>ura3Δ::λimm434 arg4::hisG his1::hisG orf19.3089::Tn7-URA3</i>	Mitchell Lab
EMH172	<u><i>ura3Δ::λimm434 arg4::hisG his1::hisG orf19.3483::Tn7-UAU1</i></u> <i>ura3Δ::λimm434 arg4::hisG his1::hisG orf19.3483::Tn7-URA3</i>	Mitchell Lab
SGH343	<u><i>ura3Δ::λimm434 arg4::hisG his1::hisG hgt8::Tn7-UAU1</i></u> <i>ura3Δ::λimm434 arg4::hisG his1::hisG hgt8::Tn7-URA3</i>	Mitchell Lab
SGH348	<u><i>ura3Δ::λimm434 arg4::hisG his1::hisG can1::Tn7-UAU1</i></u> <i>ura3Δ::λimm434 arg4::hisG his1::hisG can1::Tn7-URA3</i>	Mitchell Lab
SGH352	<u><i>ura3Δ::λimm434 arg4::hisG his1::hisG orf19.278::Tn7-UAU1</i></u> <i>ura3Δ::λimm434 arg4::hisG his1::hisG orf19.278::Tn7-URA3</i>	Mitchell Lab
SGH368	<u><i>ura3Δ::λimm434 arg4::hisG his1::hisG elf1::Tn7-UAU1</i></u> <i>ura3Δ::λimm434 arg4::hisG his1::hisG elf1::Tn7-URA3</i>	Mitchell Lab
SGH370	<u><i>ura3Δ::λimm434 arg4::hisG his1::hisG aah1::Tn7-UAU1</i></u> <i>ura3Δ::λimm434 arg4::hisG his1::hisG aah1::Tn7-URA3</i>	Mitchell Lab
SGH371	<u><i>ura3Δ::λimm434 arg4::hisG his1::hisG met3::Tn7-UAU1</i></u> <i>ura3Δ::λimm434 arg4::hisG his1::hisG met3::Tn7-URA3</i>	Mitchell Lab
SGH372	<u><i>ura3Δ::λimm434 arg4::hisG his1::hisG sit1::Tn7-UAU1</i></u> <i>ura3Δ::λimm434 arg4::hisG his1::hisG sit1::Tn7-URA3</i>	Mitchell Lab

SGH373	<u>ura3Δ::λimm434 arg4::hisG his1::hisG orf19.3665::Tn7-UAU1</u> <u>ura3Δ::λimm434 arg4::hisG his1::hisG orf19.3665::Tn7-URA3</u>	Mitchell Lab
SGH374	<u>ura3Δ::λimm434 arg4::hisG his1::hisG gpd1::Tn7-UAU1</u> <u>ura3Δ::λimm434 arg4::hisG his1::hisG gpd1::Tn7-URA3</u>	Mitchell Lab
SGH377	<u>ura3Δ::λimm434 arg4::hisG his1::hisG orf19.1676::Tn7-UAU1</u> <u>ura3Δ::λimm434 arg4::hisG his1::hisG orf19.1676::Tn7-URA3</u>	Mitchell Lab
SGH380	<u>ura3Δ::λimm434 arg4::hisG his1::hisG pho2::Tn7-UAU1</u> <u>ura3Δ::λimm434 arg4::hisG his1::hisG pho2::Tn7-URA3</u>	Mitchell Lab
RJS486	<u>ura3Δ::λimm434 arg4::hisG his1::hisG fad3::Tn7-UAU1</u> <u>ura3Δ::λimm434 arg4::hisG his1::hisG fad3::Tn7-URA3</u>	Mitchell Lab
RJS492	<u>ura3Δ::λimm434 arg4::hisG his1::hisG orf19.4563::Tn7-UAU1</u> <u>ura3Δ::λimm434 arg4::hisG his1::hisG orf19.4563::Tn7-URA3</u>	Mitchell Lab
RJS493	<u>ura3Δ::λimm434 arg4::hisG his1::hisG orf19.3477::Tn7-UAU1</u> <u>ura3Δ::λimm434 arg4::hisG his1::hisG orf19.3477::Tn7-URA3</u>	Mitchell Lab
RJS494	<u>ura3Δ::λimm434 arg4::hisG his1::hisG smm1::Tn7-UAU1</u> <u>ura3Δ::λimm434 arg4::hisG his1::hisG smm1::Tn7-URA3</u>	Mitchell Lab
RJS497	<u>ura3Δ::λimm434 arg4::hisG his1::hisG orf19.154::Tn7-UAU1</u> <u>ura3Δ::λimm434 arg4::hisG his1::hisG orf19.3477::Tn7-URA3</u>	Mitchell Lab
RJS517	<u>ura3Δ::λimm434 arg4::hisG his1::hisG gap1::Tn7-UAU1</u> <u>ura3Δ::λimm434 arg4::hisG his1::hisG gap1::Tn7-URA3</u>	Mitchell Lab
RJS519	<u>ura3Δ::λimm434 arg4::hisG his1::hisG rhr2::Tn7-UAU1</u> <u>ura3Δ::λimm434 arg4::hisG his1::hisG rhr2::Tn7-URA3</u>	Mitchell Lab
CJN702	<u>ura3Δ::λimm434 arg4::hisG his1::hisG::pHIS1 bcr1::ARG4</u> <u>ura3Δ::λimm434 arg4::hisG his1::hisG bcr1::URA3</u>	(Nobile and Mitchell, 2005)
JVD005	<u>ura3Δ::λimm434 arg4::hisG his1::hisG::pHIS1 rhr2::ARG4</u> <u>ura3Δ::λimm434 arg4::hisG his1::hisG rhr2::URA3</u>	Mitchell Lab
JVD006	<u>ura3Δ::λimm434 arg4::hisG his1::hisG::pHIS1-RHR2 rhr2::ARG4</u> <u>ura3Δ::λimm434 arg4::hisG his1::hisG rhr2::URA3</u>	Mitchell Lab
JVD009	<u>ura3Δ::λimm434 arg4::hisG his1::hisG::pHIS1 bcr1::ARG4 RHR2::pAgTEF1-NAT1-AgTEF1UTR-TDH3-RHR2</u> <u>ura3Δ::λimm434 arg4::hisG his1::hisG bcr1::URA3 RHR2</u>	Mitchell Lab
JVD017-018	<u>ura3Δ::λimm434 arg4::hisG his1::hisG::pHIS1 rhr2::ARG4 ALS1::pAgTEF1-NAT1-AgTEF1UTR-TDH3-ALS1</u> <u>ura3Δ::λimm434 arg4::hisG his1::hisG rhr2::URA3 ALS1</u>	Mitchell Lab

JVD020-021	<u>ura3Δ::λimm434 arg4::hisG his1::hisG::pHIS1 rhr2::ARG4 HWP1::pAgTEF1-NAT1-AgTEF1UTR-TDH3-HWP1</u> ura3Δ::λimm434 arg4::hisG his1::hisG rhr2::URA3 HWP1	Mitchell Lab
JVD025	<u>ura3Δ::λimm434 arg4::hisG his1::hisG::pHIS1 rhr2::ARG4 ALS3::pAgTEF1-NAT1-AgTEF1UTR-TDH3-ALS3</u> ura3Δ::λimm434 arg4::hisG his1::hisG rhr2::URA3 ALS3	Mitchell Lab
tye7Δ/Δ	<u>arg4Δ leu2Δ his1Δ URA3 IRO1 tye7::HIS1</u> arg4Δ leu2Δ his1Δ ura3Δ::imm434 iro1Δ::imm434 tye7::LEU2	(Homan et al., 2009)
JVD039	<u>ura3Δ::λimm434 arg4::hisG his1::hisG::pHIS1 rhr2::ARG4 ALS3::pAgTEF1-NAT1-AgTEF1UTR-TDH3-ALS3</u> ura3Δ::λimm434 arg4::hisG his1::hisG rhr2::URA3 BCR1	Mitchell Lab
JVD051	<u>ura3Δ::λimm434 arg4::hisG his1::hisG::pHIS1 rhr2::ARG4 ALS3::pAgTEF1-NAT1-AgTEF1UTR-TDH3-ALS3</u> ura3Δ::λimm434 arg4::hisG his1::hisG rhr2::URA3 UME6	Mitchell Lab
JVD065	<u>ura3Δ::λimm434 arg4::hisG his1::hisG::pHIS1 rhr2::ARG4 ALS3::pAgTEF1-NAT1-AgTEF1UTR-TDH3-ALS3</u> ura3Δ::λimm434 arg4::hisG his1::hisG rhr2::URA3 BRG1	Mitchell Lab
JVD101-102	<u>ura3Δ::λimm434 arg4::hisG his1::hisG::pHIS1 orf19.1889::ARG4</u> ura3Δ::λimm434 arg4::hisG his1::hisG orf19.1889::URA3	Mitchell Lab
JVD105-107	<u>ura3Δ::λimm434 arg4::hisG his1::hisG::pHIS1-ORF19.1889 orf19.1889::ARG4</u> ura3Δ::λimm434 arg4::hisG his1::hisG orf19.1889::URA3	Mitchell Lab
JVD090-091	<u>ura3Δ::λimm434 arg4::hisG his1::hisG::pHIS1 orf19.2202Δ orf19.1889::ARG4</u> ura3Δ::λimm434 arg4::hisG his1::hisG orf19.2202Δ orf19.1889::URA3	Mitchell Lab
JVD121-122	<u>leu2::cdARG4 leu2Δ his1Δ URA3 IRO1 sfl2::HIS1</u> arg4Δ leu2Δ his1Δ ura3Δ::imm434 iro1Δ::imm434 sfl2::LEU2	Mitchell Lab
JVD127-128	<u>leu2::SFL2-cdARG4 leu2Δ his1Δ URA3 IRO1 sfl2::HIS1</u> arg4Δ leu2Δ his1Δ ura3Δ::imm434 iro1Δ::imm434 sfl2::LEU2	Mitchell Lab
SF40a-b	<u>ura3Δ::λimm434 arg4::hisG his1::hisG sln1::Tn7-UAU1</u> ura3Δ::λimm434 arg4::hisG his1::hisG sln1::Tn7-URA3	Mitchell Lab
TA40-43	<u>ura3Δ::λimm434 arg4::hisG his1::hisG::pHIS1 cek1::ARG4</u> ura3Δ::λimm434 arg4::hisG his1::hisG cek1::URA3	Mitchell Lab
JVD131	<u>arg4Δ leu2Δ his1Δ URA3 IRO1 tec1::HIS1</u> arg4Δ leu2Δ his1Δ ura3Δ::imm434 iro1Δ::imm434 tec1::LEU2	(Homan et al., 2009)
JVD132	<u>arg4Δ leu2Δ his1Δ URA3 IRO1 mig1::HIS1</u> arg4Δ leu2Δ his1Δ ura3Δ::imm434 iro1Δ::imm434 mig1::LEU2	(Homan et al., 2009)
JVD133	<u>arg4Δ leu2Δ his1Δ URA3 IRO1 ahr1::HIS1</u> arg4Δ leu2Δ his1Δ ura3Δ::imm434 iro1Δ::imm434 ahr1::LEU2	(Homan et al., 2009)
JVD134	<u>arg4Δ leu2Δ his1Δ URA3 IRO1 brg1::HIS1</u> arg4Δ leu2Δ his1Δ ura3Δ::imm434 iro1Δ::imm434 brg1::LEU2	(Homan et al., 2009)

	<i>arg4Δ leu2Δ his1Δ ura3Δ::imm434 iro1Δ::imm434 brg1::LEU2</i>	2009)
CW542	<u><i>ARG4 leu2Δ his1Δ URA3 IRO1</i></u> <i>arg4Δ leu2Δ his1Δ ura3Δ::imm434 iro1Δ::imm434</i>	Mitchell lab
SN152	<u><i>arg4Δ leu2Δ his1Δ URA3 IRO1</i></u> <i>arg4Δ leu2Δ his1Δ ura3Δ::imm434 iro1Δ::imm434</i>	(Noble and Johnson, 2005)

## Plugins for biofilm image processing

The plugins were written in JAVA using several functions that are openly available from the ImageJ community. All the mentioned plugins can be installed very easily either in ImageJ or FIJI.

### 1.1 An ImageJ plugin for quantifying biofilm volume from the acquired image stack

The following plugin was written with an aim to aid our efforts of assessing biofilm formation capabilities of diverse strain under examination. The code essentially count the number of pixels in a given biofilm image stack. A thresholding operation in combination with an operation to remove background is usually performed before running this plugin for quantitation purposes. After thresholding, running this plugin yields a value that corresponds to the fluorescent biofilm volume placed in area of the field of view.

#### Code

```
package Biofilms;

import java.awt.Button;
//import java.awt.event.ActionListener;
import ij.IJ;
import ij.ImagePlus;
import ij.ImageStack;
import ij.WindowManager;
import ij.gui.GenericDialog;
import ij.gui.WaitForUserDialog;
//import ij.gui.WaitForUserDialog;
import ij.plugin.PlugIn;

/**
 * @author Lanni,F and Desai,JV
 *
 */
public class Biofilm_volume_estimator_ implements PlugIn {
    private static double StackSize;
    private static double PixLength;
    private static double FocusIncrement;
    private static double Volume;
    static int SizeofStack;
    int nSlices;
    protected boolean locked = false;
    private Button button;
    static int width=1500,height=1500;//initial values assigned
    public static ImagePlus imp;

    public void run (String arg) {
        ImagePlus imp = WindowManager.getCurrentImage();//gets the current
image and assigns it for imp
        /* The following is needed for implementing run method for the
PlugIn interface*/
        if (imp==null || (imp!=null && imp.getStackSize()<2)) {
            IJ.error("This command requires an image stack.");
            return;
        }
        /* A generic dialog is initiated from GUI interface, which will get
user input about pixel
* parameters and image-stack parameters*/

        WaitForUserDialog wd = new WaitForUserDialog("Action required from
User", "Adjust the threshold from Image Menu and then press OK");
        button = new Button(" OK ");
        wd.show();
        wd.getButton();
    }
}
```

```

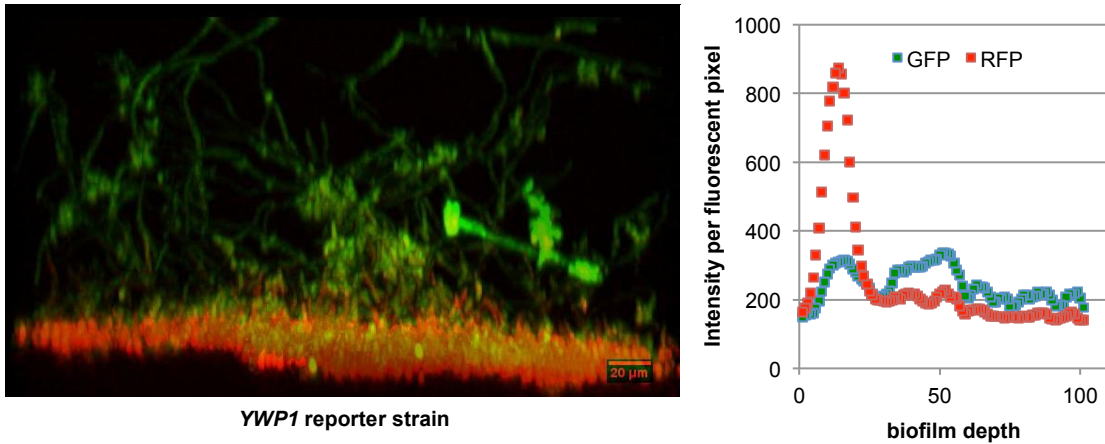
GenericDialog gd = new GenericDialog("Biomass estimator...");//new
object "gd" initiated of GenericDialog
gd.addNumericField("Enter stack size: ", StackSize, 0);//It has
three numeric fields, where the first will be assigned to width
gd.addNumericField("Enter pixel length in um: ", PixLength, 0);
gd.addNumericField("Enter the focus-increment", FocusIncrement, 0);
gd.showDialog();//this will show the dialog-box
StackSize = gd.getNextNumber();//assign the first input to
StackSize
PixLength = gd.getNextNumber();//the second input is assigned to
PixLength
FocusIncrement = gd.getNextNumber();//the third input is assigned
to FocusIncrement
ImageStack stack = imp.getImageStack();//this will assign the
processor of the image-stack to "stack"
int numberOfSlices = imp.getStackSize();
int PixelCount = 0;//a parameter is initiated which will iterate
over images to count pixels
/*the loops are established. The first loop will iterate over
images of the stack
* while the second loop will iterate over pixels, length over
height
*/
for (int i=1; i<=numberOfSlices; i++) {
    imp.unlock();
    int w=stack.getWidth();
    int h=stack.getHeight();
    for(int u=0; u<w; u++){
        for(int v=0; v<h; v++){
            double p=(double)
(stack.getProcessor(i).getPixelValue(u,v));//getPixelValue, works with double, for int
getPixel
/* An if statement to count the pixel,
Whenever a pixel is encountered having value>0
* it is counted
*/
            if (p>0){
                PixelCount = PixelCount+1;
            }
            /*A status bar wrt PixelCount is
established*/
            IJ.showStatus("Estimating biomass...");
            IJ.showProgress(i+1, numberOfSlices);
        }
    }
}
Volume = (PixelCount*FocusIncrement*PixLength*PixLength);
IJ.showMessage("The biofilm volume is " + Volume + " cubic
micron");
}
}

```

## 1.2 An ImageJ plugin to quantify fluorescent intensity per stained pixel for given image planes in an image stack

This plugin was written with an aim to quantify the spatial gene expression patterns from a biofilm image stack. The code essentially serves to count the number of pixels with intensity above a specific threshold in a given image plane. It then quantifies a ratio of total intensity in given plane/the number of pixels above a specified threshold. For example, the biofilm side-view in Figure 16 shows RFP as a marker for expression of *YWP1*. As shown in the plot of the fluorescence quantification, RFP expression is predominantly focused in the basal layer of the biofilm.

**Figure 16: Imaging and quantification of *YWP1* reporter expression in a biofilm.**



### Code

```

package Biofilms;

import java.awt.Button;
import ij.IJ;
import ij.ImagePlus;
import ij.ImageStack;
import ij.WindowManager;
import ij.gui.GenericDialog;
import ij.gui.WaitForUserDialog;
import ij.measure.ResultsTable;
import ij.plugin.PlugIn;
import ij.plugin.filter.Analyzer;

/**
 * @author Lanni, F and Desai, JV
 *
 */
public class Gene_Expression_Estimator_ implements PlugIn {
    private static double Threshold;
    static int SizeofStack;
    int nSlices;
    protected boolean locked = false;
    private Button button;
    static int width=1500,height=1500;//initial values assigned
    public static ImagePlus imp;

    public void run (String arg) {
        ImagePlus imp = WindowManager.getCurrentImage();//gets the current
image and assigns it for imp
        /* The following is needed for implementing run method for the
PlugIn interface*/
        if (imp==null || (imp!=null && imp.getStackSize()<2)) {
            IJ.error("This command requires an image stack.");
            return;
        }
        /* A generic dialog is initiated from GUI interface, which will get
user input about pixel
        * parameters and image-stack parameters*/

        GenericDialog gd = new GenericDialog("Gene expression
estimator...");//new object "gd" initiated of GenericDialog
        gd.addNumericField("Enter the background counts ", Threshold,
0);//It has three numeric fields, where the first will be assigned to width
        gd.showDialog();//this will show the dialog-box
    }
}

```

```

        Threshold = gd.getNextNumber();
        ImageStack stack = imp.getImageStack();//this will assign the
processor of the image-stack to "stack"
        int numberOfSlices = imp.getStackSize();

        ResultsTable rt = Analyzer.getResultsTable();
        if ( rt == null) {
            rt = new ResultsTable();
            Analyzer.setResultsTable(rt);
        }

        for (int i=1; i<=numberOfSlices; i++) {
            imp.unlock();
            int w=stack.getWidth();
            int h=stack.getHeight();
            int PixelCount = 0;//a parameter is initiated which will
iterate over images to count pixels
            /*the loops are established. The first loop will iterate
over images of the stack
            * while the second loop will iterate over pixels, length
over height
            */
            double p = 0;

            double TotalIntensity = 0;
            for(int u=0; u<w; u++){
                for(int v=0; v<h; v++){
                    p=(double)
(stack.getProcessor(i).getPixelValue(u,v));//getPixelValue, works with double, for int
getPixel
                    double Intensity = p;
                    /* An if statement to count the pixel,
Whenever a pixel is encountered having value>0
                    * it is counted
                    */
                    if (p>Threshold){
                        PixelCount = PixelCount+1;
                        TotalIntensity =
Intensity+TotalIntensity;
                    }
                }
            }

            double SlicePixelCount = PixelCount;
            rt.incrementCounter();
            rt.addValue("Number of Stained Pixel", SlicePixelCount);
            rt.addValue("Total Intensity", TotalIntensity);
            rt.addValue("Intensity per stained pixel",
TotalIntensity/SlicePixelCount);
        }

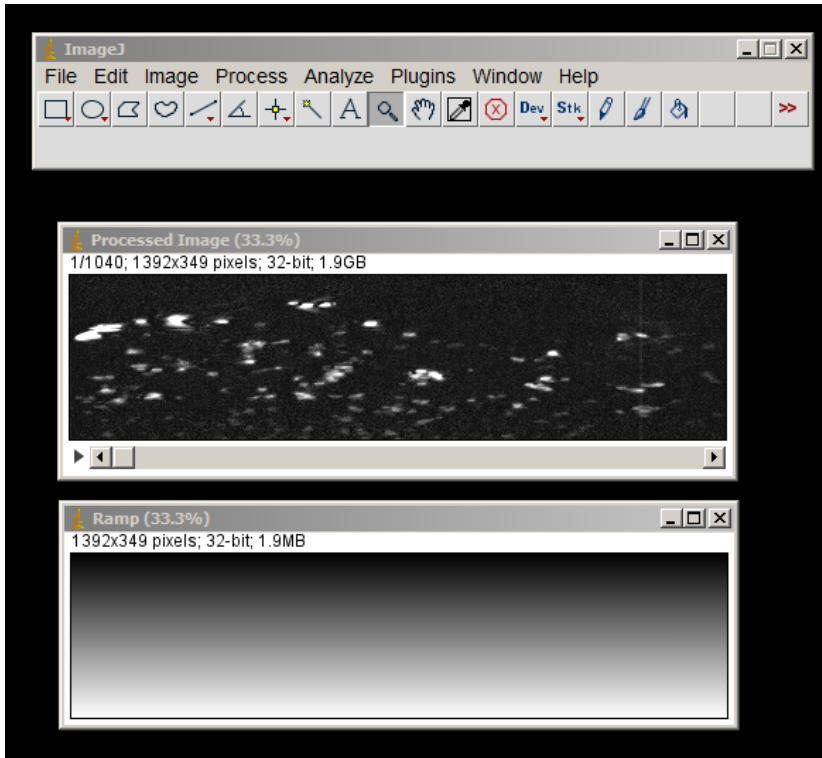
        rt.show("Results");
    }
}

```

### 1.3 An ImageJ plugin to correct the scattering light intensity attenuation in a biofilm image stack

Even after refractive index matching through plastic embedding, light intensity attenuation is often observed while imaging the thick biofilm specimen from an apical to basal layer. It was observed that a significant improvement to the image presentation could be achieved if the image stack was corrected by multiplying with a linear ramp image. The slope of this ramp for multiplication depends upon how significant the attenuation is. A plugin was written with an aim to automate this ramp generation. The plugin relies on user to provide information regarding the stack size, and intensity values of the brightest pixel at apical and basal layer image planes respectively. Once provided, this information is utilized to generate a ramp as shown in Figure 17, which the user can multiply to a resliced biofilm image stack.

**Figure 17: An image of a ramp, constructed to correct intensity attenuation arising while biofilm serial-image-stack acquisition.**



The image at top is the resliced image stack while the image at bottom is the ramp to be multiplied to the resliced stack for attenuation correction.

## Code

```
package Biofilms;
import ij.*;
import ij.process.*;
import ij.gui.*;
import ij.plugin.*;

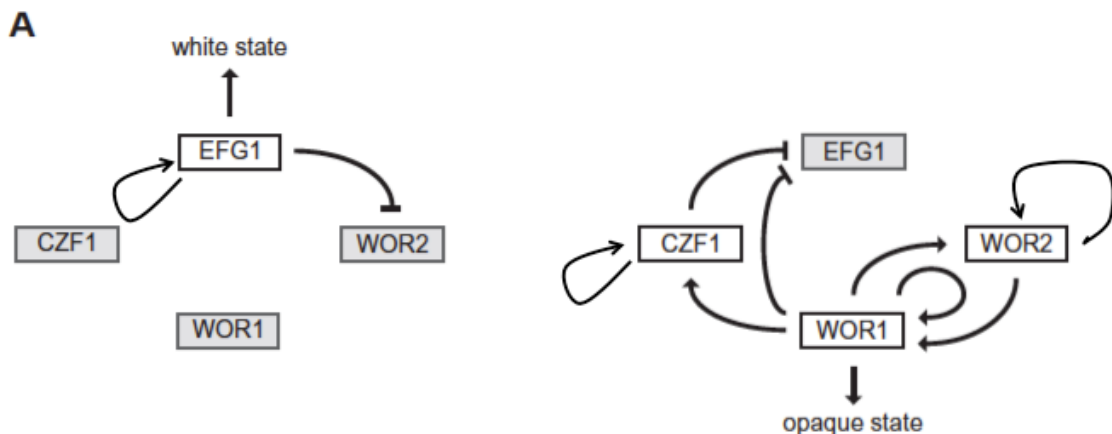
public class Ramp_for_Intensity_Correction_ implements PlugIn {
    String title = "Ramp";//variable "title" assigned to "Ramp" with type String
    static int width=512,height=1500;//initial values assigned
    static double brightness1=6000, brightness2=1500;
    static int factor=1;
    /*method initialized with return type void*/
    public void run(String arg) {
        GenericDialog gd = new GenericDialog("Rampmaker Settings");//new object "gd"
        initiated of GenericDialog
        gd.addNumericField("Enter stack size: ", width, 0);//It has two numeric fields,
        where the first will be assigned to width
        gd.addNumericField("Height: ", height, 0);
        gd.addNumericField("Brightest pixel of the first frame:", brightness1, 0);
        gd.addNumericField("Brightest pixel of the last frame:", brightness2, 0);
        gd.showDialog();//method to showDialog which will display the object "gd"
        if (gd.wasCanceled()) return;
        width = (int)gd.getNextNumber();//width assigned to the first numeric field of gd
        height = (int)gd.getNextNumber();//height assigned to the second numeric field
        double brightness1=(double)gd.getNextNumber();
        double brightness2=(double)gd.getNextNumber();
        double factor=(double) (brightness1/brightness2);
        ImagePlus imp = IJ.createImage(title, "32-bit ramp", width, height, 1);//New
        ImagePlus initiated from the FloatProcessor, with type 32-bit ramp
        ImageProcessor ip = imp.getProcessor();
        /*Multiplying each pixels to the factor*/
        int w=ip.getWidth();
        int h=ip.getHeight();
        for (int u=0; u<w; u++){
            for (int v=0; v<h; v++){
                double p=(double) ip.getPixelValue(u,v);//getPixelValue,
                works with double, for int getPixel
                double p1 = p*(factor-1);
                ip.putPixelValue(u,v,p1);//putPixelValue(x,y,p), works with
                double
            }
        }
        IJ.run(imp, "Add...", "value=1");//running the ImageJ command Add... 1
        ImageProcessor ip2 = ip.rotateRight();//running the ImageJ command rotateRight
        assigning the rotated image to a different processor ip2
        imp.setProcessor(imp.getTitle(), ip2);//setting ip2 to the ImagePlus imp
        imp.show();//showing the imageplus object "imp"
    }
}
```

## A mathematical model for cell fate decision in *Candida albicans*

*Candida albicans* is a commensal fungus in humans, however in immunocompromised individuals, it causes life-threatening infections with mortality rates close to 40% (Andes et al., 2012; Finkel and Mitchell, 2011). The success of this fungus as a successful commensal and an opportunistic pathogen can be attributed to its ability to survive successfully in diverse host niches. This ability partly derives from *Candida's* ability to exist in several distinct cell types. Two such cell types are the white and the opaque cell-types of *C. albicans*. The switch was first described by Slutsky et. al. where they observed two different kinds of colony forming phenotypes, white - shiny and opaque - dull (Slutsky et al., 1987). In addition to difference in appearance, these cell-types differ markedly from each other in shape, ability to mate, metabolic preferences, and virulence (Lohse and Johnson, 2009). Both the cell-types are genetically identical, therefore the switch is epigenetic in nature and is brought out by differential regulation of about 10% of the genome (Lohse and Johnson, 2009).

The switch from the common white cell types to opaque cells occurs stochastically every 10000 cell divisions (Lohse and Johnson, 2009). The reverse switch occur at similar frequency at 24°C. However, the switching frequency increases considerably at 37°C as well as under other certain conditions, such as oxygen, carbon dioxide, and nutrient depletion (Lohse and Johnson, 2009). Through a series of functional genomics and epistasis experiments, a circuit of four transcription factors has been described that regulates this white-opaque switching (Zordan et al., 2007). The circuit is shown below in Figure 18. Usually the common white cells are stably maintained in that state by the action of Efg1 which is highly enriched in white cell type (Hernday et al., 2013). The other three protein coding genes are severely down regulated in white cell type, but highly up regulated in opaque cell type, thus stably maintaining it.

**Figure 18: A wiring diagram of the transcriptional circuit regulating the white-opaque cell switch in *C. albicans*.**



Several studies have identified key white- and opaque-specific target genes for the four transcription factors described above (Hernday et al., 2013). Two other transcriptional regulators have also been described recently (Hernday et al., 2013). However, clear understanding is lacking regarding how certain factors can modulate switching frequency. A quantitative analysis can certainly be helpful in this regard however designing and implementing a plethora of experiments to enlist quantitative details regarding each reaction in the circuit is impractical.

Mathematical modeling and simulation is a very good alternative to that. Not only the model can be used to describe the phenomenon happening in biological context but also provide an opportunity to formulate novel hypotheses. With that motivation, I have developed an ODE (ordinary differential equations) model for transcriptional regulation of white-opaque switching in *C. albicans*. The model described here closely mimics the behavior of this circuit as observed experimentally. Local sensitivity analysis was performed to identify key parameters and reactions governing the stability of the switch as well as the frequency of switching.

#### 1.4 Methods

##### The model

The model described here has 8 variables, 4 each corresponding to RNA and protein species of the four transcription factors respectively. Total 8 reactions with 21 different parameters were written in form of ODEs. The equations are as follow and the parameters are described in Table 1.

$$\begin{aligned} \frac{d[EFG1]}{dt} &= \left[ \beta_{EFG1} \left( \frac{[Efg1]}{([Efg1] + K_E)} + \frac{K_{CE}K_{W1E}}{([Czf1] + K_{CE})([Wor1] + K_{W1E})} \right) \right. \\ &\quad \left. + \beta_0 \left( \frac{K_{CE}K_{W1E}}{([Czf1] + K_{CE})([Wor1] + K_{W1E})} \right) \right] - \alpha[EFG1] \\ \frac{d[Efg1]}{dt} &= \beta'[EFG1] - \alpha_E[Efg1] \end{aligned}$$

$$\begin{aligned} \frac{d[WOR2]}{dt} &= \left[ \beta_{WOR2} \left( \frac{[Wor2]}{([Wor2] + K_{W2})} + \frac{K_{W2E}}{(K_{W2E} + [Efg1])} \right) + \beta_0 \left( \frac{K_{W2E}}{(K_{W2E} + [Efg1])} \right) \right] - \alpha[WOR2] \\ \frac{d[Wor2]}{dt} &= \beta'[WOR2] - \alpha_{w2}[Wor2] \end{aligned}$$

$$\begin{aligned} \frac{d[WOR1]}{dt} &= \left[ \beta_0 + \beta_{WOR1} \left( \frac{[Wor1]}{([Wor1] + K_{W1})} + \frac{[Wor2]}{([Wor2] + K_{W1W2})} \right) \right] - \alpha[WOR1] \\ \frac{d[Wor1]}{dt} &= \beta'[WOR1] - \alpha_{w1}[Wor1] \end{aligned}$$

$$\begin{aligned} \frac{d[Czf1]}{dt} &= \left[ \beta_0 + \beta_{CZF1} \left( \frac{[Czf1]}{([Czf1] + K_C)} + \frac{[Wor1]}{([Wor1] + K_{W1C})} \right) \right] - \alpha[CZF1] \\ \frac{d[Czf1]}{dt} &= \beta'[CZF1] - \alpha_C[Czf1] \end{aligned}$$

## Parameter estimation

Starting guesses for parameter values were obtained by searching through literature. The initial starting values for  $\beta, \beta_0, \beta',$  and  $\alpha$  were obtained from Elowitz et. al. (Elowitz and Leibler, 2000). The starting values for protein degradation rate constant were estimated from the time-course profile of the four proteins (Lohse and Johnson, 2010). The DNA binding affinity values were measured at least for one transcription factor binding to one promoter (Lohse et al., 2010). The initial values for affinity were taken around to be same for each affinity parameter. The initial concentration of the protein species was arbitrarily taken to be 10000 molecules/cell for Wor1, Wor2 and Czf1, while 3333 molecules/cell for Efg1, in order to mimic the physiological condition of white cell type.

The parameter estimation and optimization was attempted by minimizing the following cost (error) function using MATLAB's *fminsearch*. The cost function is simply a sum of squared error function computed from the normalized data from the model's output and the normalized experimental time course data. For this purpose the observed time course data was partitioned into 26 time points and the relative concentration data was extrapolated from the curve, which was then normalized to 0-100 ranges before using to estimate and evaluate the error function. The data from model were also normalized to a range of 0-100 and the error was estimated. The optimization was terminated when a nicely fit data was observed/*fminsearch* did not show any further improvements on error minimization. The parameters obtained from this are being used in Markov chain Monte Carlo (MCMC) simulations to further refine the parameter estimates and to get an idea about the parameter distributions across whole parameter space. Total 2500000 iterations are MCMC iterations will be performed as the convergence test for 200000 iterations failed when analyzed using Geweke criterion. Due to limitation of computational resources, full implementation of MCMC routine is still in progress.

## Parameter sensitivity analysis

Time varying normalized sensitivity was estimated using *sens\_ind* which implements internal numerical differentiation approach (provided by Ericka). The analysis gives absolute sensitivity coefficients:  $w_{ij} = \frac{dy_i(t)}{d(par_j)}$ , where,  $y_i =$  ith variable,  $par_j =$  jth parameter.

The absolute sensitivity coefficient was normalized by multiplying with:  $\frac{par_j}{y_{i,max}}$

Therefore,

$$Normalized\ sensitivity\ S_{ij} = \frac{par_j}{y_{i,max}} * \frac{dy_i(t)}{d(par_j)}$$

In order to generate parameter rankings for their effects on model, the relative sensitivity coefficients were measured using the following along the time axis as described by Yue et. al. (Yue et al., 2006)

$$RS_{ij} = \frac{1}{N} \sqrt{\sum_{k=1}^N (S_{ij}(k))^2}$$

Additionally overall sensitivity of a parameter on model was calculated using the following formulae (Yue et al., 2006);

$$OS_j = \frac{1}{N} \sqrt{\sum_{k=1}^N \sum_{i=1}^8 ((S_{ij}(k))^2)}$$

## 1.5 Results

### The model and model parameters

The model was built on simple rules of writing ODE for transcriptional and translational dynamics.

i.e.,

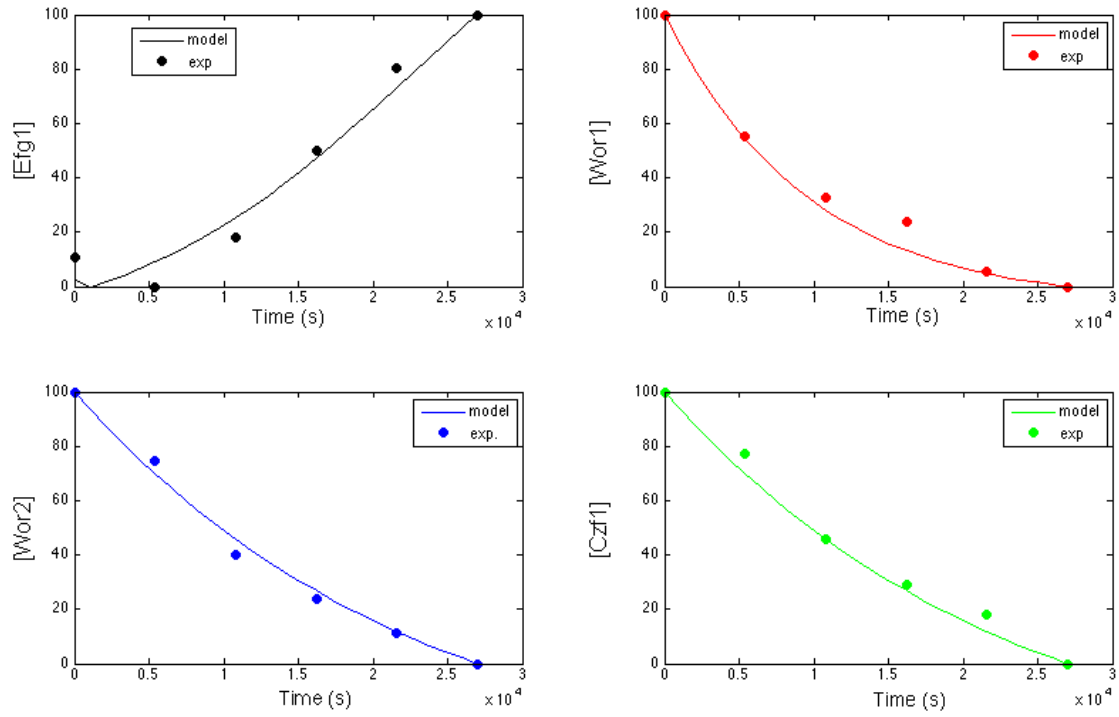
$$\frac{d[mRNA]}{dt} = [\beta(\text{Probability of activator bound} + \text{Probability of repressor not bound}) + \beta_0(\text{Probability of repressor bound})] - \alpha[mRNA]$$

$$\frac{d[Protein]}{dt} = \beta'[mRNA] - \alpha'[Protein]$$

To reduce complexity, the degradation rate constants for different RNA ( $\alpha$ ), transcriptional leakage rate constant ( $\beta_0$ ) and translational efficiency ( $\beta'$ ) were assumed to be identical for all the considered species in the model. Initializing with all the parameters as described in methods and optimizing with the Nelder-Mead simplex algorithm using MATLAB's *fminsearch* after multiple random restarts gave a relatively acceptable parameter values, as shown in Table 4. The time-course profiles for all four transcriptional regulators using this parameter vector are shown in Figure 19, along with the experimental data. The  $r^2$  value was calculated in order to analyze the goodness of fit, and  $r^2 = 0.9863$  indicates a very good fit between the model output and the observed data. The  $r^2$  value was calculated using the equation below:

$$r^2 = 1 - \frac{\sum_i (y_{i,model} - y_{i,exp})^2}{\sum_i (y_{i,model} - \text{mean}(y_{exp}))^2}$$

**Figure 19: Time-course of the cell-switch model output in terms of normalized protein concentrations of the four transcription factors.**



The solid lines in each panel represent the normalized concentration from model the filled markers represent normalized experimental data.

**Table 4: Estimated values of the parameters regulating the white-opaque cell switching.**

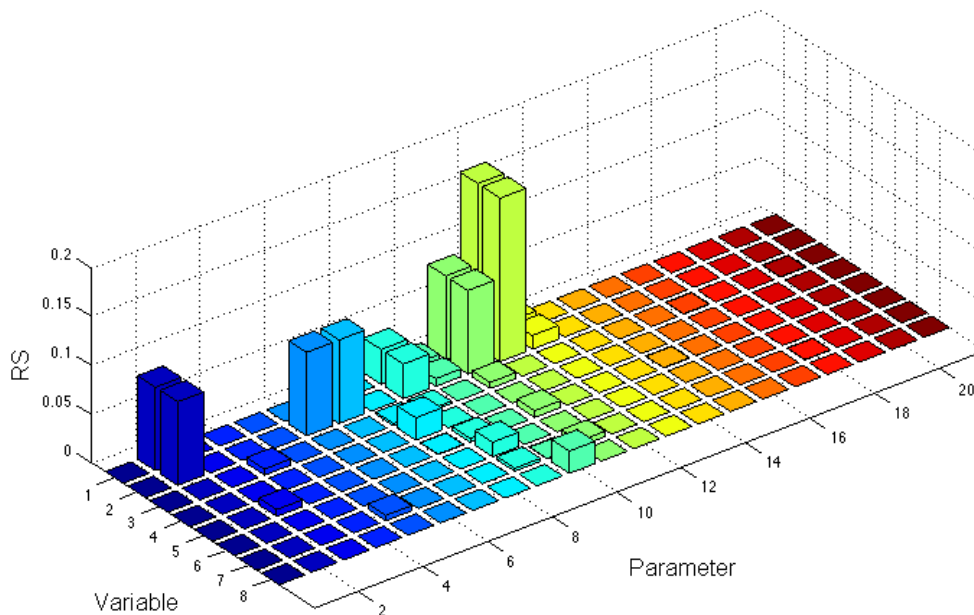
	<b>Parameter</b>	<b>Value</b>	<b>Description and units</b>
1	$\beta$	7.40E-05	Basal promoter activity (assumed similar for all promoters here)
2	$\beta_{EFG1}$	0.3763	Maximum promoter activity for the subscribed transcription factor genes (mRNA molecules/unit time)
3	$\beta_{WOR1}$	0.4086	Maximum promoter activity for the subscribed transcription factor genes (mRNA molecules/unit time)
4	$\beta_{WOR2}$	0.4844	Maximum promoter activity for the subscribed transcription factor genes (mRNA molecules/unit time)
5	$\beta_{CZF1}$	0.3137	Maximum promoter activity for the subscribed transcription factor genes (mRNA molecules/unit time)
6	$\beta'$	2.72E-07	Translational efficiency (protein molecules/mRNA molecule*unit time)
7	$\alpha_E$	0.0142	Protein degradation rate constant (/unit time)
8	$\alpha_{W2}$	4.35E-05	Protein degradation rate constant (/unit time)
9	$\alpha_{W1}$	0.000104	Protein degradation rate constant (/unit time)
10	$\alpha_C$	4.35E-05	Protein degradation rate constant (/unit time)
11	$\alpha$	0.099	mRNA degradation rate constant (/unit time)
12	$K_{CE}$	20190	Affinity of Czf1 for <i>EFG1</i> promoter (dissociation constant, molecules/cellvolm.)
13	$K_{W1E}$	939	Affinity of Wor1 for <i>EFG1</i> promoter (dissociation constant, molecules/cellvolm.)
14	$K_{W2E}$	18.1	Affinity of Wor2 for <i>EFG1</i> promoter (dissociation constant, molecules/cellvolm.)
15	$K_{W1}$	3.4	Affinity of Wor1 for positive autoregulation (dissociation constant)
16	$K_{W1W2}$	8.79	Affinity of Wor1 for <i>WOR2</i> promoter (dissociation constant, molecules/cellvolm.)
17	$K_{W2W1}$	328.9	Affinity of Wor1 for <i>WOR2</i> promoter (dissociation constant, molecules/cellvolm.)
18	$K_{W1C}$	2.82	Affinity of Wor1 for <i>CZF1</i> promoter (dissociation constant, molecules/cellvolm.)

19	$K_E$	51	Affinity of Efg1 for <i>EFG1</i> promoter (dissociation constant, molecules/cellvolm.)
20	$K_{W2}$	56.33	Affinity of Wor2 for <i>WOR2</i> promoter (dissociation constant, molecules/cellvolm.)
21	$K_C$	12.46	Affinity of Czf1 for <i>CZF1</i> promoter (dissociation constant, molecules/cellvolm.)

Sensitivity analysis points towards a role of Efg1 and protein degradation rate constants in switching

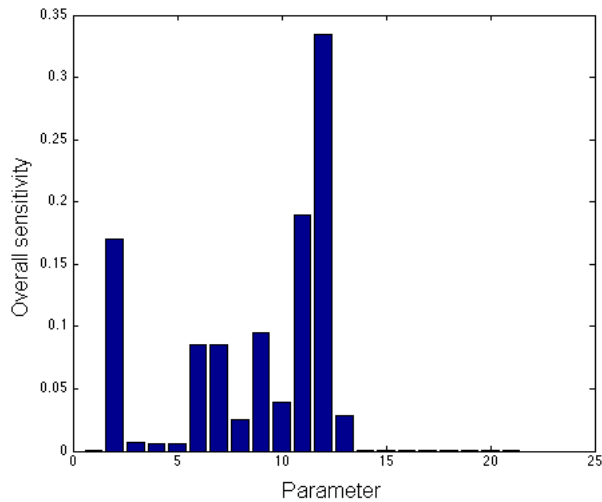
Time varying sensitivity analysis served to highlight the most critical parameters of this system. Sensitivity essentially describes how much the variable at a given is changing with respect to a minor perturbation in given parameter. I analyzed sensitivities for all variables w.r.t all the parameters. For comparative purposes, normalized or relative sensitivity was computed as described in methods. Figure 20 shows a bar chart of relative sensitivities for all variables w.r.t the parameters. Figure 20 shows that many parameters have impact on model mainly through impacting one variable, Efg1 protein concentration. Additionally, protein degradation rate constants (parameters 7-10) have most prominent effects on model, as indicated by high value of the relative sensitivity coefficient (RS), as shown in Figure 20.

**Figure 20: Relative sensitivity coefficients for the RNA and protein species' concentrations w.r.t the 21 parameters.**



The RS value gives an idea about sensitivity of one particular parameter w.r.t. a single variable. I calculated one more measure, the overall sensitivity coefficient (OS), which gives an idea of overall impact of all involved reaction species w.r.t a parameter. Figure 21 shows the plot of OS values for all the 21 parameters. Based on that a total of 8/21 parameters are considered the most sensitive for white-opaque switching.

**Figure 21: Overall sensitivity for the cell-switch model w.r.t the 21 parameters.**



## 1.6 Discussion

In *C. albicans* several experimental studies have helped define roles of transcriptional factors in regulating the white-opaque phenotypic switch (Hernday et al., 2013; Lohse and Johnson, 2009; Zordan et al., 2007). Several nice experiments established the circuit shown in Figure 18, however there was no description of how certain factor makes the switch more frequent than its natural frequency. For example, it has been well established that higher temperature makes the opaque to white transition very rapid and almost 100% of cells in opaque population switch to white state (Rikkerink et al., 1988). Additionally, it is still unclear that which transcription factors and which steps contribute the most to this cell-type switching. These types of questions can be approached methodically by the mathematical model. The presented ODE model serves to capture the observed dynamics really nicely, as the optimized parameters yield the output that conforms nicely to observed data (Figure 2).

An ODE model allows inferring information that would otherwise be difficult to deduce. For example, local sensitivity analysis effectively yields an idea about which parameters are likely the most sensitive parameters for a given model. This approach essentially analyzes the magnitude of change in a dependent variable's signal (here, the protein or mRNA concentration) when any parameter is perturbed slightly (Bentele et al., 2004; Perumal and Gunawan, 2011). The higher the magnitude of change, the higher is the sensitivity to that parameter.

I carried out this analysis to identify that the parameters  $K_{CE}$  (binding of Czf1 to EFG1 promoter),  $\alpha$  (mRNA degradation),  $\beta_{EFG1}$  (EFG1 transcription),  $\beta'$  (protein translation),  $\alpha_E$  (Efg1 protein degradation),  $\alpha_{W1}$  (Wor1 protein degradation),  $\alpha_C$  (Czf1 protein degradation), and  $\alpha_{W2}$  (Wor2 protein degradation) are the most sensitive parameters. On the other hand all other parameters did show least sensitivity to the perturbations. Thus, this calculation of overall sensitivity coefficients (OS, Figure 4) shows that the reactions affecting Efg1 protein levels are very important in regulating switching (because of the highly sensitive  $\beta_{EFG1}$  and  $K_{CE}$ ). Additionally, protein degradation rate constants also show high sensitivity. This may make sense as one can think that altered temperature have effects on protein degradation rates and thus the switching frequency. Thus, it may be possible that the observed higher switching frequency from opaque to white state at higher temperature is mainly mediated by the protein degradation rate parameters.

## 1.7 Conclusion

In conclusion, it can be inferred that the reactions regulating Efg1 protein levels as well as the protein degradation rate reactions are key players in regulating the switching from opaque to white cell type.

The MCMC simulation is currently in progress, which will give an idea about the parameter distribution and also help in further refinement of model. It will also help to corroborate the sensitivity analysis data. Additionally, results of sensitivity analysis will be used to do principal component analysis which will aid in dimensionality reduction. Subsequently, the model will be made more comprehensive by adding two more regulators which were recently described to play roles in regulating the switch.

# Phenotypic screen to uncover genes with potential roles in biofilm development

**Table 5: Phenotypic profile for biofilm up-regulated gene mutants.**

Name	ORF ID	Fold-change (biofilm/planktonic)	Functional analysis of genes using homozygous insertion mutant strains				
			Visual analysis of biofilm formation (Spider medium, 24 hrs) <sup>¶</sup>	Filamentation assay (Spider medium, 37°C) <sup>§</sup>	Relative adherence*	Fold-change in yeast-cell reporter expression in mixed biofilms (relative to wild-type)**	Survival after fluconazole treatment (relative to wild-type) <sup>§</sup>
<i>RHR2</i>	<i>orf19.5437</i>	70.19	Normal	Normal	0.54	1.275	0.76
<i>CAN1</i>	<i>orf19.97</i>	34.96	Normal	Normal	1.34	0.99	1.00
<i>AAH1</i>	<i>orf19.2251</i>	23.86	Normal	Normal	0.71	1.07	1.52
<i>orf19.3483</i>	<i>orf19.3483</i>	14.70	Normal	Normal	0.76	-	1.30
<i>SIT1</i>	<i>orf19.2179</i>	12.17	Normal	Normal	2.00	0.905	1.27
<i>GPD1</i>	<i>orf19.1756</i>	10.94	Normal	Normal	0.66	1.24	1.48
<i>FCY21</i>	<i>orf19.1357</i>	9.97	Normal	Normal	no assigned value (cell-clumps in the channel)	0.39	1.12
<i>orf19.278</i>	<i>orf19.278</i>	9.14	Normal	Normal	0.43	1.24	1.58
<i>MET3</i>	<i>orf19.5025</i>	8.71	Normal	Normal	0.65	1.815	1.50
<i>HGT8</i>	<i>orf19.2021</i>	8.58	Normal	Normal	1.13	1.205	1.11
<i>GRF10/PHO2</i>	<i>orf19.4000</i>	8.40	Normal	Normal	1.46	1.81	1.03
<i>ELF1</i>	<i>orf19.7332</i>	7.43	Normal	Normal	1.20	1.85	1.00
<i>orf19.773</i>	<i>orf19.773</i>	7.40	Normal	Normal	0.95	3.27	1.04
<i>orf19.28</i>	<i>orf19.28</i>	6.95	Normal	Normal	0.93	0.96	-
<i>orf19.3089</i>	<i>orf19.3089</i>	6.86	Normal	Normal	0.66	0.99	1.25
<i>orf19.3665</i>	<i>orf19.3665</i>	6.78	Normal	Normal	3.45	0.73	1.08
<i>orf19.3477</i>	<i>orf19.3477</i>	6.70	Normal	Normal	2.67	2.04	0.63
<i>SMM1</i>	<i>orf19.1362</i>	6.17	Normal	Normal	1.07	2.19	0.63
<i>orf19.1388</i>	<i>orf19.1388</i>	6.14	Normal	Normal	0.86	1.43	0.88
<i>FAD3</i>	<i>orf19.4933</i>	6.10	Normal	Normal	0.93	0.71	0.72
<i>orf19.154</i>	<i>orf19.154</i>	5.37	Normal	Normal	0.70	-	1.28
<i>orf19.1676</i>	<i>orf19.1676</i>	5.05	Normal	Normal	0.99	2.215	1.06
<i>GAP1</i>	<i>orf19.4304</i>	4.55	Normal	Normal	2.38	1.44	0.74
<i>orf19.4563</i>	<i>orf19.4563</i>	4.26	Normal	Normal	0.57	1.49	1.34
<i>HPT1</i>	<i>orf19.5832</i>	4.17	Normal	Normal	0.55	3.72	1.50

<sup>¶</sup> Biofilms were grown as described under methods and examined visually after 24 hours to detect any gross defect

<sup>§</sup> Filamentation was assessed by inoculating overnight culture to fresh Spider media and assaying germ-tube formation after 90 minutes of growth 37°C

\* Adherence was assayed as outlined under methods using the Fluxion assay. The multiple values correspond to the independent mutant isolates

\*\* Yeast-cell reporter expression is reported relative to the wild-type. The values indicated in table are average of the values for independent isolates.

<sup>§</sup> Relative viability after the drug treatment was evaluated using the XTT dye reduction assay as described under methods. The values indicated in table are average of the values for independent isolates.

The cells highlighted in green indicate a statistically significant change relative to wild-type ( $p < 0.05$ ). (Cells were highlighted in green only when the examined independent isolates gave statistically significant change in a same direction, relative to wild-type).

## Bibliography

- Al-Fattani, M.A., and Douglas, L.J. (2006). Biofilm matrix of *Candida albicans* and *Candida tropicalis*: chemical composition and role in drug resistance. *Journal of medical microbiology* 55, 999-1008.
- Almeida, R.S., Wilson, D., and Hube, B. (2009). *Candida albicans* iron acquisition within the host. *FEMS yeast research* 9, 1000-1012.
- Andes, D., Nett, J., Oschel, P., Albrecht, R., Marchillo, K., and Pitula, A. (2004). Development and characterization of an in vivo central venous catheter *Candida albicans* biofilm model. *Infection and immunity* 72, 6023-6031.
- Andes, D.R., Safdar, N., Baddley, J.W., Playford, G., Reboli, A.C., Rex, J.H., Sobel, J.D., Pappas, P.G., Kullberg, B.J., and Mycoses Study, G. (2012). Impact of treatment strategy on outcomes in patients with candidemia and other forms of invasive candidiasis: a patient-level quantitative review of randomized trials. *Clin Infect Dis* 54, 1110-1122.
- Askew, C., Sellam, A., Epp, E., Hogues, H., Mullick, A., Nantel, A., and Whiteway, M. (2009). Transcriptional regulation of carbohydrate metabolism in the human pathogen *Candida albicans*. *PLoS pathogens* 5, e1000612.
- Bahn, Y.S. (2008). Master and commander in fungal pathogens: the two-component system and the HOG signaling pathway. *Eukaryotic cell* 7, 2017-2036.
- Baillie, G.S., and Douglas, L.J. (1999). Role of dimorphism in the development of *Candida albicans* biofilms. *Journal of medical microbiology* 48, 671-679.
- Banerjee, M., Thompson, D.S., Lazzell, A., Carlisle, P.L., Pierce, C., Monteagudo, C., Lopez-Ribot, J.L., and Kadosh, D. (2008). UME6, a novel filament-specific regulator of *Candida albicans* hyphal extension and virulence. *Molecular biology of the cell* 19, 1354-1365.
- Bastidas, R.J., Heitman, J., and Cardenas, M.E. (2009). The protein kinase Tor1 regulates adhesin gene expression in *Candida albicans*. *PLoS pathogens* 5, e1000294.
- Bastmeyer, M., Deising, H.B., and Bechinger, C. (2002). Force exertion in fungal infection. *Annual review of biophysics and biomolecular structure* 31, 321-341.
- Basu, R., Munteanu, E.L., and Chang, F. (2014). Role of turgor pressure in endocytosis in fission yeast. *Molecular biology of the cell* 25, 679-687.
- Bentele, M., Lavrik, I., Ulrich, M., Stosser, S., Heermann, D.W., Kalthoff, H., Krammer, P.H., and Eils, R. (2004). Mathematical modeling reveals threshold mechanism in CD95-induced apoptosis. *The Journal of cell biology* 166, 839-851.
- Bentley, D.R., Balasubramanian, S., Swerdlow, H.P., Smith, G.P., Milton, J., Brown, C.G., Hall, K.P., Evers, D.J., Barnes, C.L., Bignell, H.R., *et al.* (2008). Accurate whole human genome sequencing using reversible terminator chemistry. *Nature* 456, 53-59.
- Berman, J., and Sudbery, P.E. (2002). *Candida Albicans*: a molecular revolution built on lessons from budding yeast. *Nature reviews Genetics* 3, 918-930.
- Bink, A., Vandenbosch, D., Coenye, T., Nelis, H., Cammue, B.P., and Thevissen, K. (2011). Superoxide dismutases are involved in *Candida albicans* biofilm persistence against miconazole. *Antimicrobial agents and chemotherapy* 55, 4033-4037.
- Bishop, A.C., Ganguly, S., Solis, N.V., Cooley, B.M., Jensen-Seaman, M.I., Filler, S.G., Mitchell, A.P., and Patton-Vogt, J. (2013). Glycerophosphocholine Utilization by *Candida albicans*: ROLE OF THE Git3 TRANSPORTER IN VIRULENCE. *The Journal of biological chemistry* 288, 33939-33952.
- Biswas, S., Van Dijck, P., and Datta, A. (2007). Environmental sensing and signal transduction pathways regulating morphopathogenic determinants of *Candida albicans*. *Microbiology and molecular biology reviews* : MMBR 71, 348-376.
- Blankenship, J.R., Fanning, S., Hamaker, J.J., and Mitchell, A.P. (2010). An extensive circuitry for cell wall regulation in *Candida albicans*. *PLoS pathogens* 6, e1000752.
- Blankenship, J.R., and Mitchell, A.P. (2006). How to build a biofilm: a fungal perspective. *Current opinion in microbiology* 9, 588-594.
- Bonhomme, J., Chauvel, M., Goyard, S., Roux, P., Rossignol, T., and d'Enfert, C. (2011). Contribution of the glycolytic flux and hypoxia adaptation to efficient biofilm formation by *Candida albicans*. *Molecular microbiology* 80, 995-1013.

Brand, A. (2012). Hyphal growth in human fungal pathogens and its role in virulence. *International journal of microbiology* 2012, 517529.

Brand, A., and Gow, N.A. (2009). Mechanisms of hypha orientation of fungi. *Current opinion in microbiology* 12, 350-357.

Brand, A., Lee, K., Veses, V., and Gow, N.A. (2009). Calcium homeostasis is required for contact-dependent helical and sinusoidal tip growth in *Candida albicans* hyphae. *Molecular microbiology* 71, 1155-1164.

Bruno, V.M., and Mitchell, A.P. (2004). Large-scale gene function analysis in *Candida albicans*. *Trends in microbiology* 12, 157-161.

Carlisle, P.L., Banerjee, M., Lazzell, A., Monteagudo, C., Lopez-Ribot, J.L., and Kadosh, D. (2009). Expression levels of a filament-specific transcriptional regulator are sufficient to determine *Candida albicans* morphology and virulence. *Proceedings of the National Academy of Sciences of the United States of America* 106, 599-604.

Celton, M., Goelzer, A., Camarasa, C., Fromion, V., and Dequin, S. (2012). A constraint-based model analysis of the metabolic consequences of increased NADPH oxidation in *Saccharomyces cerevisiae*. *Metabolic engineering* 14, 366-379.

Chaffin, W.L. (2008). *Candida albicans* cell wall proteins. *Microbiology and molecular biology reviews* : MMBR 72, 495-544.

Chaffin, W.L., Lopez-Ribot, J.L., Casanova, M., Gozalbo, D., and Martinez, J.P. (1998). Cell wall and secreted proteins of *Candida albicans*: identification, function, and expression. *Microbiology and molecular biology reviews* : MMBR 62, 130-180.

Chandra, J., Kuhn, D.M., Mukherjee, P.K., Hoyer, L.L., McCormick, T., and Ghannoum, M.A. (2001). Biofilm formation by the fungal pathogen *Candida albicans*: development, architecture, and drug resistance. *Journal of bacteriology* 183, 5385-5394.

Chandra, J., Long, L., Ghannoum, M.A., and Mukherjee, P.K. (2011). A rabbit model for evaluation of catheter-associated fungal biofilms. *Virulence* 2, 466-474.

Cheng, S., Clancy, C.J., Xu, W., Schneider, F., Hao, B., Mitchell, A.P., and Nguyen, M.H. (2013). Profiling of *Candida albicans* gene expression during intra-abdominal candidiasis identifies biologic processes involved in pathogenesis. *The Journal of infectious diseases* 208, 1529-1537.

Clasquin, M.F., Melamud, E., Singer, A., Gooding, J.R., Xu, X., Dong, A., Cui, H., Campagna, S.R., Savchenko, A., Yakunin, A.F., *et al.* (2011). Riboneogenesis in yeast. *Cell* 145, 969-980.

Correia, A., Lermann, U., Teixeira, L., Cerca, F., Botelho, S., da Costa, R.M., Sampaio, P., Gartner, F., Morschhauser, J., Vilanova, M., *et al.* (2010). Limited role of secreted aspartyl proteinases Sap1 to Sap6 in *Candida albicans* virulence and host immune response in murine hematogenously disseminated candidiasis. *Infection and immunity* 78, 4839-4849.

Dalle, F., Wachtler, B., L'Ollivier, C., Holland, G., Bannert, N., Wilson, D., Labruere, C., Bonnin, A., and Hube, B. (2010). Cellular interactions of *Candida albicans* with human oral epithelial cells and enterocytes. *Cellular microbiology* 12, 248-271.

Daniels, K.J., Park, Y.N., Srikantha, T., Pujol, C., and Soll, D.R. (2013). Impact of environmental conditions on the form and function of *Candida albicans* biofilms. *Eukaryotic cell* 12, 1389-1402.

Davis, T.R., Zucchi, P.C., and Kumamoto, C.A. (2013). Calmodulin binding to Dfi1p promotes invasiveness of *Candida albicans*. *PLoS one* 8, e76239.

Desai, J.V., Bruno, V.M., Ganguly, S., Stamper, R.J., Mitchell, K.F., Solis, N., Hill, E.M., Xu, W., Filler, S.G., Andes, D.R., *et al.* (2013). Regulatory role of glycerol in *Candida albicans* biofilm formation. *mBio* 4, e00637-00612.

Donlan, R.M. (2001). Biofilms and device-associated infections. *Emerging infectious diseases* 7, 277-281.

Donlan, R.M. (2002). Biofilms: microbial life on surfaces. *Emerging infectious diseases* 8, 881-890.

Dranginis, A.M., Rauceo, J.M., Coronado, J.E., and Lipke, P.N. (2007). A biochemical guide to yeast adhesins: glycoproteins for social and antisocial occasions. *Microbiology and molecular biology reviews* : MMBR 71, 282-294.

Elowitz, M.B., and Leibler, S. (2000). A synthetic oscillatory network of transcriptional regulators. *Nature* 403, 335-338.

Ene, I.V., and Bennett, R.J. (2009). Hwp1 and related adhesins contribute to both mating and biofilm formation in *Candida albicans*. *Eukaryotic cell* 8, 1909-1913.

Fan, J., Whiteway, M., and Shen, S.H. (2005). Disruption of a gene encoding glycerol 3-phosphatase from *Candida albicans* impairs intracellular glycerol accumulation-mediated salt-tolerance. *FEMS microbiology letters* **245**, 107-116.

Fanning, S., Xu, W., Beaurepaire, C., Suhan, J.P., Nantel, A., and Mitchell, A.P. (2012a). Functional control of the *Candida albicans* cell wall by catalytic protein kinase A subunit Tpk1. *Molecular microbiology* **86**, 284-302.

Fanning, S., Xu, W., Solis, N., Woolford, C.A., Filler, S.G., and Mitchell, A.P. (2012b). Divergent targets of *Candida albicans* biofilm regulator Bcr1 in vitro and in vivo. *Eukaryotic cell* **11**, 896-904.

Finkel, J.S., and Mitchell, A.P. (2011). Genetic control of *Candida albicans* biofilm development. *Nature reviews Microbiology* **9**, 109-118.

Finkel, J.S., Xu, W., Huang, D., Hill, E.M., Desai, J.V., Woolford, C.A., Nett, J.E., Taff, H., Norice, C.T., Andes, D.R., *et al.* (2012). Portrait of *Candida albicans* adherence regulators. *PLoS pathogens* **8**, e1002525.

Finkel, J.S., Yudanin, N., Nett, J.E., Andes, D.R., and Mitchell, A.P. (2011). Application of the systematic "DAMP" approach to create a partially defective *C. albicans* mutant. *Fungal genetics and biology* : FG & B **48**, 1056-1061.

Fox, E.P., and Nobile, C.J. (2012). A sticky situation: untangling the transcriptional network controlling biofilm development in *Candida albicans*. *Transcription* **3**, 315-322.

Fu, Y., Rieg, G., Fonzi, W.A., Belanger, P.H., Edwards, J.E., Jr., and Filler, S.G. (1998). Expression of the *Candida albicans* gene ALS1 in *Saccharomyces cerevisiae* induces adherence to endothelial and epithelial cells. *Infection and immunity* **66**, 1783-1786.

Ganguly, S., Bishop, A.C., Xu, W., Ghosh, S., Nickerson, K.W., Lanni, F., Patton-Vogt, J., and Mitchell, A.P. (2011). Zap1 control of cell-cell signaling in *Candida albicans* biofilms. *Eukaryotic cell* **10**, 1448-1454.

Ganguly, S., and Mitchell, A.P. (2011). Mucosal biofilms of *Candida albicans*. *Current opinion in microbiology* **14**, 380-385.

Ganguly, S., and Mitchell, A.P. (2012). Mini-blaster-mediated targeted gene disruption and marker complementation in *Candida albicans*. *Methods in molecular biology* **845**, 19-39.

Garcia, M.C., Lee, J.T., Ramsook, C.B., Alsteens, D., Dufrene, Y.F., and Lipke, P.N. (2011). A role for amyloid in cell aggregation and biofilm formation. *PLoS one* **6**, e17632.

Garcia-Sanchez, S., Aubert, S., Iraqui, I., Janbon, G., Ghigo, J.M., and d'Enfert, C. (2004). *Candida albicans* biofilms: a developmental state associated with specific and stable gene expression patterns. *Eukaryotic cell* **3**, 536-545.

Gaur, N.K., Klotz, S.A., and Henderson, R.L. (1999). Overexpression of the *Candida albicans* ALA1 gene in *Saccharomyces cerevisiae* results in aggregation following attachment of yeast cells to extracellular matrix proteins, adherence properties similar to those of *Candida albicans*. *Infection and immunity* **67**, 6040-6047.

Geiss, G.K., Bumgarner, R.E., Birditt, B., Dahl, T., Dowidar, N., Dunaway, D.L., Fell, H.P., Ferree, S., George, R.D., Grogan, T., *et al.* (2008). Direct multiplexed measurement of gene expression with color-coded probe pairs. *Nature biotechnology* **26**, 317-325.

Gillum, A.M., Tsay, E.Y., and Kirsch, D.R. (1984). Isolation of the *Candida albicans* gene for orotidine-5'-phosphate decarboxylase by complementation of *S. cerevisiae* ura3 and *E. coli* pyrF mutations. *Molecular & general genetics* : MGG **198**, 179-182.

Gow, N.A., and Hube, B. (2012). Importance of the *Candida albicans* cell wall during commensalism and infection. *Current opinion in microbiology* **15**, 406-412.

Granger, B.L. (2012). Insight into the antiadhesive effect of yeast wall protein 1 of *Candida albicans*. *Eukaryotic cell* **11**, 795-805.

Granger, B.L., Flenniken, M.L., Davis, D.A., Mitchell, A.P., and Cutler, J.E. (2005). Yeast wall protein 1 of *Candida albicans*. *Microbiology* **151**, 1631-1644.

Gutierrez-Escribano, P., Zeidler, U., Suarez, M.B., Bachellier-Bassi, S., Clemente-Blanco, A., Bonhomme, J., Vazquez de Aldana, C.R., d'Enfert, C., and Correa-Bordes, J. (2012). The NDR/LATS kinase Cbk1 controls the activity of the transcriptional regulator Bcr1 during biofilm formation in *Candida albicans*. *PLoS pathogens* **8**, e1002683.

Hashash, R., Younes, S., Bahnan, W., El Koussa, J., Maalouf, K., Dimassi, H.I., and Khalaf, R.A. (2011). Characterisation of Pga1, a putative *Candida albicans* cell wall protein necessary for proper adhesion and biofilm formation. *Mycoses* **54**, 491-500.

Hawser, S.P., Baillie, G.S., and Douglas, L.J. (1998). Production of extracellular matrix by *Candida albicans* biofilms. *Journal of medical microbiology* *47*, 253-256.

Hawser, S.P., and Douglas, L.J. (1994). Biofilm formation by *Candida* species on the surface of catheter materials in vitro. *Infection and immunity* *62*, 915-921.

Hernday, A.D., Lohse, M.B., Fordyce, P.M., Nobile, C.J., DeRisi, J.L., and Johnson, A.D. (2013). Structure of the transcriptional network controlling white-opaque switching in *Candida albicans*. *Molecular microbiology* *90*, 22-35.

Hiller, E., Heine, S., Brunner, H., and Rupp, S. (2007). *Candida albicans* Sun41p, a putative glycosidase, is involved in morphogenesis, cell wall biogenesis, and biofilm formation. *Eukaryotic cell* *6*, 2056-2065.

Hohmann, S. (2002). Osmotic stress signaling and osmoadaptation in yeasts. *Microbiology and molecular biology reviews* : MMBR *66*, 300-372.

Homann, O.R., Dea, J., Noble, S.M., and Johnson, A.D. (2009). A phenotypic profile of the *Candida albicans* regulatory network. *PLoS genetics* *5*, e1000783.

Hornby, J.M., Jensen, E.C., Lisec, A.D., Tasto, J.J., Jahnke, B., Shoemaker, R., Dussault, P., and Nickerson, K.W. (2001). Quorum sensing in the dimorphic fungus *Candida albicans* is mediated by farnesol. *Applied and environmental microbiology* *67*, 2982-2992.

Hoyer, L.L., Green, C.B., Oh, S.H., and Zhao, X. (2008). Discovering the secrets of the *Candida albicans* agglutinin-like sequence (ALS) gene family--a sticky pursuit. *Medical mycology* *46*, 1-15.

Hoyer, L.L., and Hecht, J.E. (2001). The ALS5 gene of *Candida albicans* and analysis of the Als5p N-terminal domain. *Yeast* *18*, 49-60.

Kamai, Y., Kubota, M., Kamai, Y., Hosokawa, T., Fukuoka, T., and Filler, S.G. (2001). New model of oropharyngeal candidiasis in mice. *Antimicrobial agents and chemotherapy* *45*, 3195-3197.

Kaserer, A.O., Andi, B., Cook, P.F., and West, A.H. (2009). Effects of osmolytes on the SLN1-YPD1-SSK1 phosphorelay system from *Saccharomyces cerevisiae*. *Biochemistry* *48*, 8044-8050.

Khamooshi, K., Sikorski, P., Sun, N., Calderone, R., and Li, D. (2014). The Rbf1, Hfl1 and Dbp4 of *Candida albicans* regulate common as well as transcription factor-specific mitochondrial and other cell activities. *BMC genomics* *15*, 56.

Klotz, S.A., Gaur, N.K., Lake, D.F., Chan, V., Rauceo, J., and Lipke, P.N. (2004). Degenerate peptide recognition by *Candida albicans* adhesins Als5p and Als1p. *Infection and immunity* *72*, 2029-2034.

Kojic, E.M., and Darouiche, R.O. (2004). *Candida* infections of medical devices. *Clin Microbiol Rev* *17*, 255-267.

Kumamoto, C.A. (2005). A contact-activated kinase signals *Candida albicans* invasive growth and biofilm development. *Proceedings of the National Academy of Sciences of the United States of America* *102*, 5576-5581.

Kumamoto, C.A. (2008). Molecular mechanisms of mechanosensing and their roles in fungal contact sensing. *Nature reviews Microbiology* *6*, 667-673.

Kumamoto, C.A., and Vines, M.D. (2005). Alternative *Candida albicans* lifestyles: growth on surfaces. *Annual review of microbiology* *59*, 113-133.

LaFleur, M.D., Kumamoto, C.A., and Lewis, K. (2006). *Candida albicans* biofilms produce antifungal-tolerant persister cells. *Antimicrobial agents and chemotherapy* *50*, 3839-3846.

Leonhard, M., Moser, D., Reumueller, A., Mancusi, G., Bigenzahn, W., and Schneider-Stickler, B. (2010). Comparison of biofilm formation on new Phonax and Provox 2 voice prostheses - a pilot study. *Head & neck* *32*, 886-895.

Lermann, U., and Morschhauser, J. (2008). Secreted aspartic proteases are not required for invasion of reconstituted human epithelia by *Candida albicans*. *Microbiology* *154*, 3281-3295.

Li, F., and Palecek, S.P. (2003). EAP1, a *Candida albicans* gene involved in binding human epithelial cells. *Eukaryotic cell* *2*, 1266-1273.

Li, F., and Palecek, S.P. (2008). Distinct domains of the *Candida albicans* adhesin Eap1p mediate cell-cell and cell-substrate interactions. *Microbiology* *154*, 1193-1203.

Li, F., Svarovsky, M.J., Karlsson, A.J., Wagner, J.P., Marchillo, K., Oshel, P., Andes, D., and Palecek, S.P. (2007). Eap1p, an adhesin that mediates *Candida albicans* biofilm formation in vitro and in vivo. *Eukaryotic cell* *6*, 931-939.

Lindsay, A.K., Deveau, A., Piispanen, A.E., and Hogan, D.A. (2012). Farnesol and cyclic AMP signaling effects on the hypha-to-yeast transition in *Candida albicans*. *Eukaryotic cell* *11*, 1219-1225.

Lipke, P.N., Garcia, M.C., Alsteens, D., Ramsook, C.B., Klotz, S.A., and Dufrene, Y.F. (2012). Strengthening relationships: amyloids create adhesion nanodomains in yeasts. *Trends in microbiology* *20*, 59-65.

Liu, Y., and Filler, S.G. (2011). *Candida albicans* Als3, a multifunctional adhesin and invasin. *Eukaryotic cell* *10*, 168-173.

Lockhart, J.A. (1965). An analysis of irreversible plant cell elongation. *Journal of theoretical biology* *8*, 264-275.

Lohse, M.B., and Johnson, A.D. (2009). White-opaque switching in *Candida albicans*. *Current opinion in microbiology* *12*, 650-654.

Lohse, M.B., and Johnson, A.D. (2010). Temporal anatomy of an epigenetic switch in cell programming: the white-opaque transition of *C. albicans*. *Molecular microbiology* *78*, 331-343.

Lohse, M.B., Zordan, R.E., Cain, C.W., and Johnson, A.D. (2010). Distinct class of DNA-binding domains is exemplified by a master regulator of phenotypic switching in *Candida albicans*. *Proceedings of the National Academy of Sciences of the United States of America* *107*, 14105-14110.

Lu, Y., Su, C., Unoje, O., and Liu, H. (2014). Quorum sensing controls hyphal initiation in *Candida albicans* through Ubr1-mediated protein degradation. *Proceedings of the National Academy of Sciences of the United States of America* *111*, 1975-1980.

Ma, H., Kunes, S., Schatz, P.J., and Botstein, D. (1987). Plasmid construction by homologous recombination in yeast. *Gene* *58*, 201-216.

Marrie, T.J., and Costerton, J.W. (1984). Scanning and transmission electron microscopy of in situ bacterial colonization of intravenous and intraarterial catheters. *Journal of clinical microbiology* *19*, 687-693.

Martins, M., Henriques, M., Lopez-Ribot, J.L., and Oliveira, R. (2012). Addition of DNase improves the in vitro activity of antifungal drugs against *Candida albicans* biofilms. *Mycoses* *55*, 80-85.

Martins, M., Uppuluri, P., Thomas, D.P., Cleary, I.A., Henriques, M., Lopez-Ribot, J.L., and Oliveira, R. (2010). Presence of extracellular DNA in the *Candida albicans* biofilm matrix and its contribution to biofilms. *Mycopathologia* *169*, 323-331.

Menon, V., De Bernardis, F., Calderone, R., and Chauhan, N. (2008). Transcriptional profiling of the *Candida albicans* Ssk1p receiver domain point mutants and their virulence. *FEMS yeast research* *8*, 756-763.

Menon, V., Li, D., Chauhan, N., Rajnarayanan, R., Dubrovskaya, A., West, A.H., and Calderone, R. (2006). Functional studies of the Ssk1p response regulator protein of *Candida albicans* as determined by phenotypic analysis of receiver domain point mutants. *Molecular microbiology* *62*, 997-1013.

Minc, N., Boudaoud, A., and Chang, F. (2009). Mechanical forces of fission yeast growth. *Current biology* : CB *19*, 1096-1101.

Monriot, C., Boisrame, A., Da Costa, G., Chauvel, M., Sautour, M., Bougnoux, M.E., Bellon-Fontaine, M.N., Dalle, F., d'Enfert, C., and Richard, M.L. (2013). Rbt1 Protein Domains Analysis in *Candida albicans* Brings Insights into Hyphal Surface Modifications and Rbt1 Potential Role during Adhesion and Biofilm Formation. *PLoS one* *8*, e82395.

Morales, D.K., and Hogan, D.A. (2010). *Candida albicans* interactions with bacteria in the context of human health and disease. *PLoS pathogens* *6*, e1000886.

Mortazavi, A., Williams, B.A., McCue, K., Schaeffer, L., and Wold, B. (2008). Mapping and quantifying mammalian transcriptomes by RNA-Seq. *Nature methods* *5*, 621-628.

Mukherjee, P.K., Chandra, J., Kuhn, D.M., and Ghannoum, M.A. (2003). Mechanism of fluconazole resistance in *Candida albicans* biofilms: phase-specific role of efflux pumps and membrane sterols. *Infection and immunity* *71*, 4333-4340.

Mukherjee, P.K., Mohamed, S., Chandra, J., Kuhn, D., Liu, S., Antar, O.S., Munyon, R., Mitchell, A.P., Andes, D., Chance, M.R., *et al.* (2006). Alcohol dehydrogenase restricts the ability of the pathogen *Candida albicans* to form a biofilm on catheter surfaces through an ethanol-based mechanism. *Infection and immunity* *74*, 3804-3816.

Murillo, L.A., Newport, G., Lan, C.Y., Habelitz, S., Dungan, J., and Agabian, N.M. (2005). Genome-wide transcription profiling of the early phase of biofilm formation by *Candida albicans*. *Eukaryotic cell* 4, 1562-1573.

Nett, J., Lincoln, L., Marchillo, K., Massey, R., Holoyda, K., Hoff, B., VanHandel, M., and Andes, D. (2007). Putative role of beta-1,3 glucans in *Candida albicans* biofilm resistance. *Antimicrobial agents and chemotherapy* 51, 510-520.

Nett, J.E., Crawford, K., Marchillo, K., and Andes, D.R. (2010a). Role of Fks1p and matrix glucan in *Candida albicans* biofilm resistance to an echinocandin, pyrimidine, and polyene. *Antimicrobial agents and chemotherapy* 54, 3505-3508.

Nett, J.E., Lepak, A.J., Marchillo, K., and Andes, D.R. (2009). Time course global gene expression analysis of an in vivo *Candida* biofilm. *The Journal of infectious diseases* 200, 307-313.

Nett, J.E., Marchillo, K., Spiegel, C.A., and Andes, D.R. (2010b). Development and validation of an in vivo *Candida albicans* biofilm denture model. *Infection and immunity* 78, 3650-3659.

Nett, J.E., Sanchez, H., Cain, M.T., Ross, K.M., and Andes, D.R. (2011). Interface of *Candida albicans* biofilm matrix-associated drug resistance and cell wall integrity regulation. *Eukaryotic cell* 10, 1660-1669.

Nobile, C.J., Andes, D.R., Nett, J.E., Smith, F.J., Yue, F., Phan, Q.T., Edwards, J.E., Filler, S.G., and Mitchell, A.P. (2006a). Critical role of Bcr1-dependent adhesins in *C. albicans* biofilm formation in vitro and in vivo. *PLoS pathogens* 2, e63.

Nobile, C.J., Fox, E.P., Nett, J.E., Sorrells, T.R., Mitrovich, Q.M., Hernday, A.D., Tuch, B.B., Andes, D.R., and Johnson, A.D. (2012). A recently evolved transcriptional network controls biofilm development in *Candida albicans*. *Cell* 148, 126-138.

Nobile, C.J., and Mitchell, A.P. (2005). Regulation of cell-surface genes and biofilm formation by the *C. albicans* transcription factor Bcr1p. *Current biology : CB* 15, 1150-1155.

Nobile, C.J., and Mitchell, A.P. (2009). Large-scale gene disruption using the UAU1 cassette. *Methods in molecular biology* 499, 175-194.

Nobile, C.J., Nett, J.E., Andes, D.R., and Mitchell, A.P. (2006b). Function of *Candida albicans* adhesin Hwp1 in biofilm formation. *Eukaryotic cell* 5, 1604-1610.

Nobile, C.J., Nett, J.E., Hernday, A.D., Homann, O.R., Deneault, J.S., Nantel, A., Andes, D.R., Johnson, A.D., and Mitchell, A.P. (2009). Biofilm matrix regulation by *Candida albicans* Zap1. *PLoS biology* 7, e1000133.

Nobile, C.J., Schneider, H.A., Nett, J.E., Sheppard, D.C., Filler, S.G., Andes, D.R., and Mitchell, A.P. (2008a). Complementary adhesin function in *C. albicans* biofilm formation. *Current biology : CB* 18, 1017-1024.

Nobile, C.J., Solis, N., Myers, C.L., Fay, A.J., Deneault, J.S., Nantel, A., Mitchell, A.P., and Filler, S.G. (2008b). *Candida albicans* transcription factor Rim101 mediates pathogenic interactions through cell wall functions. *Cellular microbiology* 10, 2180-2196.

Noble, S.M., and Johnson, A.D. (2005). Strains and strategies for large-scale gene deletion studies of the diploid human fungal pathogen *Candida albicans*. *Eukaryotic cell* 4, 298-309.

Norice, C.T., Smith, F.J., Jr., Solis, N., Filler, S.G., and Mitchell, A.P. (2007). Requirement for *Candida albicans* Sun41 in biofilm formation and virulence. *Eukaryotic cell* 6, 2046-2055.

Pahlman, A.K., Granath, K., Ansell, R., Hohmann, S., and Adler, L. (2001). The yeast glycerol 3-phosphatases Gpp1p and Gpp2p are required for glycerol biosynthesis and differentially involved in the cellular responses to osmotic, anaerobic, and oxidative stress. *The Journal of biological chemistry* 276, 3555-3563.

Peleg, A.Y., Hogan, D.A., and Mylonakis, E. (2010). Medically important bacterial-fungal interactions. *Nature reviews Microbiology* 8, 340-349.

Peltroche-Llacsahuanga, H., Goyard, S., d'Enfert, C., Prill, S.K., and Ernst, J.F. (2006). Protein O-mannosyltransferase isoforms regulate biofilm formation in *Candida albicans*. *Antimicrobial agents and chemotherapy* 50, 3488-3491.

Perez, A., Pedros, B., Murgui, A., Casanova, M., Lopez-Ribot, J.L., and Martinez, J.P. (2006). Biofilm formation by *Candida albicans* mutants for genes coding fungal proteins exhibiting the eight-cysteine-containing CFEM domain. *FEMS yeast research* 6, 1074-1084.

Perez, J.C., Kumamoto, C.A., and Johnson, A.D. (2013). *Candida albicans* commensalism and pathogenicity are intertwined traits directed by a tightly knit transcriptional regulatory circuit. *PLoS biology* 11, e1001510.

Perumal, T.M., and Gunawan, R. (2011). Understanding dynamics using sensitivity analysis: caveat and solution. *BMC systems biology* 5, 41.

Phan, Q.T., Myers, C.L., Fu, Y., Sheppard, D.C., Yeaman, M.R., Welch, W.H., Ibrahim, A.S., Edwards, J.E., Jr., and Filler, S.G. (2007). Als3 is a *Candida albicans* invasin that binds to cadherins and induces endocytosis by host cells. *PLoS biology* 5, e64.

Proseus, T.E., Ortega, J.K., and Boyer, J.S. (1999). Separating growth from elastic deformation during cell enlargement. *Plant physiology* 119, 775-784.

Puri, S., Kumar, R., Chadha, S., Tati, S., Conti, H.R., Hube, B., Cullen, P.J., and Edgerton, M. (2012). Secreted aspartic protease cleavage of *Candida albicans* Msb2 activates Cek1 MAPK signaling affecting biofilm formation and oropharyngeal candidiasis. *PLoS one* 7, e46020.

Ramage, G., Bachmann, S., Patterson, T.F., Wickes, B.L., and Lopez-Ribot, J.L. (2002a). Investigation of multidrug efflux pumps in relation to fluconazole resistance in *Candida albicans* biofilms. *J Antimicrob Chemother* 49, 973-980.

Ramage, G., Saville, S.P., Wickes, B.L., and Lopez-Ribot, J.L. (2002b). Inhibition of *Candida albicans* biofilm formation by farnesol, a quorum-sensing molecule. *Applied and environmental microbiology* 68, 5459-5463.

Ramage, G., VandeWalle, K., Lopez-Ribot, J.L., and Wickes, B.L. (2002c). The filamentation pathway controlled by the Efg1 regulator protein is required for normal biofilm formation and development in *Candida albicans*. *FEMS microbiology letters* 214, 95-100.

Rauceo, J.M., De Armond, R., Otoo, H., Kahn, P.C., Klotz, S.A., Gaur, N.K., and Lipke, P.N. (2006). Threonine-rich repeats increase fibronectin binding in the *Candida albicans* adhesin Als5p. *Eukaryotic cell* 5, 1664-1673.

Richard, M.L., Nobile, C.J., Bruno, V.M., and Mitchell, A.P. (2005). *Candida albicans* biofilm-defective mutants. *Eukaryotic cell* 4, 1493-1502.

Rikkerink, E.H., Magee, B.B., and Magee, P.T. (1988). Opaque-white phenotype transition: a programmed morphological transition in *Candida albicans*. *Journal of bacteriology* 170, 895-899.

Robbins, N., Uppuluri, P., Nett, J., Rajendran, R., Ramage, G., Lopez-Ribot, J.L., Andes, D., and Cowen, L.E. (2011). Hsp90 governs dispersion and drug resistance of fungal biofilms. *PLoS pathogens* 7, e1002257.

Rosignol, T., Ding, C., Guida, A., d'Enfert, C., Higgins, D.G., and Butler, G. (2009). Correlation between biofilm formation and the hypoxic response in *Candida parapsilosis*. *Eukaryotic cell* 8, 550-559.

Salgado, P.S., Yan, R., Taylor, J.D., Burchell, L., Jones, R., Hoyer, L.L., Matthews, S.J., Simpson, P.J., and Cota, E. (2011). Structural basis for the broad specificity to host-cell ligands by the pathogenic fungus *Candida albicans*. *Proceedings of the National Academy of Sciences of the United States of America* 108, 15775-15779.

Sandini, S., Stringaro, A., Arancia, S., Colone, M., Mondello, F., Murtas, S., Girolamo, A., Mastrangelo, N., and De Bernardis, F. (2011). The MP65 gene is required for cell wall integrity, adherence to epithelial cells and biofilm formation in *Candida albicans*. *BMC microbiology* 11, 106.

Sen, M., Shah, B., Rakshit, S., Singh, V., Padmanabhan, B., Ponnusamy, M., Pari, K., Vishwakarma, R., Nandi, D., and Sadhale, P.P. (2011). UDP-glucose 4, 6-dehydratase activity plays an important role in maintaining cell wall integrity and virulence of *Candida albicans*. *PLoS pathogens* 7, e1002384.

Shapiro, R.S., Robbins, N., and Cowen, L.E. (2011). Regulatory circuitry governing fungal development, drug resistance, and disease. *Microbiology and molecular biology reviews* : MMBR 75, 213-267.

Singleton, D.R., Masuoka, J., and Hazen, K.C. (2001). Cloning and analysis of a *Candida albicans* gene that affects cell surface hydrophobicity. *Journal of bacteriology* 183, 3582-3588.

Slutsky, B., Staebell, M., Anderson, J., Risen, L., Pfaller, M., and Soll, D.R. (1987). "White-opaque transition": a second high-frequency switching system in *Candida albicans*. *Journal of bacteriology* 169, 189-197.

Srikantha, T., Daniels, K.J., Pujol, C., Kim, E., and Soll, D.R. (2013). Identification of genes upregulated by the transcription factor Bcr1 that are involved in impermeability, impenetrability, and drug resistance of *Candida albicans*  $\alpha$ /alpha biofilms. *Eukaryotic cell* 12, 875-888.

Staab, J.F., Bradway, S.D., Fidel, P.L., and Sundstrom, P. (1999). Adhesive and mammalian transglutaminase substrate properties of *Candida albicans* Hwp1. *Science* 283, 1535-1538.

Stewart, P.S., and Franklin, M.J. (2008). Physiological heterogeneity in biofilms. *Nature reviews Microbiology* 6, 199-210.

Stichternoth, C., and Ernst, J.F. (2009). Hypoxic adaptation by Efg1 regulates biofilm formation by *Candida albicans*. *Applied and environmental microbiology* 75, 3663-3672.

Su, C., Lu, Y., and Liu, H. (2013). Reduced TOR signaling sustains hyphal development in *Candida albicans* by lowering Hog1 basal activity. *Molecular biology of the cell* 24, 385-397.

Sudbery, P.E. (2011). Growth of *Candida albicans* hyphae. *Nature reviews Microbiology* 9, 737-748.

Sun, J.N., Solis, N.V., Phan, Q.T., Bajwa, J.S., Kashleva, H., Thompson, A., Liu, Y., Dongari-Bagtzoglou, A., Edgerton, M., and Filler, S.G. (2010). Host cell invasion and virulence mediated by *Candida albicans* Ssa1. *PLoS pathogens* 6, e1001181.

Synnott, J.M., Guida, A., Mulhern-Haughey, S., Higgins, D.G., and Butler, G. (2010). Regulation of the hypoxic response in *Candida albicans*. *Eukaryotic cell* 9, 1734-1746.

Taff, H.T., Nett, J.E., Zarnowski, R., Ross, K.M., Sanchez, H., Cain, M.T., Hamaker, J., Mitchell, A.P., and Andes, D.R. (2012). A *Candida* biofilm-induced pathway for matrix glucan delivery: implications for drug resistance. *PLoS pathogens* 8, e1002848.

Thomas, D.P., Bachmann, S.P., and Lopez-Ribot, J.L. (2006). Proteomics for the analysis of the *Candida albicans* biofilm lifestyle. *Proteomics* 6, 5795-5804.

Tournu, H., and Van Dijck, P. (2012). *Candida* biofilms and the host: models and new concepts for eradication. *International journal of microbiology* 2012, 845352.

Trapnell, C., Pachter, L., and Salzberg, S.L. (2009). TopHat: discovering splice junctions with RNA-Seq. *Bioinformatics (Oxford, England)* 25, 1105-1111.

Tronchin, G., Bouchara, J.P., and Robert, R. (1989). Dynamic changes of the cell wall surface of *Candida albicans* associated with germination and adherence. *European journal of cell biology* 50, 285-290.

Uppuluri, P., Chaturvedi, A.K., Srinivasan, A., Banerjee, M., Ramasubramaniam, A.K., Kohler, J.R., Kadosh, D., and Lopez-Ribot, J.L. (2010). Dispersion as an important step in the *Candida albicans* biofilm developmental cycle. *PLoS pathogens* 6, e1000828.

Wachtler, B., Citiulo, F., Jablonowski, N., Forster, S., Dalle, F., Schaller, M., Wilson, D., and Hube, B. (2012). *Candida albicans*-epithelial interactions: dissecting the roles of active penetration, induced endocytosis and host factors on the infection process. *PloS one* 7, e36952.

Wang, X., and Fries, B.C. (2011). A murine model for catheter-associated candiduria. *Journal of medical microbiology* 60, 1523-1529.

Weissman, Z., and Kornitzer, D. (2004). A family of *Candida* cell surface haem-binding proteins involved in haemin and haemoglobin-iron utilization. *Molecular microbiology* 53, 1209-1220.

Wilson, R.A., and Talbot, N.J. (2009). Under pressure: investigating the biology of plant infection by *Magnaporthe oryzae*. *Nature reviews Microbiology* 7, 185-195.

Wilson, R.B., Davis, D., and Mitchell, A.P. (1999). Rapid hypothesis testing with *Candida albicans* through gene disruption with short homology regions. *Journal of bacteriology* 181, 1868-1874.

Yeater, K.M., Chandra, J., Cheng, G., Mukherjee, P.K., Zhao, X., Rodriguez-Zas, S.L., Kwast, K.E., Ghannoum, M.A., and Hoyer, L.L. (2007). Temporal analysis of *Candida albicans* gene expression during biofilm development. *Microbiology* 153, 2373-2385.

Yue, H., Brown, M., Knowles, J., Wang, H., Broomhead, D.S., and Kell, D.B. (2006). Insights into the behaviour of systems biology models from dynamic sensitivity and identifiability analysis: a case study of an NF-kappaB signalling pathway. *Molecular bioSystems* 2, 640-649.

Zhao, X., Daniels, K.J., Oh, S.H., Green, C.B., Yeater, K.M., Soll, D.R., and Hoyer, L.L. (2006). *Candida albicans* Als3p is required for wild-type biofilm formation on silicone elastomer surfaces. *Microbiology* 152, 2287-2299.

Zhao, X., Oh, S.H., Yeater, K.M., and Hoyer, L.L. (2005). Analysis of the *Candida albicans* Als2p and Als4p adhesins suggests the potential for compensatory function within the Als family. *Microbiology* 151, 1619-1630.

- Zhu, W., and Filler, S.G. (2010). Interactions of *Candida albicans* with epithelial cells. *Cellular microbiology* *12*, 273-282.
- Zhu, W., Phan, Q.T., Boonthung, P., Solis, N.V., Loo, J.A., and Filler, S.G. (2012). EGFR and HER2 receptor kinase signaling mediate epithelial cell invasion by *Candida albicans* during oropharyngeal infection. *Proceedings of the National Academy of Sciences of the United States of America* *109*, 14194-14199.
- Zhu, Z., Wang, H., Shang, Q., Jiang, Y., Cao, Y., and Chai, Y. (2013). Time course analysis of *Candida albicans* metabolites during biofilm development. *Journal of proteome research* *12*, 2375-2385.
- Znaidi, S., Nesseir, A., Chauvel, M., Rossignol, T., and d'Enfert, C. (2013). A comprehensive functional portrait of two heat shock factor-type transcriptional regulators involved in *Candida albicans* morphogenesis and virulence. *PLoS pathogens* *9*, e1003519.
- Zordan, R.E., Miller, M.G., Galgoczy, D.J., Tuch, B.B., and Johnson, A.D. (2007). Interlocking transcriptional feedback loops control white-opaque switching in *Candida albicans*. *PLoS biology* *5*, e256.
- Zucchi, P.C., Davis, T.R., and Kumamoto, C.A. (2010). A *Candida albicans* cell wall-linked protein promotes invasive filamentation into semi-solid medium. *Molecular microbiology* *76*, 733-748.